SLAC-PUB-5562
May1991
(N)

COUPLING IMPEDANCE FOR MODERN ACCELERATORS*

S. A. Heifets and S. Kheifets
Stanford Linear Accelerator Center, Stanford University, Stanford, CA 94309

CONTENTS

* Work supported by Department of Energy contract DE-AC03-76SF00515.

Submitted to American Institute of Physics Conference Proceedings, Particle Accelerators, 1991

LIST OF SYMBOLS

Throughout the paper, boldface letters denote vectors.

Latin letters

$A(p)$	expansion coefficients
A_{LN}^{nl}	coefficients of Eq. (4.23)
a	beam pipe radius
$\mathbf{a}$	transverse vector defining an offset of a bunch
$B_n^{\pm}$	expansion coefficients
B_p	expansion coefficients
b	beam pipe radius
c	velocity of light
d	beam pipe radius
$d_n^{\pm}$	expansion coefficients
$\mathbf{E}(\mathrm{r},t)$	electric field
$\mathbf{E}_\omega(z,\mathrm{r},\theta)$	Fourier harmonic of the electric field
$\mathbf{E}_m$	azimuthal harmonic for mth mode
$E_m^{(\pm)}(k,r)$	azimuthal harmonics for mth mode
$\mathcal{E}$	particle energy
$\Delta\mathcal{E}$	energy loss
e	particle charge
$G_k(\mathrm{r},\mathrm{r}')$	time Fourier harmonic of the Green's function
$\hat{G}_{kp}(r,r')$	space Fourier harmonic of the Green's function
$G_1(r,d)$	$= K_1(\tau r) + I_1(\tau r)\, K_0(\tau d)/I_0(\tau d)$
$G_0(r,d)$	$= K_0(\tau r) - I_0(\tau r)\, K_0(\tau d)/I_0(\tau d)$
g	cavity gap
$\widetilde{g}$	$= g/2b$
g_1	taper length
$\mathbf{H}(\mathrm{r},t)$	magnetic field
$\mathbf{H}_\omega(z,\mathrm{r},\theta)$	Fourier harmonic of the magnetic field
H_m	Hankel functions of the first kind of the mth order
I_m	modified Bessel functions of the first kind of the mth order
J_m	Bessel functions of the first kind of the mth order
$\mathbf{j}_\omega$	Fourier harmonic of the current density
K_m	modified Bessel functions of the second kind of the mth order
k	$= \omega/c$, wave number
$\widetilde{k}$	$= kb$
Δk	averaging interval of wave numbers
δk	difference between neighboring resonance frequencies
L	length of variation of the cavity shape

L	longitudinal period of a periodic structure
M	number of cavities in an array
m	azimuthal mode number, e.g. monopole $m = 0$, dipole $m = 1$, etc.
N	$= 0, 1, \ldots, M-1,$ cavity number in an array
n_0	the integer closest to $\tilde{k}$
$\mathbf{n}$	the unit vector normal to the surface
P_L^l	right-hand sides of Eq. (4.23)
p_i	$= a_i/b\,, \quad i = 1, 2$
Q	$= qk/\pi c\gamma^2\beta^2$
Q_λ	quality factor of a resonance λ
q	$= eN,$ total charge of a bunch
R	$= \lvert\mathbf{r} - \mathbf{r}'\rvert = \sqrt{(z-z')^2 + r^2 + r'^2 - 2rr'\cos\theta}$
R_λ	shunt impedance of a mode λ
r_0	bunch offset
$\mathbf{r}$	transverse offset of the trailing particle
$r_b(z)$	equation for a boundary in the (r, z) plane
S	surface
$d\mathbf{S}$	$= \mathbf{n}\, dS,$ surface element
s	distance inside a bunch
s_B	bunch spacing
t	time
U_λ	energy stored in a mode λ
dV	volume element
V_λ	eigenfunctions of a mode λ
$\mathbf{v}$	particle velocity
W	total field energy
$w_l(s)$	longitudinal point wake function
$w_\perp(s, \mathbf{r})$	transverse point wake function
w_l^R	longitudinal resistive point wake function
$w_\perp^R$	transverse resistive point wake function
x_n, t_n, y_n, z_n	normalized expansion coefficients
Y_m	Bessel functions of the second kind of the mth order
Z_l^R	longitudinal resistive impedance
$Z_\perp^R$	transverse resistive impedance
$Z_{cav}(k)$	the impedance of a cavity
$Z_{coll}(k)$	the impedance of a collimator
$Z_{in}(k)$	the impedance of a step-in
$Z_{out}(k)$	the impedance of a step-out
Z_T	longitudinal impedance of a taper
$Z_l(\omega, \mathbf{r})$	longitudinal impedance
$Z_\perp(\omega, \mathbf{r})$	transverse impedance
Z_0	$= 4\pi/c \equiv 377\ \Omega$

Z_1	real part of the impedance
Z_2	imaginary part of the impedance
Z_l^{NB}	narrow-band longitudinal impedance
$Z_\perp^{NB}$	narrow-band transverse impedance

Greek letters

α_p^2	$= (2\pi ap/L)^2 + 4\pi ka^2p/L$
β	$= v/c$, relative particle velocity
γ	$= \mathcal{E}/mc^2$, Lorentz factor
γ_λ	resonance width of a mode λ
γ_{nm}	resonance width of a mode nm
$\delta(r)$	the Dirac's radial δ-function
$\vartheta(x)$	step function, $\vartheta(x) = 1$ for $x > 0$, $\vartheta(x) = 0$ for $x < 0$.
ζ_n	effective surface impedance
ζ_N	local distance in the Nth cavity
η	parameter of a transition from a cavity regime to a step regime
κ_l	longitudinal loss factor
κ_λ^l	loss factor of a mode λ
κ_{in}^l	loss factor of a step-in
κ_{out}^l	loss factor of a step-out
$\kappa_\perp$	transverse loss factor
λ_n	$= n\pi/g$
λ_{dn}	$= \sqrt{k^2 - \nu_n^2/d^2}$, $Im\ \lambda_{dn} > 0$
$\widetilde{\lambda}_d$	$= \sqrt{\widetilde{k}^2 - \nu_n^2}$
μ_n	$= b\sqrt{k^2 - \lambda_n^2}$
μ	$= gk/2$
ν_n	nth root of J_0, $\nu_1 < \nu_2 < \ldots < \nu_\infty$
χ_n	$= g\lambda_{bn}/2$
χ_p	$= a\Omega$
$\rho(s, \mathbf{r})$	normalized longitudinal charge density
ρ_ω	Fourier component of the charge density
σ	rms bunch length
$\sigma_\perp$	transverse *rms* size of a bunch
σ_R	resistivity
τ	$= k/\gamma\beta$
Ω	$= \sqrt{k^2 - p^2 + 2ik\varepsilon}$, $\varepsilon \to 0$
ω_λ	frequency of a mode λ
$\omega_{c.o.}$	$\simeq c/a$, cutoff frequency
∇^2	the Laplace operator
$o(\epsilon)$	terms of the order of ϵ

COUPLING IMPEDANCE FOR MODERN ACCELERATORS

S. A. Heifets and S. A. Kheifets
Stanford Linear Accelerator Center, Stanford University, Stanford, CA 94309

ABSTRACT

A systematic review of theoretical results for the longitudinal and transverse impedances obtained by different methods is presented. The paper comprises definitions, general theorems, modal analysis, a diffraction model, and analytical results. Several new results are included. In particular, necessary and sufficient conditions are given for the independence of the impedance from the beam longitudinal direction. The impedances of two basic simple structures—that of a *cavity* and that of a *step*—are studied in detail. The transition from the regime of a cavity to the regime of a step is explained, an approximate formula describing this transition is given, and the criterion for determining the applicability of each regime is established. The asymptotic behavior of the impedance for a finite number M of periodically arranged cavities as a function of M is studied. The different behaviors of the impedance for a single cavity and that for an infinite number of cavities are explained as resulting from the interference of the diffracted waves. A criterion for determining the transition in the impedance behavior from small M to large M is presented.

I. INTRODUCTION

The major problem of accelerator physics today is to increase the stored beam current. This is important for both existing and future high energy accelerators, since the rate of events in experiments with high energy particles drops with the energy $\mathcal{E}$, and increasing the beam current improves the yield.

The current stored in a modern high energy accelerator is limited by collective instabilities (provided, of course, that the single-particle motion is stable, as is the case for all accelerators). Collective instabilities could arise either from direct electromagnetic (EM) interaction of particles in the same bunch, or indirectly, since a particle beam in an accelerator generates an electromagnetic field while passing through discontinuities and variations in the cross-sectional shape of the vacuum chamber.

Direct interaction between relativistic particles of the same bunch on a straight trajectory becomes negligible with increasing energy, since the Coulomb repulsion between the particles is compensated with an accuracy $1/\gamma^2 \ll 1$, $\gamma = \mathcal{E}/mc^2$, by their magnetic attraction. All the space-charge effects (such as the Laslett tune shift [79]), which are dominant at low particle energies, can be disregarded as $\gamma \to \infty$. The interaction of particles on a bend trajectory comprises a very interesting subject [104] but will not be considered here (see also Refs. 8, 15, 59, 82, and 98).

Stability of the ultrarelativistic particle motion depends mostly (apart from the beam-beam interaction) on the interaction of the particle with electromagnetic *wakefields* generated in accelerator structures by the particles moving ahead of it. The wakefields in turn interact with the particles and may cause such collective effects as single- and multibunch collective instabilities, bunch lengthening, increase in the bunch energy spread, its emittance growth, etc. [39, 127]. The discussion of the collective effects can be found, for example, in Refs. 16, 17, 54, and 97. The properties of the wakefields and the methods for their calculation in the ultrarelativistic limit $\gamma \to \infty$ are the subjects of this paper.

The wakefield can be considered as a linear response of the system to an external excitation produced in our case by a beam current. In general, the response may be expressed in terms of a Green's function. However, in most cases it is sufficient to consider the average effect of the accelerator structure: an energy loss of a particle and a transverse abrupt change in the particle momenta (kick), which a particle experiences when passing through the structure. *Wake functions* describe such average effects of an accelerator structure. They depend both on the beam current distribution in the bunch and on the properties of the beam environment.

To find the *bunch wake function* excited in a given structure by a *bunch* of particles, it is helpful first to find the *point wake function* excited in it by a *point charge*. After the point wake function is found, the bunch wake function can be determined by its convolution with the charge distribution. Finding the point wake function requires study of the propagation, diffraction, and interference of the radiated EM waves.

In general, the point wake function has three components. In what follows, we distinguish between two types of point wake functions: (1) the *longitudinal* point wake function, i.e. its projection on the axis of the structure, and (2) the *transverse* point wake function, the two-dimensional vector perpendicular to the axis of the structure.

The point wake function describes the interaction of a particle with its environment in the time domain [5]. The same interaction can also be described in the frequency domain by the Fourier transform of the point wake function—the *coupling impedance* [4, 124]. In what follows we consider the *longitudinal* and *transverse* impedances.

The range of frequencies ω studied here extends up to some high frequency which is well above the cutoff frequency of the beam pipe of radius a, but is also such that the corresponding dimensionless wave number is still small compared to the particle Lorentz factor: $1 \ll \omega a/c \ll \gamma$. This range is sufficient for studying the stability of the shortest bunches used in or designed for modern accelerators. Below the cutoff frequency, impedance is defined by a few eigenmodes and can easily be found by means of existing numerical codes. For $\omega > c\gamma/a$ the impedance falls off exponentially.

From its definition it is clear that the coupling impedance is a property of the beam environment, but not of the beam itself. This is the main advantage of the coupling impedance concept. The real (resistive) part of the longitudinal impedance describes the energy loss. The imaginary part of the impedance is responsible for an incoherent tune shift and bunch lengthening. If the frequency

shifts of any two low-order synchrotron modes lead to their degeneracy, transverse mode coupling (also called fast head-tail instability) occurs. Other instabilities, such as microwave longitudinal instability and transverse fast blowup instability depend on the absolute value of the impedance. It is worth mentioning that single-bunch instabilities are due to the *high-frequency impedance*, whereas multibunch instabilities depend on the low-frequency *narrow-band* impedance.

The narrow-band impedance may be described as a sum of narrow resonances. Each resonance is produced by a localized mode whose frequency is below or not much above the cutoff frequency of openings present in the structure. In the time domain, this corresponds to a slow-decaying oscillating wake function. In the high-frequency region, well above the cutoff frequency, the resonances overlap, producing a smooth frequency dependance of the impedance. In the time domain, this defines the short-range behavior of the wake function.

The high-frequency impedance describes interactions of particles due to the presence of abrupt changes of the beam pipe cross section as well as high-frequency tails of resonant structures such as radio-frequency (rf) cavities, bellows, vacuum ports, etc. It is significant if the bunch length is small compared to the beam pipe radius. Until recently the bunch length in all accelerators was larger than the beam pipe radius, and consequently the detailed behavior of the high-frequency impedance was not a major concern. It was usually approximated by single broad resonance parameters that were estimated from an experiment. This model of the high-frequency impedance is usually referred to as a *broad-band impedance* [55]. However, the new generation of accelerators, such as high energy colliders, synchrotron light sources, storage rings designed to yield large numbers of mesons (ϕ- and B-factories), etc., utilizes very short bunches, and therefore the energy loss is defined largely by the high-frequency impedance. This makes desirable a careful analytic analysis of the high-frequency behavior of the longitudinal impedance [10]. This subject is emphasized here.

This paper is restricted to theoretical methods and results for the impedance, and does not discuss measurement techniques or purely numerical methods of the impedance calculations.

The impedance of a given structure can be measured on a test bench either by using a small dielectric probe and then interpreting the results according to the Slatter theory [102], or by using a short current pulse sent through a wire [33, 99]. The impedance of the whole accelerator can be estimated from measurements of bunch lengthening, the coherent tune shifts, etc. Lambertson [77] and Palumbo and Vaccaro [99] have discussed this subject.

Numerical calculation of the point wake function is not a simple task because of the singularity of the charge distribution. Numerical methods are more appropriate for finding the bunch wake functions for nonsingular charge distributions [117, 118]. They are also the only methods applicable to complex structures. Nevertheless, such calculations require significant time even with the most advanced computers.

A more conventional method consists of finding the impedance and using its inverse Fourier transformation to find the point wake function. Clearly, use of this method demands knowledge of the impedance up to very high frequencies.

Direct numerical calculation of the impedance similarly faces difficulties from the enormous number of resonance contributions that should be taken into account [111], which justifies development of the analytical and semianalytical methods described here. Such methods not only provide useful formulae for estimating the impedance but also give insight into the physics of the wakefield generation.

Whenever possible we check our results by the numeric code TBCI [119], which allows calculation of the bunch wake functions in the time domain. Another useful code for this purpose is ABCI [19].

Throughout our discussion we assume that the particle energy is constant and does not change as a result of the radiation in the structure. We also neglect small oscillations of a particle moving in an accelerator. In other words, we assume that the vector of the particle velocity $\mathbf{v}$ is constant (at least while the particle is traveling through the structure under consideration) and is directed parallel to the axis of the structure, which is the z-axis in the coordinate system we have chosen. The particular case of a beam circulating in a toroidal cavity where $|\mathbf{v}| = constant$ has been considered by Warnock and Morton [114, 115], Ng [86,87], and Ng and Warnock [88].

We also neglect the resistivity of the metal walls (exception in Section II.D). In the ultrarelativistic limit, the resistive corrections are negligibly small and are outside the scope of this paper. The assumption of superconductivity allows us to impose simple boundary conditions on the EM field, which substantially simplify our derivations.

Our main objective is to review the properties of the point wake function (in the time domain) or, equivalently, the behavior of the coupling impedance (in the frequency domain). The basic concepts are defined in Section II.

In Section III several general theorems concerning the impedances are stated. Here we give the Panofsky-Wenzel [96] relation of the transverse and longitudinal point wake functions, and consequently the relation of the transverse and longitudinal impedances. We then present the radial dependence of impedance modes due to Weiland [120]. Two useful results follows: (1) an expression of the impedance in the high-frequency region in terms of low-frequency eigenmodes, and (2) a proof of the independence of the impedance from the direction of the bunch motion along $\pm z$.

Section IV is devoted to evaluation of the narrow-band impedance for a step, a cavity, and a collimator using the field matching technique. A perturbation method is developed which simplifies calculations, and a hypothesis explaining the appearance of trapped modes is suggested.

In Section V a simple diffraction approach for evaluating the high-frequency impedance is developed. For two structures for which exact methods exist and the impedances are known, this simple approach is shown to give correct results.

In Section VI we present some analytical calculations of the high-frequency impedance. These can be done only in limited, cylindrically symmetric, simple cases, such as a cavity or a step in a waveguide cross section. Nevertheless, there are several reasons to consider these cases analytically.

(1) Analytical considerations improve our understanding of the details of the radiation process.

(2) Analytical results complement the purely numerical results of existing codes, and provide an answer in parameter regions where existing codes have difficulties.

(3) Analytical results for a cavity and for a step are interesting in themselves. Sometimes, other more complicated structures can be considered as combinations of cavities and steps. A good approximation for the coupling impedance of such a structure could be a sum of contributions of its parts. Solutions for several interesting structures can be obtained from the two cases studied here. For example, a cylindrical pipe of radius a ending with an infinite flange is a special case of a step in a pipe cross section from radius a to radius b in the limit as $b \to \infty$.

Because of the enormity of the field, we cannot present a comprehensive description of all the results obtained up to now, nor can we mention all the relevant papers. Our aim is to provide an introduction to the present status of the field, with a representive list of references.

II. BASIC DEFINITIONS

A. The longitudinal impedance

The longitudinal point wake function w_l is defined as the energy loss $\Delta\mathcal{E}_1$ of a test particle with charge e, that follows, at a distance s, a point-like bunch having total charge $q = eN$ [3, 4]:

$$\Delta\mathcal{E}_1 \equiv eqw_l(s) . \tag{2.1}$$

If the electric field $\mathbf{E}$ excited by the charge q is known, then the point wake function can be found by integrating the instantaneous work produced by the field on a trailing ultrarelativistic particle with an offset $\mathbf{r}$:

$$w_l(s,\mathbf{r}) \equiv -\frac{1}{q}\int_{-\infty}^{\infty} dt\ \mathbf{v}\cdot\mathbf{E}(z,\mathbf{r},t)|_{z=vt-s}\ ,\ v \approx c\ . \tag{2.2}$$

Note that the field $\mathbf{E}(z,\mathbf{r},t)$ does *not* include the self-interaction of the particle. The radiated part of the field satisfies the homogeneous wave equation and the radiation condition $|\mathbf{E}| \to 0$ as $z \to \pm\infty$ [57].

Equations (2.1) and (2.2) can also be derived by considering the energy flow of the EM field. The field of a particle moving along the axis z of a smooth pipe has only two nonzero components: the radial electric E_r and the azimuthal magnetic H_θ. The energy flow described by the Poynting vector $\mathbf{P} \sim \mathbf{E}\times\mathbf{H}$ is directed along the axis z and remains constant. There is no energy loss in this case. The field of a particle changes at a discontinuity of the vacuum pipe, causing the energy loss. In the first approximation, the loss is given by the product of the z component of the electric field E_z at the discontinuity and the unperturbed azimuthal component H_θ. This gives a nonzero radial energy flux, producing Eqs. (2.1) and (2.2).

*The dimensions of the longitudinal wake function are V/C (volt per coulomb) in the MKS system and 1/cm in the CGS system. For this reason we chose not to call this quantity the wake potential as is usually done. Dimensions of the longitudinal impedance in these systems are Ω (ohm) in the MKS system and sec/cm in the CGS system.

In general, the radiated field depends on the transverse offsets of both the trailing and the leading particles. The dependence on the transverse offset of the trailing particle r is explicitly indicated in Eq. (2.2).

We define the Fourier harmonic of a function $f(t)$ by

$$f(\omega) \equiv \int_{-\infty}^{\infty} dt\ f(t)\ e^{i\omega t} . \tag{2.3}$$

The longitudinal impedance $Z_l(\omega, \mathbf{r})$ is defined as a Fourier harmonic of the point wake function:

$$Z_l(\omega, \mathbf{r}) \equiv \frac{1}{v} \int_{-\infty}^{\infty} ds\ w_l(s, \mathbf{r})\ e^{i\omega s/v} . \tag{2.4}$$

If the particle velocity has only the longitudinal component v_z, the longitudinal impedance is expressed in terms of the Fourier harmonic of the longitudinal electric field:

$$Z_l(\omega, \mathbf{r}) \equiv -\frac{1}{q} \int_{-\infty}^{\infty} dz\ E_{z\omega}(z, \mathbf{r})\ e^{-i\omega z/v} . \tag{2.5}$$

For a single bunch, the energy loss κ_l per particle averaged over the particle distribution in the bunch is given by the convolution of the point wake function with the normalized longitudinal particle density $\rho(s, \mathbf{r})$, $\int ds\ dr\, \rho(s, \mathbf{r}) = 1$:

$$\kappa_l \equiv \langle w_l(s) \rangle = \int ds_1 d\mathbf{r}_1\, ds_2 d\mathbf{r}_2\ \rho(s_1, \mathbf{r}_1)\, \rho(s_2, \mathbf{r}_2)\ w_l(s_1 - s_2, \mathbf{r}_1, \mathbf{r}_2) . \tag{2.6}$$

In the case when the transverse dimensions of the bunch are small, $\rho(s, \mathbf{r})$ can be approximated by $\rho(s)\delta(\mathbf{r})$ and the loss factor is

$$\kappa_l = \frac{1}{2\pi} \int d\omega\ Z_l(\omega)\ |\hat{\rho}(\omega)|^2 . \tag{2.7}$$

Here $Z_l(\omega) \equiv Z_l(\omega, 0)$ and $\hat{\rho}(\omega)$ is the Fourier harmonic of $\rho(s)$.

For a particular case of a Gaussian longitudinal distribution of the bunch density with the rms length σ

$$\rho(s) = \frac{1}{\sqrt{2\pi\sigma^2}}\ e^{-s^2/2\sigma^2} , \tag{2.8}$$

its Fourier harmonic is real

$$\hat{\rho}(\omega) = e^{-\omega^2\sigma^2/2c^2} , \tag{2.9}$$

and there is no need to take the absolute value in Eq. (2.7).

For resonant structures such as radio-frequency resonators, cavities, etc., the impedance has narrow maxima at the resonance frequencies. Hence, the *narrow-band* impedance may be represented by the sum of resonances:

$$Z_l^{NB}(\omega) = i\sum_\lambda \kappa_\lambda^l \left(\frac{1}{\omega - \omega_\lambda + i\gamma_\lambda} + \frac{1}{\omega + \omega_\lambda + i\gamma_\lambda} \right) , \qquad (2.10)$$

where ω_λ, γ_λ, and κ_λ^l are the frequencies, widths, and loss factors of the λth resonance, respectively. In the complex ω-plane these parameters define the positions of the poles and their residues. Equation (2.10) is usually written in the form

$$Z_l^{NB}(\omega) \;=\; \sum_\lambda \frac{R_\lambda}{1 + iQ_\lambda(\omega_\lambda/\omega - \omega/\omega_\lambda)} , \qquad (2.11)$$

where κ_λ^l and γ_λ are related to the shunt impedance R_λ and the quality factor Q_λ:

$$\kappa_\lambda^l \;=\; \frac{\omega_\lambda R_\lambda}{2Q_\lambda} , \qquad \gamma_\lambda^l \;=\; \frac{\omega_\lambda}{2Q_\lambda} . \qquad (2.12)$$

For example, for the fundamental mode of a typical rf resonator $(R/Q)_0 \approx 200\ \Omega$, and for $\omega_0 \approx 500$ MHz, the loss factor $\kappa_0^l \approx 0.35\ \mathrm{cm}^{-1}$.* In the time domain, the point wake function that corresponds to the narrow-band impedance Eq. (2.10) is

$$w_l(s) \;=\; 2\sum_\lambda \kappa_\lambda^l \cos\left(\omega_\lambda s/v\right)\; e^{-\omega_\lambda s/2Q_\lambda v} , \qquad s > 0 . \qquad (2.13)$$

The action of a bunch on a trailing particle at some large distance s is dominated by a few low-frequency higher-order modes (HOM). On the other hand, for $s = 0$ [123],

$$w_l(0) \;=\; \sum_\lambda \kappa_\lambda^l . \qquad (2.14)$$

The seeming discrepancy between this formula and Eq. (2.13) is a consequence of the *fundamental theorem of beam loading* [123]. The factor 1/2 appears because a particle is subject to the wake function produced only by the charge preceding it and hence "feels" on average 1/2 of its own charge. Since there is no EM field in front of an ultrarelativistic particle, it follows from the causality principle that $w_l(s) = 0$ for $s < 0$. The energy loss per particle into a single mode λ of an infinitely short bunch is

$$\frac{\Delta\mathcal{E}_\lambda}{N} = e^2\kappa_\lambda^l . \qquad (2.15)$$

*Sometimes the loss factor is expressed in units of volts per picocoulomb (V/pC), $1\ \mathrm{V/pC} = 1.11\ \mathrm{cm}^{-1}$.

The loss factor κ_λ^l can be expressed [123] in terms of the eigenfunction E_z^λ corresponding to the mode λ:

$$\kappa_\lambda^l = \frac{|V_\lambda|^2}{4U_\lambda}, \tag{2.16}$$

where

$$V_\lambda = \int dz E_z^\lambda(z) \; e^{-i\omega z/v} \tag{2.17}$$

and U_λ is the energy stored in the mode λ.

In practice, the loss factors and the resonance frequencies of the low modes are found numerically by using a suitable computer code such as URMEL [121], SUPERFISH [40], AMOS [23] or others for two-dimensional (2-D) structures. For 3-D calculations one can use code MAFIA [74], ARGUS [84] or MAGIC [22].

In the case when the bunch wake functions are excited by a train of equidistant bunches with bunch spacing s_B, the interference of the fields excited in the same structure by different bunches of the train has to be taken into account [124]. The loss factor of a given mode in the limit $v \to c$ should be multiplied by a factor $F(k_\lambda s_B/2Q_\lambda, k_\lambda s_B)$, where $k_\lambda = \omega_\lambda/c$ and Q_λ are the mode wave number and the quality factor, respectively. The function F of two arguments is

$$F(x,y) \equiv \frac{\sinh x}{\cosh x - \cos y}. \tag{2.18}$$

If $Q_\lambda \gg 1$ and the condition for the resonance excitation $k_\lambda s_B = 2\pi n$, n an integer, is fulfilled, the loss factor can be substantially enhanced, i.e.

$$F \sim \frac{4Q_\lambda}{2\pi n}. \tag{2.19}$$

Modal analysis is an effective way to calculate the impedance for frequencies below or comparable to the cutoff frequency $\omega_{c.o.} \sim c/a$, where a is the beam pipe radius. For higher frequencies, the density of the resonances increases. In addition, since such an EM field may propagate in the beam pipe, the widths of the resonances get large. In this case the impedance as a function of the frequency becomes extremely complicated. Observable effects though, can always be described by an expression containing the convolution of the impedance with the spectral density of the bunch. Hence, only the average impedance plays a role. Such a *high-frequency impedance* is a smooth function of the frequency.

B. The transverse impedance

A particle moving in a cylindrically symmetric structure that is uniform in the longitudinal direction with an offset, generates transverse EM field propagating with the particle. However, in the ultrarelativistic case, the transverse electric and magnetic forces cancel each other, and hence the net transverse kick is zero. Any disruption of the uniformity impairs this balance, and a particle experiences transverse force that depends on both the bunch and the particle offsets. For a small magnitude of the bunch offset r_0, the transverse EM field is proportional

to r_0. The dependence on the bunch offset can be removed from all the expressions by dividing them by r_0. The conventional definition of the transverse wake function is done in this way. The price for this is different dimensions of the respective transverse and longitudinal wake functions, loss factors, and impedances.

Correspondingly, the transverse point wake function is defined as the integrated transverse kick caused by the transverse component of the radiated field divided by the bunch offset r_0:

$$w_\perp(s,\mathbf{r}) \equiv -\frac{1}{qr_0}\int\limits_{-\infty}^{\infty} dz \left(\mathbf{E}+\frac{\mathbf{v}}{c}\times\mathbf{H}\right)_\perp (z,\mathbf{r},t)|_{t=(z+s)/v} . \tag{2.20}$$

The transverse impedance $Z_\perp(\omega)$ is defined as the ωth Fourier harmonic of $-iw_\perp$:

$$Z_\perp(\omega,\mathbf{r}) = -\frac{i}{v}\int\limits_{-\infty}^{\infty} ds\; w_\perp(s,\mathbf{r})\; e^{i\omega s/v} , \tag{2.21}$$

or, cf. Eq. (2.5),

$$Z_\perp(\omega,\mathbf{r}) = -\frac{i}{qr_0}\int\limits_{-\infty}^{\infty} dz \left(\mathbf{E}_\omega+\frac{\mathbf{v}}{c}\times\mathbf{H}_\omega\right)_\perp e^{-i\omega z/v} . \tag{2.22}$$

The transverse loss factor is defined analogously to Eq. (2.7):

$$\kappa_\perp \equiv \langle w_\perp\rangle = \frac{i}{2\pi}\int d\omega |\hat{\rho}(\omega)|^2\; Z_\perp(\omega) . \tag{2.23}$$

Here $Z_\perp(\omega)\equiv Z_\perp(\omega,0)$.

The transverse narrow-band impedance can be represented by a sum over the pole terms:

$$Z_\perp^{NB}(\omega) = i\sum_\lambda \kappa_\lambda^\perp \left(\frac{1}{\omega-\omega_\lambda+i\gamma_\lambda}-\frac{1}{\omega+\omega_\lambda+i\gamma_\lambda}\right) . \tag{2.24}$$

This gives the transverse point wake function

$$w_\perp(s) = 2\sum_\lambda \kappa_\lambda^\perp\; \sin(\omega_\lambda s/v)\; e^{-\omega_\lambda s/2Q_\lambda v} , \qquad s>0 . \tag{2.25}$$

Similarly to Eq. (2.16) the transverse loss factors $\kappa_\lambda^\perp$ can also be expressed [2, 5] in terms of the eigenfunctions V_λ:

$$\kappa_\lambda^\perp = \frac{c}{\omega_\lambda r_0}\frac{V_\lambda^*\nabla_\perp V_\lambda}{U_\lambda} , \tag{2.26}$$

where $\nabla_\perp$ means the derivative over r.

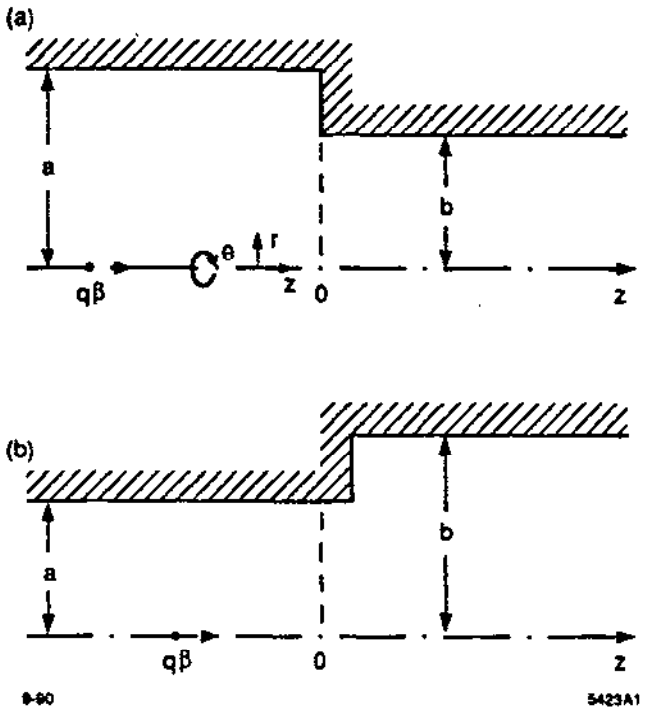

Figure 2.1 Geometry of the waveguide cross-section step and the coordinate system: (a) incoming charge, (b) outgoing charge.

C. The loss factor for a step

To illustrate the concept of a longitudinal loss factor, we estimate it here for a simple example of an abrupt change in the cross section of a circular waveguide from radius a to radius b (a step); see Fig. 2.1.

We start by considering a particle moving in free space. It is convenient to direct the z-axis along the particle trajectory. For an ultrarelativistic particle, a good approximation for the nonzero components of the field in the region $r < \gamma/k$ is

$$E_{\omega r} = \frac{2q}{cr} e^{ikz} , \tag{2.27}$$

$$H_{\omega\theta} = \frac{2q}{cr} e^{ikz} . \tag{2.28}$$

The field propagates synchronously with the charge. In the region $kr > \beta\gamma$ the field is exponentially small. The total field energy of the charge is given by

$$W = 2\pi \int_{-\infty}^{\infty} dt \int_{0}^{\infty} r dr \, \frac{c}{4\pi} (\mathbf{E} \times \mathbf{H})_z = -2\pi c \int_{r_{min}}^{\infty} r dr \int_{0}^{c\gamma/r} d\omega \, |E_{\omega r}|^2 . \tag{2.29}$$

With the field from Eq. (2.27), the integral diverges at small r:

$$W \simeq \frac{q^2\gamma}{r_{min}} . \tag{2.30}$$

If $r_{\min}$ is the classical electron radius e^2/mc^2, the energy of the synchronous component of the field W is of the order of the energy of a particle $\mathcal{E}$: $W \simeq \mathcal{E}$, and it actually depends on the definition of the electron mass and the charge of a particle. For a rigid bunch of N particles the contribution of all particles

$$|E_{\omega\tau}|^2 = \left(\frac{2q}{c\tau}\right)^2 \sum_{i,j} e^{ik(z_i - z_j)} \qquad (2.31)$$

can be found by replacing the sum by the integral over the normalized distribution function $\rho(z)$:

$$|E_{\omega\tau}|^2 = \left(\frac{2Ne}{c\tau}\right)^2 \int dz_1\, dz_2\, \rho(z_1)\, \rho(z_2)\; e^{ik(z_1 - z_2)}\,. \qquad (2.32)$$

For a Gaussian bunch with rms length σ the energy per particle is

$$W = \frac{Ne^2}{\sqrt{\pi}\sigma} \ln\frac{\gamma\sigma}{r_{\min}}\,. \qquad (2.33)$$

Consider now a particle moving in a circular waveguide of radius a. For $\gamma\sigma > a$ the energy of the synchronous component of the field moving with the particle is

$$W(a) = \frac{Ne^2}{\sqrt{\pi}\sigma} \ln\frac{a}{r_{\min}}\,. \qquad (2.34)$$

Suppose now that the particle passes through an abrupt change of the pipe cross section. Then the change in the energy of the synchronous component of the field ΔW is the difference $W(a) - W(b)$:

$$\Delta W = \frac{Ne^2}{\sqrt{\pi}\sigma} \ln\frac{b}{a}\,. \qquad (2.35)$$

We must distinguish two cases: a particle entering a narrowing pipe (a step-in) and a particle exiting into a broadening pipe (a step-out). The energy loss in these two cases is defined by the term ΔW and the radiated energy $\Delta\mathcal{E}_{rad}$:

$$\kappa^l_{in} = \Delta\mathcal{E}_{rad} - \Delta W\,, \qquad (2.36)$$

$$\kappa^l_{out} = \Delta\mathcal{E}_{rad} + \Delta W\,. \qquad (2.37)$$

For the step-in case, the radiation propagates in the direction opposite to the direction of the particle motion. Hence, the interaction of the field with the particle is small, $\kappa^l_{in} \approx 0$. The energy of the radiation is taken out of the synchronous component of the field: $\Delta\mathcal{E}_{rad} \approx \Delta W$. From Eq. (2.37) for the step-out case, we obtain

$$\kappa^l_{out} = 2\Delta W = \frac{2Ne^2}{\sqrt{\pi}\sigma} \ln\frac{b}{a}\,. \qquad (2.38)$$

More accurate calculation shows that κ^l_{in} is not exactly zero but has a small negative value. This corresponds to the gain of energy [14, 67] that can be interpreted

as the attraction by the image charge. Thus, κ^l_{out} is less than given by Eq. (2.38). Nevertheless, the difference is always the constant

$$\kappa^l_{out} - \kappa^l_{in} \;=\; 2\Delta W \;=\; \frac{2Ne^2}{\sqrt{\pi}\sigma}\;\ln\frac{b}{a}\,. \tag{2.39}$$

Since below the cutoff frequency of a pipe no radiation occurs, $\Delta\mathcal{E}_{rad} = 0$, for a long bunch $\sigma > a$ it follows from Eqs. (2.36) and (2.37) that $\kappa^l_{in} = -\Delta W$ and $\kappa^l_{out} = \Delta W$, i.e. the absolute value of the energy loss or gain ΔW in such a case equals half the value of the energy loss κ^l_{out} for a step-out. The above consideration for the energy loss is also applicable to the longitudinal impedance; see Section IV.C.

D. The resistive wall impedance

One particular source of the high-frequency impedance is the resistivity of the beam pipe walls. Although the effects of the resistivity in the ultrarelativistic case are small and are neglected here, we present formulae for the point wake functions and the impedances for comparison with those produced by discontinuities of the waveguide.

The longitudinal point wake function generated by the image current flowing in the wall of radius a with resistivity σ_R decays asymptotically with the distance s behind the leading particle as $s^{-3/2}$ [16, 85]:

$$w^R_l(s) = \frac{1}{2\pi a}\;\sqrt{\frac{c}{\sigma_R}}\;\left(\frac{1}{s}\right)^{3/2} \qquad \text{for}\;\; s > 0\,. \tag{2.40}$$

The corresponding resistive impedance per unit length is inductive and increases with frequency:

$$Z^R_l = (1-i)\,\frac{Z_0}{4\pi a}\;\sqrt{\frac{\omega}{2\pi\sigma_R}}\,. \tag{2.41}$$

Here $Z_0 = 4\pi/c \equiv 377$ ohm.

Similarly, the transverse point wake function decays asymptotically with the distance s behind the leading particle as $s^{-1/2}$:

$$w^R_\perp = \frac{1}{\pi a^3}\;\sqrt{\frac{c}{\sigma_R\, s}} \qquad \text{for}\;\; s > 0\,. \tag{2.42}$$

The corresponding resistive impedance per unit length decreases with frequency:

$$Z^R_\perp = (1-i)\;\frac{1}{a^3}\;\sqrt{\frac{1}{2\pi\sigma_R\,\omega}}\,. \tag{2.43}$$

III. SOME GENERAL THEOREMS

In this section we discuss several useful general statements regarding the coupling impedances.

A. The Panofsky-Wenzel theorem

The Panofsky-Wenzel theorem [96] gives the relation between the longitudinal and transverse point wake functions:

$$\frac{\partial w_\perp(s,\mathbf{r})}{\partial s} \;=\; \frac{1}{r_0}\,\nabla_\perp\, w_l(s,\mathbf{r})\;. \tag{3.1}$$

This relationship follows directly from the definitions of Eqs. (2.2) and (2.20) and Maxwell's equation $ik\mathbf{H} = \nabla \times \mathbf{E}$, provided that transverse components of the radiated field are zero at infinity:

$$\lim \mathbf{E}_\perp(z,\mathbf{r},t) = 0 \qquad \text{as} \quad z \to \pm\infty\;. \tag{3.2}$$

By applying the Fourier transformation in the longitudinal coordinate s to both sides of Eq. (3.1), one obtains the expression for the transverse impedance in terms of the transverse gradient of the longitudinal impedance:

$$Z_\perp(s,\mathbf{r}) \;=\; \frac{v}{\omega r_0}\,\nabla_\perp\, Z_l(s,\mathbf{r})\;. \tag{3.3}$$

B. The radial dependence of the impedance

For *cylindrically symmetric* structures the radial dependence of the coupling impedances *in the ultrarelativistic case* was found explicitly by Weiland [120]. To obtain his result, note that the radiated part of the EM field satisfies the homogeneous wave equation. For its Fourier harmonic $\mathbf{E}_\omega$, the equation is

$$\nabla^2\,\mathbf{E}_\omega + k^2\,\mathbf{E}_\omega \;=\; 0\;, \qquad k \;=\; \frac{\omega}{c}\;. \tag{3.4}$$

The synchronous component of the field, i.e. the component whose phase velocity equals the velocity c of the particle, is then defined as

$$\mathbf{E}_k(r,\theta) \;\equiv\; \int\limits_{-\infty}^{\infty} dz\;\mathbf{E}_\omega(z,r,\theta)\;\; e^{-ikz}\;. \tag{3.5}$$

The boundary conditions for $\mathbf{E}_\omega(z,r,\theta)$ mix components of $\mathbf{E}_k(r,\theta)$ with different k. However, for cylindrically symmetric structures, the boundary conditions do not mix the azimuthal harmonics $\mathbf{E}_m$, which are the coefficients in the expansion:

$$\mathbf{E}_k(r,\theta) \;=\; \sum_m \mathbf{E}_m(k,r)\;\; e^{im\theta}\;. \tag{3.6}$$

Hence, the azimuthal harmonics can be treated independently from each other.

The equations for the projections of the azimuthal harmonics are easy to obtain by using Eqs. (3.4) and (3.5):

$$\left(\frac{1}{r}\,\frac{\partial}{\partial r}\,r\,\frac{\partial}{\partial r}-\frac{m^2}{r^2}\right)\,E_m^{(z)}(k,r)=0\,, \tag{3.7}$$

$$\left(\frac{1}{r}\,\frac{\partial}{\partial r}\,r\,\frac{\partial}{\partial r}-\frac{(m\pm 1)^2}{r^2}\right)\,E_m^{(\pm)}(k,r)=0\,, \tag{3.8}$$

where $E_m^{(\pm)}\equiv E_m^{(r)}\pm iE_m^{(\theta)}$. The solutions of Eqs. (3.7) and (3.8) which are finite on the axis $r=0$ are

$$E_m^{(z)}(k,r)\;=\Upsilon_m^{(z)}(k)r^m\,,\qquad m\geq 0\,, \tag{3.9}$$

$$E_m^{(\pm)}(k,r)\;=\Upsilon_m^{(\pm)}(k)r^{m\pm 1}\,,\qquad (m\pm 1)\geq 0\,, \tag{3.10}$$

where functions $\Upsilon_m^{(z)}(k)$ and $\Upsilon_m^{(\pm)}(k)$ are defined by the boundary condition for $\mathbf{E}_k(r,\theta)$. Under the conditions considered here, the longitudinal and transverse impedances for each mode m can be expressed in term of $E_m^{(z)}(k,r)$:

$$Z_{lm}\;=\;-\frac{E_m^{(z)}(k,r)}{q}\;=-\;\frac{\Upsilon_m^{(z)}(k)}{q}\,r^m\,,\qquad m\geq 0\,, \tag{3.11}$$

$$Z_{rm}\;=\;-\frac{1}{qk}\,\frac{\partial E_m^{(z)}(k,r)}{\partial r}\;=-\;\frac{m\Upsilon_m^{(z)}(k)}{qk}\,r^{m-1}\,,\qquad m\geq 1\,, \tag{3.12}$$

$$Z_{\theta m}\;=\;-\frac{im}{qk}\,\frac{E_m^{(z)}(k,r)}{r}\;=-\;\frac{im\Upsilon_m^{(z)}(k)}{qk}\,r^{m-1}\,,\qquad m\geq 1\,. \tag{3.13}$$

These formulae, which agree with the Panofsky-Wenzel theorem, Eq. (3.3), give the scaling of the impedance with the offset r of the trailing particle. In the dimensionless form, $Z_{lm}\sim(r/a)^m$ and $Z_{\perp m}\sim(r/a)^{m-1}$ where a is a characteristic transverse dimension—for example the pipe radius. Usually the transverse size of the bunch $\sigma_\perp$ is much smaller than a (to prevent particle losses, usually $a\geq$ (10 to 20)$\sigma_\perp$). Hence, the monopole mode ($m=0$) dominates the longitudinal impedance, and the dipole mode ($m=1$) dominates the transverse impedance. Higher-order modes $m\geq 2$ can dilute the transverse emittance of a bunch. However, this effect is usually negligible.

From Eqs. (3.11) to (3.13), it follows that the longitudinal impedance of the azimuthally symmetric monopole mode ($m=0$) is independent of the coordinate r. The transverse impedance of this mode is zero. Hence, in this case the longitudinal impedance can be calculated by integrating the field over z at any value of the coordinate r. In particular, it is convenient to integrate the field along the pipe wall and its continuation inside the structure. Since the longitudinal field on the wall is zero, the integration is restricted to the line inside the structure only. With subsequent rescaling of the respective impedance with the offset r, this procedure can be applied to any other mode m as well.

For the *dipole* mode $m = 1$ from Eq. (3.12), it follows that

$$Z_{r1} = \frac{Z_{l1}|_{r=a}}{ka} . \tag{3.14}$$

In what follows we consider the longitudinal impedance. The transverse impedance can be obtained from it by applying either Eq. (3.14) for $m \stackrel{+}{=} 1$, or the Panofsky-Wenzel theorem for any m.

C. Dispersion relations and the finite frequency sum rule

Several important properties of the impedance can be derived from the analytic continuation of the impedance into the complex ω plane. First, the point wake function is real by definition. Therefore,

$$Z_l(-\omega^*) \; = \; +Z_l^*(\omega) \, , \tag{3.15}$$

where an asterisk indicates the complex conjugate value. It follows from this equation that Im $Z_l(0) = 0$. [Note that according to the definition of the transverse impedance Eq. (2.22), $Z_\perp(-\omega^*) = -Z_\perp^*(\omega)$].

Next, causality requires that in the ultrarelativistic limit $\gamma \to \infty$ there is no field in front of the charge:

$$w(s) \; = \; 0 \quad \text{for} \;\; s < 0 \, . \tag{3.16}$$

Therefore, all the singularities of the impedance must lie in the lower half of the complex ω plane. Provided that $Z_l(\omega)$ tends to zero as $|\omega| \to \infty$, the Cauchy integral formulae give the following Kramers-Kronig dispersion relations between $Z_1(\omega)$ and $Z_2(\omega)$, the real and imaginary parts of the longitudinal impedance, respectively:

$$Z_1(\omega) \; = \frac{2}{\pi} \, PV \int\limits_0^\infty d\nu \, \frac{\nu Z_2(\nu)}{\nu^2 - \omega^2} \, , \tag{3.17}$$

$$Z_2(\omega) \; = \; - \, \frac{2\omega}{\pi} \, PV \int\limits_0^\infty d\nu \, \frac{Z_1(\nu)}{\nu^2 - \omega^2} \, , \tag{3.18}$$

where PV denotes the principal value of the integral. If the impedance tends to a finite limit as $|\omega| \to \infty$, similar dispersion relations hold for the difference between the impedances at finite and infinite ω. The dispersion relations allow one to find the impedance by calculating either the real or the imaginary part only.

The dispersion relations can be used to determine the asymptotic behavior of the impedance from the parameters of its low-frequency resonances [46]. The derivation of this formula is similar to that of the finite energy sum rule [56]. Analogously, we call this result the finite frequency sum rule.

Suppose, for example, that the high-frequency tail of the impedance of some structure decreases with frequency as $\omega^{-1/2}$, cf. Eq. (6.32), and that it can be expanded for large ω into a power series in $\omega^{-1/2}$ (to the end of Section III.C, we restrict frequency ω to positive values, $\omega > 0$). We know that such asymptotic behavior has, for example, the impedance of a cavity with side pipes [24, 47, 50, 80, 81]. In this case Eq. (3.15) gives

$$Z_l(\omega) \;=\; \alpha\,\frac{(1+i)}{\sqrt{\omega}} + \frac{i\zeta}{\omega} + o(\omega^{-3/2})\;, \tag{3.19}$$

where α and ζ are two unknown real constants. We keep here the first few terms of the impedance expansion.

Consider the difference

$$\tilde{Z}(\omega) \;=\; Z_l(\omega) - \frac{\alpha(1+i)}{\sqrt{\omega}} - \frac{i\zeta}{\omega}\;. \tag{3.20}$$

The function $\tilde{Z}(\omega)$ decreases asymptotically, at least as $\omega^{-3/2}$. Its real part $\tilde{Z}_1$ satisfies the dispersion relation Eq. (3.17). Its imaginary part $\tilde{Z}_2$ has an additional pole at $\omega = 0$. Hence, the dispersion relation for it must be

$$\tilde{Z}_2(\omega) \;=\; -\frac{\zeta}{\omega} - \frac{2\omega}{\pi}\,PV\int\limits_0^\infty d\nu\,\frac{\tilde{Z}_1(\nu)}{\nu^2-\omega^2}\;. \tag{3.21}$$

To assure the correct asymptotic behavior $\tilde{Z}_2(\omega) \approx \omega^{-3/2}$ for $|\omega| \to \infty$, the following superconvergence relation must hold:

$$\int\limits_0^\infty d\nu\,\tilde{Z}_1(\nu) \;=\; \frac{\pi\zeta}{2}\;. \tag{3.22}$$

Otherwise, $\tilde{Z}_2(\omega)$ would fall off as ω^{-1}, which is too slow.

Define now a sufficiently large frequency ω_c such that for any $\omega > \omega_c$

$$Z_1(\omega) \;=\; \frac{\alpha}{\sqrt{\omega}}\left[1 + o\left(\frac{\omega_c}{\omega}\right)\right]\;. \tag{3.23}$$

Then for any $\Omega > \omega_c$, Eq. (3.22) gives

$$\int\limits_0^\Omega d\nu\left[Z_1(\nu) - \frac{\alpha}{\sqrt{\omega}}\right] \;=\; \frac{\pi\zeta}{2}\left[1 + o\left(\frac{\alpha\omega_c}{\sqrt{\Omega}}\right)\right]\;, \tag{3.24}$$

or

$$\alpha \;=\; \frac{1}{2\sqrt{\Omega}}\left[\int\limits_0^\Omega d\nu Z_1(\nu) - \frac{\pi\zeta}{2}\right]\left[1 + o\left(\frac{\omega_c}{\sqrt{\Omega}}\right)\right]\;. \tag{3.25}$$

Note that the right-hand side of this expression is independent of Ω, since α is a constant independent of ω.

In the region $\omega < \Omega$, $Z_1(\omega)$ can be represented as the sum of resonant terms. Using Eq. (2.10) we obtain

$$\alpha = \frac{\pi}{2\sqrt{\Omega}} \left(\sum_{\omega_\lambda < \Omega} \kappa_\lambda - \frac{\zeta}{2} \right) . \tag{3.26}$$

Equation (3.19) now defines the impedance for all ω in terms of the parameters of several low-frequency resonances:

$$Z_l(\omega) = i\vartheta(\Omega - \omega) \sum_{\omega_\lambda < \Omega} \kappa_\lambda^l \left(\frac{1}{\omega - \omega_\lambda + i\gamma_\lambda} + \frac{1}{\omega + \omega_\lambda + i\gamma_\lambda} \right)$$

$$+ \vartheta(\omega - \Omega) \frac{\pi(1+i)}{2\sqrt{\omega\Omega}} \left(\sum_{\omega_\lambda < \Omega} \kappa_\lambda - \frac{\zeta}{2} \right) . \tag{3.27}$$

Here $\vartheta(x)$ is the step function: $\vartheta(x) = 1$ for $x > 0$, and $\vartheta(x) = 0$ for $x < 0$. The parameters κ_λ^l, ω_λ, and γ_λ can easily be found for any given structure by one of the existing computer codes, e.g. URMEL. If Ω is large enough, $Z_l(\omega)$ obtained in this way is independent of the particular choice of Ω. The sum

$$\Sigma(\Omega) \equiv \sum_{\omega_\lambda < \Omega} \kappa_\lambda \tag{3.28}$$

can be parametrized as

$$\Sigma(\Omega) = \frac{\zeta}{2} + \frac{2\alpha}{\pi} \sqrt{\Omega} + o\left(\frac{1}{\sqrt{\Omega}} \right) , \tag{3.29}$$

from which both unknown parameters α and ζ can be found.

Figure 3.1 [43] illustrates this procedure. The sum Eq. (3.28) was calculated with the help of the code URMEL for the CEBAF cavity (the fundamental and cutoff frequencies are 1.5 GHz and 3.2 GHz, respectively) and is plotted here as a function of Ω. Parametrization by Eq. (3.29) (solid line in Fig. 3.1) gives $\zeta = 0$ and shows that α is independent of Ω for Ω larger than, say, twice the cutoff frequency.

D. The directional symmetry of the impedance

The lack of dependence of the impedance on whether the bunch is moving in the $+z$ or the $-z$ direction is an important feature of an accelerator structure. Recently Gluckstern and Zotter [29] considered a cylindrically symmetric but longitudinally asymmetric cavity with side pipes of equal radii. They were able to prove that for a relativistic particle the *longitudinal* impedance of a cavity with arbitrary shape is independent of the direction along the z-axis in which the bunch travels. Their result corroborates numerical observations of the independence of the bunch wake function obtained with the code TBCI. Bisognano [11] gives an elegant proof of the same statement. His approach is based on a reciprocity relation applied to the tensor Green's function.

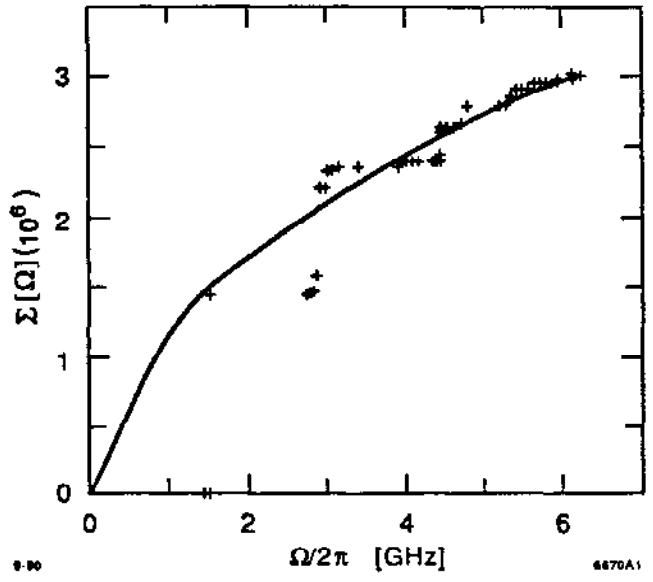

Figure 3.1 The finite frequency sum rule [see Eq. (3.28)]. Crosses represent results of numerical calculations. The curve is a parametrization by Eq. (3.29).

We follow here his idea in a somewhat simpler way [45] to obtain a more general and physically transparent proof of this property for both *longitudinal* and *transverse* impedances. The result is valid for a cavity with no azimuthal symmetry, and for arbitrary particle velocity as long as it may be considered constant. At the same time it is shown that the impedance is directionally symmetric only if the entrance and exit side beam pipes have the same cross sections.

Consider a cavity of arbitrary configuration and let a bunch travel through it along the axis z. We attach a subscript, + or −, to all quantities pertaining to the cases when the bunch travels in the positive or negative direction parallel to the z axis. To examine both the longitudinal and transverse impedances, we assume that the bunch trajectory is offset from the axis by a transverse vector $\mathbf{a}$.

The current densities have only z-component. The Fourier harmonics are

$$j_{\omega z+} = q\delta(\mathbf{r}-\mathbf{a}) \exp(i\omega z/v) , \qquad \rho_{\omega+} = j_{\omega z+}/v , \tag{3.30}$$

$$j_{\omega z-} = -q\delta(\mathbf{r}-\mathbf{a}) \exp(-i\omega z/v) , \qquad \rho_{\omega-} = -j_{\omega z-}/v . \tag{3.31}$$

Note that

$$\mathbf{j}_{\omega-} = -\mathbf{j}^*_{\omega+} , \qquad \rho_{\omega-} = \rho^*_{\omega+} . \tag{3.32}$$

The fields $\mathbf{E}_{\omega+}$ and $\mathbf{E}_{\omega-}$ excited by such sources satisfy the following wave equations:

$$\left(\nabla^2 + \frac{\omega^2}{c^2}\right) \mathbf{E}_{\omega+} = 4\pi\nabla\rho_{\omega+} - \frac{4\pi i\omega}{c^2}\,\mathbf{j}_{\omega+} , \tag{3.33}$$

$$\left(\nabla^2 + \frac{\omega^2}{c^2}\right) \mathbf{E}_{\omega-} = 4\pi\nabla\rho_{\omega-} - \frac{4\pi i\omega}{c^2}\,\mathbf{j}_{\omega-}\,, \tag{3.34}$$

as well as the boundary conditions for their tangential components:

$$\mathbf{E}_{\omega+}|_{tan} = 0\,, \qquad \mathbf{E}_{\omega-}|_{tan} = 0\,, \tag{3.35}$$

and the radiation conditions for the radiated part of the EM field:

$$\begin{cases} \lim \mathbf{E}_{+}^{rad}(z,\mathbf{r},t)|_{t=(z+s)/v} = 0\,, \\ \lim \mathbf{E}_{-}^{rad}(z,\mathbf{r},t)|_{t=(z+s)/v} = 0\,, \end{cases} \quad \text{as } z \to \pm\infty\,. \tag{3.36}$$

The longitudinal impedances Z_+ and Z_- are, cf. Eq. (2.5),

$$Z_+(\omega,\mathbf{r}) = -\frac{1}{q}\int_{-\infty}^{\infty} dz E_{z\omega+}(\mathbf{r},z)\; e^{-i\omega z/v}\,, \tag{3.37}$$

$$Z_-(\omega,\mathbf{r}) = +\frac{1}{q}\int_{-\infty}^{\infty} dz E_{z\omega-}(\mathbf{r},z)\; e^{+i\omega z/v}\,. \tag{3.38}$$

Let us find out under what conditions the fields $\mathbf{E}_{\omega+}$ and $\mathbf{E}_{\omega-}$ are complex conjugates of one another. Substituting Eq. (3.32) into Eq. (3.34) and taking its complex conjugate, we obtain

$$\left(\nabla^2 + \frac{\omega^2}{c^2}\right) \mathbf{E}^*_{\omega-} = 4\pi\nabla\rho_{\omega+} - \frac{4\pi i\omega}{c^2}\,\mathbf{j}_{\omega+}\,. \tag{3.39}$$

The boundary conditions shown in Eq. (3.35) are also valid for $\mathbf{E}^*_{\omega-}$. We now need only one additional assumption, that no incident waves accompany particles + and −; then the equations and all the boundary conditions for $\mathbf{E}^*_{\omega-}$ and $\mathbf{E}_{\omega+}$ are the same, and we may conclude that

$$\mathbf{E}^*_{\omega-} = \mathbf{E}_{\omega+}\,. \tag{3.40}$$

From the Maxwell equation $i(\omega/c)\,\mathbf{H}_\pm = \nabla \times \mathbf{E}_\pm$, it follows that

$$\mathbf{H}^*_{\omega+} = -\mathbf{H}_{\omega-}\,. \tag{3.41}$$

We now multiply Eq. (3.33) by $\mathbf{E}_{\omega-}$ and Eq. (3.34) by $\mathbf{E}_{\omega+}$, subtract the results, and integrate the difference over the volume of the cavity and the side pipes bounded by imaginary cross sections at $z = \pm\xi, \xi \to \infty$. We then obtain the *Lorentz reciprocity theorem* [20]:

$$\frac{4\pi}{c}\int dV(\mathbf{E}_{\omega-}\cdot\mathbf{j}_{\omega+} - \mathbf{E}_{\omega+}\cdot\mathbf{j}_{\omega-}) = \int d\mathbf{S}\cdot(\mathbf{E}_{\omega+}\times\mathbf{H}_{\omega-} - \mathbf{E}_{\omega-}\times\mathbf{H}_{\omega+})\,. \tag{3.42}$$

The integration on the right-hand side is performed over the surface enclosing the volume over which the integration on the left-hand side is performed, i.e. over the walls of the cavity, the walls of the side pipes, and the bounding cross sections.

Since the tangential electric field on the walls is zero, it is sufficient to perform the integration only over these cross sections. The integration over the transverse coordinates in the left side of Eq. (3.42) is performed easily by using Eq. (3.30). The remaining integration over z gives the longitudinal impedance, cf. Eqs. (3.37) and (3.38). We obtain the following expression for the difference betweem the impedances for two directions of the bunch travel:

$$\frac{4\pi q^2}{c}\,[Z_-(\omega,\mathbf{r}) - Z_+(\omega,\mathbf{r})] \;=$$

$$\int d\mathbf{S}\cdot[(\mathbf{E}_{\omega+}\times\mathbf{H}_{\omega-} - \mathbf{E}_{\omega-}\times\mathbf{H}_{\omega+})_L - (\mathbf{E}_{\omega+}\times\mathbf{H}_{\omega-} - \mathbf{E}_{\omega-}\times\mathbf{H}_{\omega+})_R]\,, \quad (3.43)$$

where the subscripts R and L refer to the beam pipe cross section at $z = \pm\xi$, respectively. By using Eqs. (3.40) and (3.41) this equation can be rewritten as

$$\frac{4\pi q^2}{c}\,[Z_-(\omega,\mathbf{r}) - Z_+(\omega,\mathbf{r})] \;=$$

$$\int d\mathbf{S}\cdot\left[(\mathbf{E}_{\omega+}\times\mathbf{H}^*_{\omega+} + \mathbf{E}^*_{\omega+}\times\mathbf{H}_{\omega+})_R - (\mathbf{E}_{\omega+}\times\mathbf{H}^*_{\omega+} + \mathbf{E}^*_{\omega+}\times\mathbf{H}_{\omega+})_L\right]. \quad (3.44)$$

The right-hand side of this equation is real. Hence, the imaginary parts of the impedances are equal:

$$\mathrm{Im}Z_+(\omega,\mathbf{r}) = \mathrm{Im}Z_-(\omega,\mathbf{r})\,. \quad (3.45)$$

The integrals in the right-hand side of Eq. (3.44) have a simple physical meaning. They give the EM field energy flow through the cross sections of the side pipes. If these cross sections are far enough from the cavity, then the only part of the EM field impinging on them is the synchronous component accompanying the bunch. This is a direct consequence of the radiation condition, Eq. (3.36), which is assumed to be fulfilled here. For the case when both side pipes have similar and equal cross sections, the synchronous components of the field at $z = \pm\infty$ are the same. It follows then from Eq. (3.44) that the two longitudinal impedances are equal. Applying now the Panofsky-Wenzel theorem, Eq. (3.3), we see that the same is true for the transverse impedances.

However, for unequal or nonsimilar pipe cross sections, the synchronous components of the two fields are different, even at $z = \pm\infty$. We cannot say that Eqs. (3.40) and (3.41) are necessarily true. In this case the real parts of the impedances for two directions may differ by a constant.

In the ultrarelativistic case, $\gamma \to \infty$, for the side pipes with round cross sections, the difference between the energies of the synchronous components in the pipes with radii a and b is proportional to the constant $\ln(b/a)$ [1], cf. Section II.C. Hence, the difference between the real parts of the impedances is proportional to the same constant. The impedance for such a case is calculated in Section IV.C [62, 63].

IV. THE MODAL ANALYSIS OF THE IMPEDANCE

We now turn to the study of the narrow-band impedance given by the sum of resonant contributions of *eigenmodes*, Eqs. (2.13) and (2.14). Effectively, only the modes that have frequencies below or comparable to the cutoff frequency $\omega_{c.o.} \simeq c/a$ of the beam pipe with radius a contribute to the narrow-band impedance [42]. The widths of the resonance peaks above the cutoff frequencies rapidly become large and their height decreases. The resonance curves overlap, producing a smooth high-frequency impedance considered in Sections V and VI.

The narrow-band impedance can be found analytically in the case when the structure may be divided into several parts for which the solutions of the Maxwell equations are known. The field for the whole structure can then be found by the *field-matching technique* [60, 128], i.e. by requiring the field to be continuous across contiguous regions.

The field-matching technique is described in Section IV.A. With its use, the exact infinite system of linear equations for unknown coefficients of the field expansions into eigenmodes is derived. For low-frequency modes, the system of coupled equations can be solved either by perturbation methods or by series truncation. We demonstrate the method of truncation for a cavity and a collimator in Section IV.B, and for a step in the waveguide cross section in Section IV.C. The method of perturbation, applicable for an arbitrary cylindrically symmetric cavity, is described in Section IV.D. Comparison of the two methods shows good agreement. In Section IV.E we briefly discuss the problem of trapped modes.

In cases of smoothly varying boundaries, the field-matching technique is hard to apply. Structures of this type are widely used in accelerators in the form of bellows. Several methods have been developed for such cases [18, 21, 61, 66, 72, 74-76]. To illustrate an approach for such cases, in Section IV.F we describe the calculation of the longitudinal narrow-band impedance for bellows [75]. Calculations of the transverse narrow-band impedance have been published [72, 76].

A. Field matching

The field-matching technique [60] will be demonstrated for axially symmetric structures, such as those sketched in Fig. 4.1 for a cavity (a) and a collimator (b). The symmetry axis is the z-axis. We chose the interfaces to be at $z \pm g/2$. The point charge q is assumed to move on the axis with speed v. The Fourier harmonic of the current density, cf. Eq. (3.30), has only the z-component:

$$j_{\omega z} = q\delta(r)\ \exp\left(ikz/\beta\right)\ , \tag{4.1}$$

where $k = \omega/c$, $\beta = v/c$, and $\delta(r)$ is Dirac's radial δ-function.

The Fourier components of the solution of the Maxwell equations that satisfy the boundary condition $E_z(z) = 0$ on the pipe wall and the radiation condition at $z = \infty$ are known [103]. We denote such a solution for the region $z > g/2$ by the

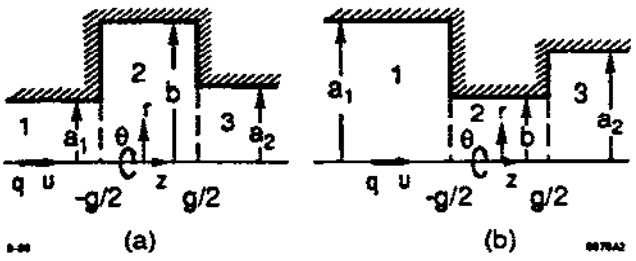

Figure 4.1 Cylindrically symmetric structures of radius b and length g with side pipes of radii a_1 and a_2; (a) a cavity, (b) a collimator.

superscript + and for the region $z < -g/2$ by the superscript −. It is convenient to introduce the following notations:

$$Q = qk/\pi c\gamma^2\beta^2 ,$$

$$G_1(r,d) = K_1(\tau r) + I_1(\tau r)\, K_0(\tau d)/I_0(\tau d) , \tag{4.2}$$

$$G_0(r,d) = K_0(\tau r) - I_0(\tau r)\, K_0(\tau d)/I_0(\tau d) , \tag{4.3}$$

where d stands for a_1 or a_2, and $\tau = k/\gamma\beta$. K_0, K_1, I_0, and I_1 are modified Bessel functions of the second and first kind of the zeroth and first order, respectively. For $\gamma >> 1$, $\gamma Q G_1(d,d) = Z_o q/4\pi^2 d$, where $Z_0 = 377\ \Omega$. With these notations

$$E^{\pm}_{\omega r} = \gamma Q G_1(r,d)\exp(ikz/\beta) - i\sum_n B^{\pm}_n(\nu_n/d)J_1(\nu_n r/d)\lambda_{dn}\exp(\pm iz\lambda_{dn}) , \tag{4.4}$$

$$E^{\pm}_{\omega z} = -iQG_0(r,d)\exp(ikz/\beta) + \sum_n B^{\pm}_n(\nu_n^2/d^2)J_0(\nu_n r/d)\exp(\pm iz\lambda_{dn}) , \tag{4.5}$$

$$H^{\pm}_{\omega\theta} = \gamma\beta QG_1(r,d)\exp(ikz/\beta) - ik\sum_n B^{\pm}_n(\nu_n/d)J_1(\nu_n r/d)\exp(\pm iz\lambda_{dn}) . \tag{4.6}$$

Here J_0 and J_1 are Bessel functions of the first kind of the zeroth and the first order, and $\nu_1 < \nu_2 < .... < \infty$ are the roots of J_0. The signs of the imaginary parts of the propagation constants $\lambda_{dn} = \sqrt{k^2 - \nu_n^2/d^2}$ should be chosen positive: Im $\lambda_{dn} > 0$. Such a choice is defined by the radiation condition, cf. Eq. (3.36).

The first terms in Eqs. (4.4) to (4.6) correspond to the synchronous component of the EM field. Each term in the sums of these expressions describes either (a) the nth diffracted wave propagating in the positive z direction, if $k > \nu_n/a_2$, or (b) an evanescent wave, if $k < \nu_n/a_2$. Similarly, for the reflected field each term describes either (a) the nth wave propagating in the negative z direction, if $k > \nu_n/a_1$, or (b) an evanescent wave, if $k < \nu_n/a_1$. For any given k, there are finite numbers of propagating waves and an infinite number of evanescent waves.

We also need to define similar expressions for the region $-g/2 < z < g/2$ with radius b (region 2 in Fig. 4.1):

$$E^0_{\omega r} = \gamma Q G_1(r,b) \ \exp(ikz/\beta)$$
$$- i \sum_n (\nu_n/b) J_1(\nu_n r/b) \lambda_{bn} [C^+ \exp(iz\lambda_{bn}) - C^- \exp(-iz\lambda_{bn})] , \quad (4.7)$$

$$E^0_{\omega z} = -iQG_0(r,b) \ \exp(ikz/\beta)$$
$$+ \sum_n (\nu_n^2/b^2) J_0(\nu_n r/b) [C^+ \exp(iz\lambda_{bn}) + C^- \exp(-iz\lambda_{bn})] , \quad (4.8)$$

$$H^0_{\omega\theta} = \gamma\beta Q G_1(r,b) \ \exp(ikz/\beta)$$
$$- ik \sum_n (\nu_n/b) J_1(\nu_n r/b) [C^+ \exp(iz\lambda_{bn}) + C^- \exp(-iz\lambda_{bn})] . \quad (4.9)$$

For certainty, the same positive sign is chosen for the propagation constant in region 2: Im $\lambda_{bn} > 0$.

Expansions of the EM field are constructed in such a way as to fulfill the boundary condition on the wall of the pipe in any region with a constant pipe radius. For example, for $r = a_2$ and for all $z > g/2$, $E^+_z(z) = 0$. On the other hand, unknown coefficients $B^\pm_n$ and $C^\pm$ have to be defined by the boundary and continuity conditions in the planes $z = \pm g/2$ between adjacent cylindrical regions: (a) the radial component of the electric field on the inner side of the wall should be equal to zero for all r, and (b) all three components of the field should be continuous through the opening.

For example, in the case of a cavity at $z = g/2$ for $a_2 < r < b$,

$$E^0_{\omega r}(r) = 0 , \quad (4.10)$$

and for $r < a_2$,

$$E^+_{\omega z}(r) = E^0_{\omega z}(r) , \quad (4.11)$$

$$E^+_{\omega r}(r) = E^0_{\omega r}(r) . \quad (4.12)$$

Analogous expressions can be written for another cavity interface at $z = -g/2$, and for a collimator.

Introduce now dimensionless variables:

$$\tilde{k} = kb , \quad (4.13)$$

$$p_i = a_i/b , \quad i = 1, 2 , \quad (4.14)$$

$$\tilde{g} = g/2b . \quad (4.15)$$

In these variables the propagation constants are

$$\tilde{\lambda}_{ain} \equiv \lambda_{ain} b = \sqrt{\tilde{k}^2 - \nu_n^2/p_i^2}\,, \qquad i = 1,\ 2\,, \tag{4.16}$$

$$\tilde{\lambda}_{bn} \equiv \lambda_{bn} b = \sqrt{\tilde{k}^2 - \nu_n^2}\,. \tag{4.17}$$

It is also convenient to redefine the expansion coefficients

$$x_n = (i\pi c/2bQ)\ \exp\left[i\tilde{g}(\tilde{k}/\beta + \tilde{\lambda}_{a1n})\right] B_n^-\,, \tag{4.18}$$

$$t_n = (i\pi c/2bQ)\ \exp\left[-i\tilde{g}(\tilde{k}/\beta + \tilde{\lambda}_{bn})\right] C_n^-\,, \tag{4.19}$$

$$y_n = (i\pi c/2bQ)\ \exp\left[i\tilde{g}(\tilde{k}/\beta - \tilde{\lambda}_{bn})\right] C_n^+\,, \tag{4.20}$$

$$z_n = -(i\pi c/2bQ)\ \exp\left[-i\tilde{g}(\tilde{k}/\beta - \tilde{\lambda}_{a2n})\right] B_n^+\,. \tag{4.21}$$

The expressions for the field components [63] in the planes $z = -g/2$ and $z = g/2$ in these variables are, correspondingly,

$$\begin{aligned} E_{\omega r}^- &= (2Q/\pi cb)\exp(-i\kappa\tilde{g}/\beta)\left[(\tilde{k}/2\gamma\beta^2)G_1(r,a_1)\right. \\ &\quad \left. +\ (1/p_1)\Sigma_n x_n \nu_n J_1(\nu_n r/a_1)\tilde{\lambda}_{a1n}\right]\,, \end{aligned} \tag{4.4a}$$

$$\begin{aligned} E_{\omega r}^0 &= (2Q/\pi cb)\exp(-i\tilde{k}\tilde{g}/\beta)\left[(\tilde{k}/2\gamma\beta^2)G_1(r,b)\right.\,, \\ &\quad \left. +\ \Sigma_n \nu_n J_1(\nu_n r/b)\tilde{\lambda}_{bn}\{t_n \exp[2i\tilde{g}(\tilde{k}/\beta + \tilde{\lambda}_{bn})] - y_n\}\right]\,, \end{aligned} \tag{4.8a}$$

$$\begin{aligned} E_{\omega z}^- &= -(2iQ/\pi cb)\exp(-i\tilde{k}\tilde{g}/\beta)\left[(\tilde{k}/2\gamma^2\beta^2)G_0(r,a_1)\right. \\ &\quad \left. +\ (1/p_1^2)\Sigma_n x_n \nu_n^2 J_0(\nu_n r/a_1)\right]\,, \end{aligned} \tag{4.4b}$$

$$\begin{aligned} E_{\omega z}^0 &= -(2iQ/\pi cb)\exp(-i\tilde{k}\tilde{g}/\beta)\left[(\tilde{k}/2\gamma^2\beta^2)G_0(r,b)\right. \\ &\quad \left. +\ \Sigma_n \nu_n^2 J_0(\nu_n r/b)\{t_n \exp[2i\tilde{g}(\tilde{k}/\beta + \tilde{\lambda}_{bn})] + y_n\}\right]\,, \end{aligned} \tag{4.8b}$$

and

$$\begin{aligned} E_{\omega r}^+ &= (2Q/\pi cb)\exp(i\tilde{k}\tilde{g}/\beta)\left[(\tilde{k}/2\gamma\beta^2)G_1(r,a_2)\right. \\ &\quad \left. +\ (1/p_2)\Sigma_n z_n \nu_n J_1(\nu_n r/a_2)\tilde{\lambda}_{a2n}\right]\,, \end{aligned} \tag{4.4c}$$

$$\begin{aligned} E_{\omega r}^0 &= (2Q/\pi cb)\exp(i\tilde{k}\tilde{g}/\beta)\left[(\tilde{k}/2\gamma\beta^2)G_1(r,b)\right. \\ &\quad \left. +\ \Sigma_n \nu_n J_1(\nu_n r/b)\tilde{\lambda}_{bn}\{t_n - y_n \exp[-2i\tilde{g}(\tilde{k}/\beta - \tilde{\lambda}_{bn})]\}\right]\,, \end{aligned} \tag{4.8c}$$

$$\begin{aligned} E_{\omega z}^+ &= -(2iQ/\pi cb)\exp(i\tilde{k}\tilde{g}/\beta)\left[(\tilde{k}/2\gamma^2\beta^2)G_0(r,a_2)\right. \\ &\quad \left. -\ (1/p_2^2)\Sigma_n z_n \nu_n^2 J_0(\nu_n r/a_2)\right]\,, \end{aligned} \tag{4.4d}$$

$$\begin{aligned} E_{\omega z}^0 &= -(2iQ/\pi cb)\exp(i\tilde{k}\tilde{g}/\beta)\left[(\tilde{k}/2\gamma^2\beta^2)G_0(r,b)\right. \\ &\quad \left. +\ \Sigma_n \nu_n^2 J_0(\nu_n r/b)\{t_n + y_n \exp[-2i\tilde{g}(\tilde{k}/\beta + \tilde{\lambda}_{bn})]\}\right]\,. \end{aligned} \tag{4.8d}$$

These expressions are valid both for a cavity for which $p_i < 1$ and for a collimator for which $p_i > 1$.

The unknown coefficients x_n, y_n, t_n, and z_n are defined by the set of linear algebraic equations that are obtained by substituting expressions for the field components into Eqs. (4.10) to (4.12) for $z = g/2$, and into similar equations for the second interface, $z = -g/2$.

If we introduce a matrix of coefficients

$$X_n^N \equiv \begin{pmatrix} X_n^1 \\ X_n^2 \\ X_n^3 \\ X_n^4 \end{pmatrix} = \begin{pmatrix} x_n \\ y_n \\ t_n \\ z_n \end{pmatrix} , \qquad N = 1, 2, 3, 4 , \tag{4.22}$$

then the set of equations can be written in a compact form:

$$\Sigma_N \Sigma_n A_{LN}^{nl} X_n^N = P_L^l , \qquad L, N = 1, 2, 3, 4 ; \quad n, l = 1, 2, \ldots, \infty . \tag{4.23}$$

Equation (4.23) constitutes an infinite system of linear algebraic equations for unknown coefficients X_n^N. The coefficients A_{LN}^{nl} and the right-hand sides P_L^l of Eq. (4.23) are presented in Table I for a cavity and in Table II for a collimator [40]. There

$$\phi_{mn}(p) = \begin{cases} \nu_n J_0(\nu_m p) J_1(\nu_n)/(\nu_n^2 - p^2 \nu_m^2) & \text{if } \nu_n \neq p\nu_m ; \\ \nu_n J_1^2(\nu_n)/(\nu_n + p\nu_m) & \text{if } \nu_n = p\nu_m . \end{cases} \tag{4.24}$$

In particular,

$$\phi_{mn}(1) = \delta_{nm} J_1^2(\nu_n)/2 .$$

In a smooth pipe for which $p_1 = p_2 = 1$, all $P_L^l = 0$. Since $Det|A_{LN}^{nl}| \neq 0$, only the trivial solution $X_n^N = 0$ exists. This means that no radiation occurs in a smooth pipe.

An equivalent system of equations can also be obtained by matching the field on the surface $r = a$ [51]. For small openings, matching at $z = \pm g/2$ is preferable because the field in the structure under consideration, in this case, is close to the field of a pillbox cavity. This type of matching is also the only one possible when the tubes have different radii. In calculations with equal side-pipe radii, the two types of matching are in close agreement.

B. The impedance of a cavity and a collimator

Suppose that the coefficients X_n^N, defined as the solution of the system Eq. (4.23), are found. Using definitions Eqs. (4.18) to (4.21), we can now find the longitudinal component of the electric field $E_z(z)$ from Eqs. (4.5) and (4.8).

TABLE I. Coefficients A^{nl}_{LN} and right-hand sides P^l_L of Eq. (4.23) for a cavity.

L / N	1	2	3	4	P^l_L
1	$2p_1^2\tilde{\lambda}_{a1n}\phi_{ln}(p_1)$	$\tilde{\lambda}_{bn}J_1^2(\nu_n)\delta_{nl}$	$-\tilde{\lambda}_{bn}J_1^2(\nu_n)\delta_{nl}E_+$	0	$J_0(\nu_l p_1)/I_0(\tau a_1)[\nu_l^2+(\tau b)^2]$
2	$\nu_n^2 J_1^2(\nu_n)\delta_{ln}$	$-2p_1^2\nu_n^2\phi_{nl}(p_1)$	$-2p_1^2\nu_n^2\phi_{nl}(p_1)E_+$	0	$-(\tau b)p_1^2\nu_l J_1(\nu_l)I_0(\tau a_1)F(a_1)/[\nu_l^2+(\tau a_1)^2]\gamma$
3	0	$\tilde{\lambda}_{bn}J_1^2(\nu_n)\delta_{nl}E_-$	$-\tilde{\lambda}_{bn}J_1^2(\nu_n)\delta_{nl}$	$2p_2^2\tilde{\lambda}_{a2n}\phi_{ln}(p_2)$	$J_0(\nu_l p_2)/I_0(\tau a_2)[\nu_l^2+(\tau b)^2]$
4	0	$-2p_2^2\nu_n^2\phi_{nl}(p_2)E_-$	$-2p_2^2\nu_n^2\phi_{nl}(p_2)$	$-\nu_n^2 J_1^2(\nu_n)\delta_{ln}$	$-(\tau b)p_2^2\nu_l J_1(\nu_l)I_0(\tau a_2)F(a_2)/[\nu_l^2+(\tau a_2)^2]\gamma$

$E_+ = \exp[2i\tilde{g}(\kappa/\beta+\tilde{\lambda}_{bn})]$, $\quad E_- = \exp[-2i\tilde{g}(\kappa/\beta-\tilde{\lambda}_{bn})]$,

$F(a) = K_0(\tau b)/I_0(\tau b) - K_0(\tau a)/I_0(\tau a)$, $\quad p_1 = a_1/b$, $\quad p_2 = a_2/b$, $\quad \tilde{g} = g/2b$.

TABLE II. Coefficients A^{nl}_{LN} and right-hand sides P^l_L of Eq. (4.23) for a collimator.

L / N	1	2	3	4	P^l_L
1	$\tilde{\lambda}_{a1n}J_1^2(\nu_n)\delta_{nl}$	$2p_1^{-2}\tilde{\lambda}_{bn}\phi_{ln}(p_1^{-1})$	$-2p_1^{-2}\tilde{\lambda}_{bn}\phi_{ln}(p_1^{-1})E_+$	0	$-J_0(\nu_l/p_1)/I_0(\tau a_1)[\nu_l^2+(\tau b)^2]$
2	$2p_1^{-2}\nu_n^2\phi_{nl}(p_1^{-1})$	$-\nu_n^2J_1^2(\nu_n)\delta_{ln}$	$-\nu_n^2J_1^2(\nu_n)\delta_{ln}E_+$	0	$-(\tau b)\nu_lJ_1(\nu_l)I_0(\tau a_1)F(a_1)/p_1^2[\nu_l^2+(\tau a_1)^2]\gamma$
3	0	$2p_2^{-2}\tilde{\lambda}_{bn}\phi_{ln}(p_2^{-1})E_-$	$-2p_2^{-2}\tilde{\lambda}_{bn}\phi_{ln}(p_2^{-1})$	$\tilde{\lambda}_{a2n}J_1^2(\nu_n)\delta_{nl}$	$-J_0(\nu_l/p_2)/I_0(\tau a_2)[\nu_l^2+(\tau b)^2]$
4	0	$-\nu_n^2J_1^2(\nu_n)\delta_{ln}E_-$	$-\nu_n^2J_1^2(\nu_n)\delta_{ln}$	$-2p_2^{-2}\nu_n^2\phi_{nl}(p_2^{-1})$	$-(\tau b)\nu_lJ_1(\nu_l)I_0(\tau a_2)F(a_2)/p_2^2[\nu_l^2+(\tau a_2)^2]\gamma$

$E_+ = \exp[2i\tilde{g}(\kappa/\beta+\tilde{\lambda}_{bn})]$, $\quad E_- = \exp[-2i\tilde{g}(\kappa/\beta-\tilde{\lambda}_{bn})]$,

$F(a) = K_0(\tau b)/I_0(\tau b) - K_0(\tau a)/I_0(\tau a)$, $\quad p_1 = a_1/b$, $\quad p_2 = a_2/b$, $\quad \tilde{g} = g/2b$.

Substituting it into formula Eq. (2.5) and performing the integration in it, we find

$$\begin{aligned} Z(k) \;=\; & -(Z_0/\pi)\Sigma_n \Big\{ x_n(\widetilde{k}/\beta - \widetilde{\lambda}_{a1n})/[1+(\tau a_1/\nu_n)^2] \\ & + \; y_n(\widetilde{k}/\beta + \widetilde{\lambda}_b)\,\{\exp[2i\widetilde{g}(\widetilde{\lambda}_b - \widetilde{k}/\beta)] - 1\}/[1+(\tau b/\nu_n)^2] \\ & - \; t_n(\widetilde{k}/\beta - \widetilde{\lambda}_b)\,\{\exp[2i\widetilde{g}(\widetilde{\lambda}_b + \widetilde{k}/\beta)] - 1\}/[1+(\tau b/\nu_n)^2] \\ & + \; z_n(\widetilde{k}/\beta + \widetilde{\lambda}_{a2n})/[1+(\tau a_2/\nu_n)^2] \Big\} \;. \end{aligned} \tag{4.25}$$

Quantities $\widetilde{k}, \widetilde{g}$, and $\widetilde{\lambda}$ are defined in Eqs. (4.13) through (4.17). Formula (4.25) is valid for both a cavity and a collimator, if the expansion coefficients x_n, y_n, t_n, and z_n in it are understood to be given by the solution of Eq. (4.23) for a cavity and for a collimator, respectively.

In the ultrarelativistic limit, $\gamma \to \infty$, the impedance can be found by integrating the field along any path displaced by r [120], cf. Section III.B:

$$\begin{aligned} Z(k) \;=\; & -(Z_0/\pi)\,\Sigma_n \Big\{ x_n J_0(\nu_n r/a_1)(\widetilde{k} - \widetilde{\lambda}_{a1n}) \\ & + \; y_n J_0(\nu_n r/b)(\widetilde{k} + \widetilde{\lambda}_b)\,\{\exp[2i\widetilde{g}(\widetilde{\lambda}_b - \widetilde{k})] - 1\} \\ & - \; t_n J_0(\nu_n r/b)(\widetilde{k} - \widetilde{\lambda}_b)\,\{\exp[2i\widetilde{g}(\widetilde{\lambda}_b + \widetilde{k})] - 1\} \\ & + \; z_n J_0(\nu_n r/a_2)(\widetilde{k} + \widetilde{\lambda}_{a2n}) \Big\} \;. \end{aligned} \tag{4.26}$$

The remarkable feature of this formula is that the right-hand side of it does *not* depend on r in spite of its explicit presence there.

In particular, for a cavity with equal side-pipe radii a, $b = pa$, a convenient choice is $r = a$, since then the regions $z > g/2$ and $z < -g/2$ do not contribute to the value of the integral:

$$\begin{aligned} Z_{cav}(k) \;=\; & -(Z_0/\pi)\,\Sigma_n J_0(\nu_n p) \Big[y_n(\widetilde{k} + \widetilde{\lambda}_b)\,\{\exp[2i\widetilde{g}(\widetilde{\lambda}_b - \widetilde{k})] - 1\} \\ & - \; t_n(\widetilde{k} - \widetilde{\lambda}_b)\,\{\exp[2i\widetilde{g}(\widetilde{\lambda}_b + \widetilde{k})] - 1\} \Big] \;. \end{aligned} \tag{4.27}$$

For a collimator a convenient choice is $r = b$. In this case, the region $-g/2 < z < g/2$ does not contribute to the value of the integral:

$$Z_{coll}(k) = -(Z_0/\pi)\,\Sigma_n [x_n J_0(\nu_n/p_1)(\widetilde{k} - \widetilde{\lambda}_b) + z_n J_0(\nu_n/p_2)(\widetilde{k} + \widetilde{\lambda}_b)] \;. \tag{4.28}$$

In general, a solution of Eq. (4.23) can be found only numerically. Two computer codes RCVTY (for the geometry sketched in Fig. 4.1a) and RCLMTR (for that in Fig. 4.1b) exist for this purpose [63]. An approximate solution is found by truncating the system to a finite size, inverting its matrix and solving for the coefficients. Such a solution is expected to be valid for modes with wavelengths larger than the diameter of the opening. For parameter values that are not too extreme, a matrix size of 20×20 is usually sufficient to obtain reasonable accuracy for the values of ka in the range $0 \le ka \lesssim 3.0$. The results are independent of the matrix size up to the maximum size of 100×100 allowed by the codes.

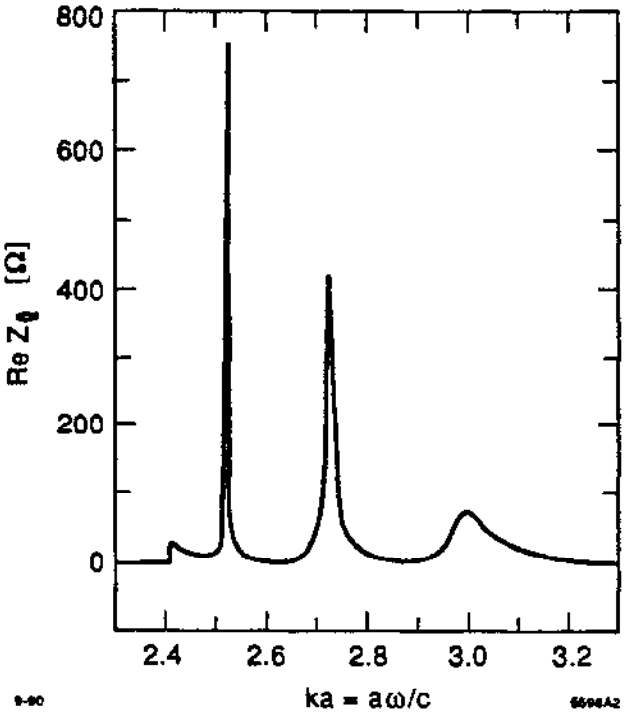

Figure 4.2 The real part of the longitudinal impedance of a cavity as a function of dimensionless parameter $ka = a\omega/c$; $a = a_1 = a_2$, $g/2b = 0.302$, $a/b = 0.152$.

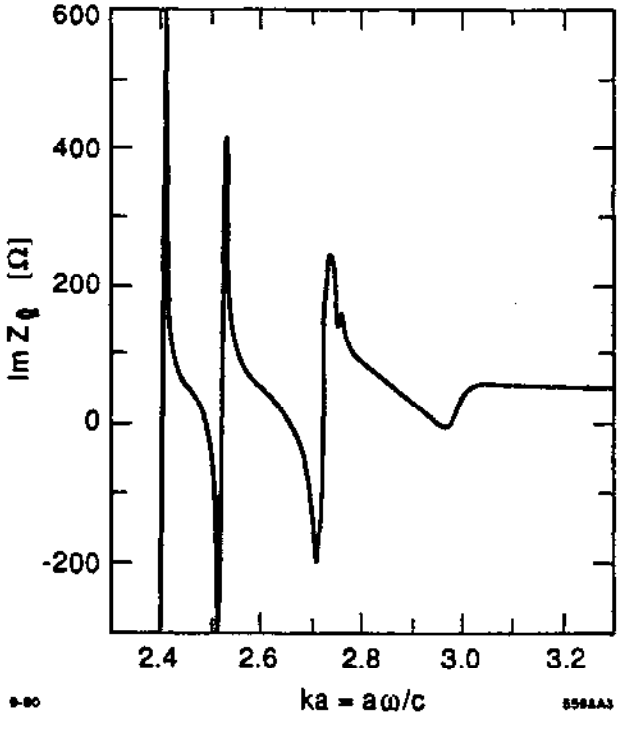

Figure 4.3 The same as Fig. 4.2, but for the imaginary part of the impedance.

The impedance of the same structure was also calculated by Henke [51] who matched the field on the surface $r = a$, $-g/2 < z < g/2$. In Figs. 4.2 and 4.3 [63] we present the real and imaginary parts of the impedance calculated with the code RCVTY. Good agreement is found with the impedance calculated by Henke [51] for all frequencies except for a small region around the cutoff frequency of the pipe $ka = 2.405$. Other calculations of the narrow-band impedance of a cavity with beam pipes have been published [105, 109, 110, 112, 113].

The dependence of the impedance on the particle energy is illustrated in Figs. 4.4 and 4.5 [63], where the real and imaginary parts of the longitudinal impedance of a cavity are plotted for several different Lorentz factors γ. The impedance for $\gamma = 100$ is indistinguishable from that for $\gamma = \infty$.

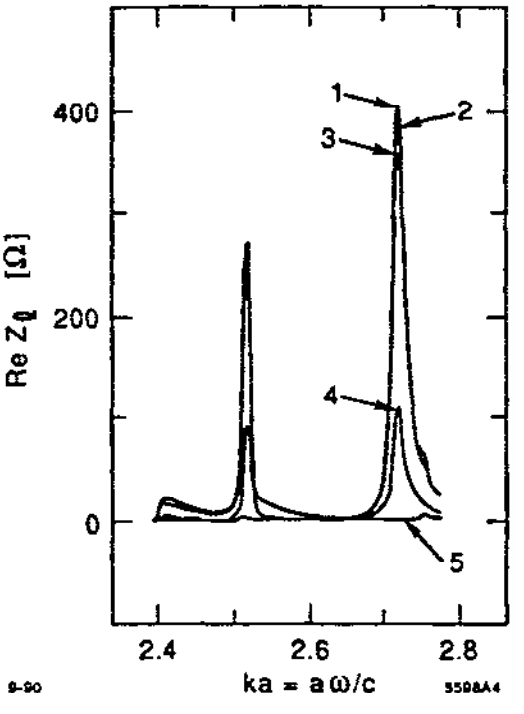

Figure 4.4 An illustration of the dependence of the real part of the impedance on γ for the same cavity shown in Fig. 4.2: (1) $\gamma = 100$, (2) $\gamma = 10$, (3) $\gamma = 5$, (4) $\gamma = 2$, (5) $\gamma = 1.4$.

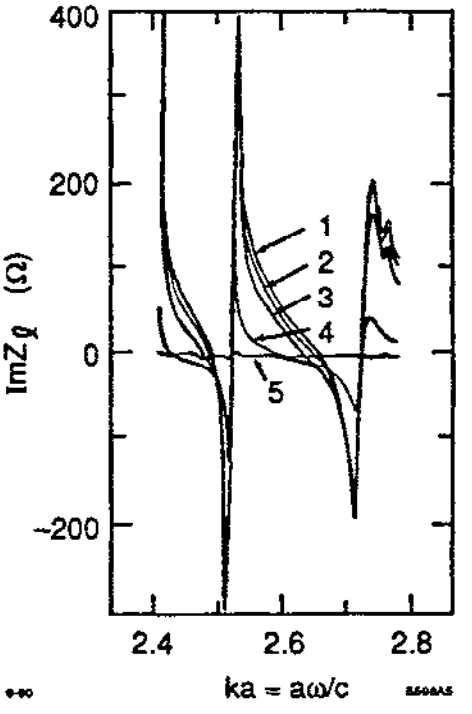

Figure 4.5 The same as Fig. 4.4, but for the imaginary part of the impedance.

To illustrate the behavior of the impedance of a collimator, the real and imaginary parts of the impedance of a thin collimator for the SLAC geometry are plotted in Figs. 4.6 and 4.7 [63]. The transverse impedance of a cavity has been calculated [52, 64, 65].

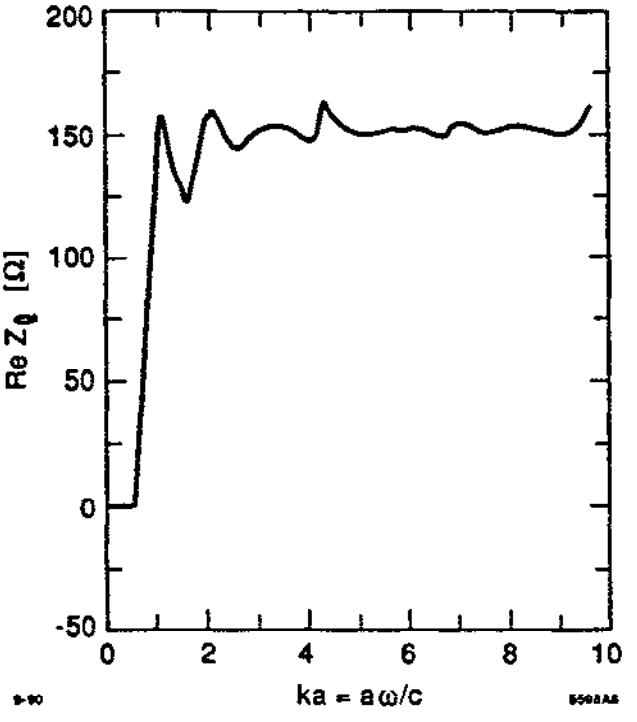

Figure 4.6 The real part of the longitudinal impedance of a very thin collimator as a function of dimensionless parameter $ka = a\omega/c$; $a = a_1 = a_2$, $g/2b = 0.217$, $a/b = 0.281$.

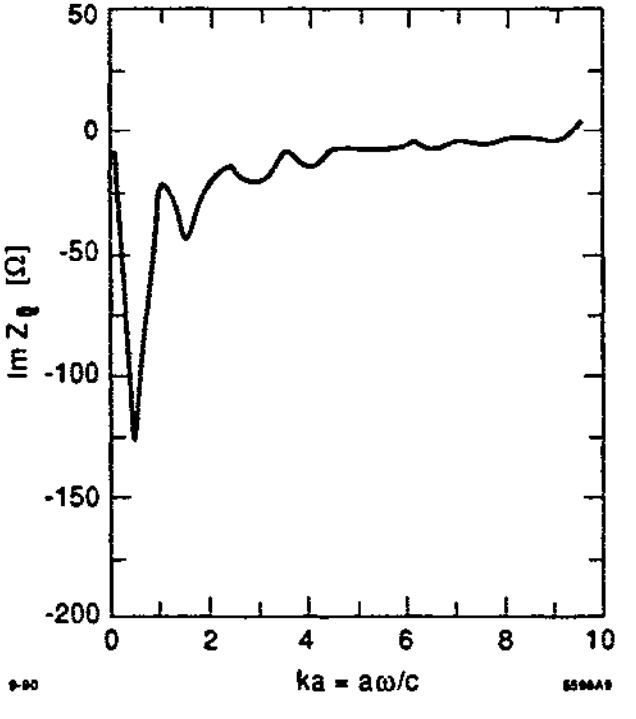

Figure 4.7 The same as Fig. 4.6, but for the imaginary part of the impedance.

C. The impedance of a step

Another important case is an infinitely long straight pipe with an abrupt change of its cross section (a step). The coupling impedance of a step for a planar geometry was considered by Hereward [53]. We give here the calculation of the coupling impedance of a step in a cylindrical pipe [67, 68]. The geometry and the coordinate system are sketched in Fig. 2.1. As discussed in Section III.D, one needs to distinguish two cases when considering a step: a charge coming out of the bigger pipe of cross section radius a and entering the narrow pipe of cross section radius b, indicated by subscript *in*; and a charge exiting from the narrow pipe and entering the bigger one, indicated by subscript *out*.

Both of these cases are included in the solution derived in the preceeding section. For example, case *in* of a charge passing through a *decreasing* cross section can be obtained by assuming $a_2 = b$ (or equivalently, $p_2 = 1$), and $g = 0$, in the equations describing a collimator. Similarly, case *out* of a charge passing through an *increasing* cross section can be obtained by assuming $a_1 = b$ (or equivalently, $p_1 = 1$), and $g = 0$, in the same equations.

Using Eq. (4.25) we find that the narrow-band longitudinal coupling impedance for a charge entering the narrow pipe is

$$Z_{in}(k) \;=\; -\frac{Z_0}{\pi} \sum_n \left[x_n(\tilde{k} - \tilde{\lambda}_a) + z_n(\tilde{k} + \tilde{\lambda}_b) \right] \;. \tag{4.29}$$

For a charge exiting the narrow pipe,

$$Z_{out}(k) \;=\; -\frac{Z_0}{\pi} \sum_n \left[x_n(\tilde{k} - \tilde{\lambda}_b) + z_n(\tilde{k} + \tilde{\lambda}_a) \right] \;. \tag{4.30}$$

Coefficients x_n and z_n here are defined by solving an infinite system of linear algebraic equations which follow from Eq. (4.23) and Tables I and II:

$$\sum_m \left[T_{lm} \pm \delta_{lm}\, \tilde{\lambda}_{al}\, J_1^2(\nu_l) \right] g_m^{\pm} \;=\; P_l \;, \tag{4.31}$$

where

$$P_l \;=\; \frac{J_0(\nu_l p)}{\nu_l^2} \;, \tag{4.32}$$

$$T_{lm} \;=\; 4\nu_m^2 p^4\, J_0(\nu_m p)\, J_0(\nu_l p) \sum_n \frac{\tilde{\lambda}_{bn}}{(\nu_n^2 - \nu_m^2 p^2)(\nu_n^2 - \nu_l^2 p^2)} \;, \tag{4.33}$$

$g_m^- \equiv -x_m$, $g_m^+ \equiv z_m$, $p = b/a$, $\tilde{\lambda}_{al} = a\lambda_{al}$, $\tilde{\lambda}_{bl} = b\lambda_{bl}$; and $a = a_1$, $b = a_2$ for Z_{in}, $b = a_1$, $a = a_2$ for Z_{out}.

It is instructive to consider two limiting cases. If there is no step, i.e. $b = a$, then $P_l = 0$ for all l, $x_l = 0$, $z_l = 0$ and no radiation occurs. In the opposite limit, when the pipe is closed, i.e. $b = 0$, $p = 0$, one obtains the exact solution

$$x_n = -\frac{1}{\nu_n^2 J_1^2(\nu_n)\sqrt{k^2a^2 - \nu_n^2}} \;, \qquad z_n = 0 \;, \tag{4.34}$$

which gives the radiation produced in a Faraday cup.

An approximate solution of Eq. (4.31) has been found numerically by truncating its matrix to a finite size, inverting it, and solving for the coefficients. For moderate values of parameters, a 20×20 matrix is sufficient to obtain reasonable accuracy. Since the magnitudes of the coefficients $g_m^{\pm}$ fall off with increasing m rather rapidly, the result does not change with larger matrix size. The narrow-band impedance behavior is illustrated in Figs. 4.8 and 4.9 [67], where the real and imaginary parts of longitudinal impedance are plotted for $p = 0.1$ as functions of the normalized frequency ka. The resonant character of the impedance is clearly exhibited.

The impedances of narrowing and widening steps are similar except that the latter is shifted up by a constant. The shift is basically proportional to the difference between the EM field energies of particles traveling in pipes with radii a and b. For a narrowing step, the radiated energy is taken out of the excess of the particle field energy in a wide pipe. As a result, the loss factor is small, cf. the area under curve 1 in Fig. 4.8. Careful examination shows that the loss factor is negative, corresponding to the gain of energy. The increase of the particle energy can be interpreted as a result of acceleration due to attraction by the image charge in the flange of the step. This effect was also noted by Chan and Schweinfurth [14]. For a widening pipe, restoration of the particle field takes place. The energy for this is taken away from the particle energy. Correspondingly, the loss factor is positive and large, cf. curve 2 in Fig. 4.8.

D. A perturbation method

An approximate solution of Eq. (4.23), obtained by truncation, is discussed above. Another approximation for the narrow-band impedance of a cavity is obtained by using a perturbation method [41, 43].

In a cavity with an opening to a waveguide (beam pipe, rf coupler, etc.), a mode above the cutoff frequency is coupled to modes propagating in the waveguide. This produces a finite width of the corresponding resonance in the narrow-band impedance (in addition to the width due to the finite wall resistivity). The narrow-band impedance exists because this coupling is small. A perturbation theory in this small parameter can be developed.

In the zeroth approximation, the field pattern inside the cavity is the same as that of the closed cavity, and tangential components of the electric field are zero on the opening. In the first approximation the matching of the normal component of the electric field defines amplitudes of the longitudinal components of the waves propagating in the waveguide. The transverse components in the waveguide are then uniquely defined, which in turn defines the tangential components of the field on the cavity opening. As a result, the relation between the normal and tangential components of the field on the opening inside the cavity can be written as

$$E_{rn} = \zeta_n H_{\theta n} , \tag{4.35}$$

where the coefficient $\zeta_n = \sqrt{1 - (\nu_n/kb)^2}$ is the effective surface impedance of the opening. For example, the frequency shift of a nth mode caused by the opening

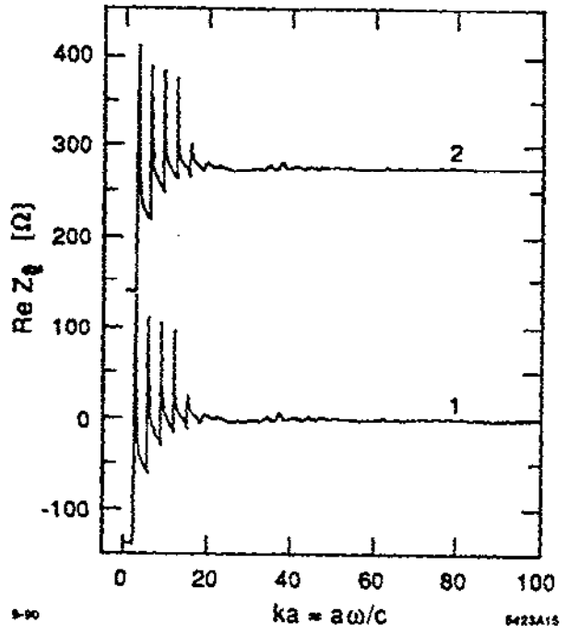

Figure 4.8 The real part of the longitudinal coupling impedance of a cross-section step as a function of parameter $ka = a\omega/c$; $b/a = 0.1$; the matrix size is 60×60; (1) Re Z_{in}, (2) Re Z_{out}.

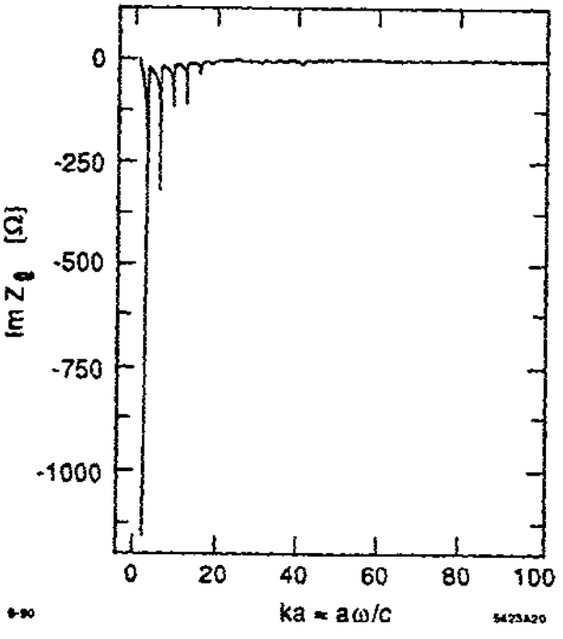

Figure 4.9 The imaginary part of the longitudinal coupling impedance of a step as a function of parameter $ka = a\omega/c$; $b/a = 0.1$; the matrix size is 60×60. The imaginary parts of both Z_{in} and Z_{out} are found to be equal, in agreement with Eq. (3.45).

can be calculated by using the well-known result [78] for the frequency shift due to surface impedance:

$$\omega_n - \omega_{0n} = -\frac{ic}{2} \frac{\int dS\, \zeta_n |\mathbf{H}_n|^2}{\int d\mathbf{S} \cdot \mathbf{r}(|\mathbf{H}_n|^2 - |\mathbf{E}_n|^2)} . \tag{4.36}$$

The same idea that modes in the cavity with a small opening are almost the same as modes in the closed cavity may be utilized for an effective truncation of the exact system of equations obtained above. To obtain a set of equations suitable for the perturbation solution, we exclude coefficients x_n and z_n from Eq. (4.23) and make the following substitution:

$$y_n = i(d_n^+ + d_n^-)\ e^{i(\mu - \chi_n)} , \tag{4.37}$$

$$t_n = i(d_n^+ - d_n^-)\ e^{-i(\mu + \chi_n)} , \tag{4.38}$$

where $\chi_n = g\lambda_{bn}/2$, with λ_{bn} defined in Eq. (4.17), and $\mu = gk/2$. Such substitution corresponds to decomposition of the field into standing waves. Coefficients $d_n^{\pm}$ are amplitudes of the longitudinal even (cosine-like) and odd (sine-like) modes. They satisfy two separate systems of equations:

$$d_n^+ = \frac{i}{\sin\chi_n} \left[P_n \sin\mu + \frac{1}{2} \sum_m T_{mn}\, d_m^+ \cos\chi_m \right] , \tag{4.39}$$

and

$$d_n^- = \frac{i}{\cos\chi_n} \left[P_n \cos\mu - \frac{1}{2} \sum_m T_{mn}\, d_m^- \sin\chi_m \right] . \tag{4.40}$$

The coefficients T_{nm} and P_n are defined as follows:

$$T_{nm} = \frac{4g\nu_m^2}{b\chi_n} \left(\frac{a}{b}\right)^4 \frac{J_0(\nu_n a/b)\ J_0(\nu_m a/b)}{J_1^2(\nu_n)}\, \sigma_{nm} , \tag{4.41}$$

where

$$\sigma_{nm} = \sum_l \frac{\sqrt{(ka)^2 - \nu_l^2}}{[\nu_l^2 - (\nu_n a/b)^2]\ [\nu_l^2 - (\nu_m a/b)^2]} , \tag{4.42}$$

and

$$P_n = (g/2b\chi_n)\ J_0(\nu_n a/b)/2\nu_n^2\ J_1^2(\nu_n) . \tag{4.43}$$

For the impedance in terms of d_n^+ and d_n^- we have

$$Z(\omega) = -\frac{Z_0}{\pi} \frac{g}{b} \sum_n \nu_n^2\ J_0(\nu_n a/b)$$

$$\times \left[(d_n^+ + d_n^-) \frac{\sin(\mu - \chi_n)}{(\mu - \chi_n)} + (d_n^+ - d_n^-) \frac{\sin(\mu + \chi_n)}{(\mu + \chi_n)} \right] . \tag{4.44}$$

The concept of narrow-band impedance presumes that the openings are small compared to the cavity surface. In this case, the field pattern inside the

cavity is expected to be perturbed only slightly by the presence of the side tubes, and to be similar to that of the closed cavity [24]. Therefore, in the vicinity of the eigenfrequencies of the unperturbed cavity for which

$$\sin\chi_n \approx 0\ , \qquad \chi_n \approx \chi^0_{nm} = m\pi\ , \qquad \text{for } n \text{ even}\ , \tag{4.45}$$

and

$$\cos\chi_n \approx 0\ , \qquad \chi_n \approx \chi^0_{nm} = (m+1/2)\pi\ , \qquad \text{for } n \text{ odd}\ , \tag{4.46}$$

only diagonal modes $d^{\pm}_n$ need be retained in the sums in Eqs. (4.39) and (4.40). This gives

$$d^+_n = \frac{iP_n \sin\mu}{\sin\chi_n + \frac{i}{2}\,T_{nn}\cos\chi_n}\ , \tag{4.47}$$

and

$$d^-_n = \frac{iP_n \cos\mu}{\cos\chi_n - \frac{i}{2}\,T_{nn}\sin\chi_n}\ . \tag{4.48}$$

Other amplitudes $d^{\pm}_l$, where $l \neq n$, describe the mixing of the modes of a closed cavity and are zero in this approximation. This approximation can be refined, however, by substituting Eqs. (4.47) and (4.48) into the right-hand side of Eqs. (4.39) and (4.40). This will give $d^{\pm}_m \neq 0$. Repeating the substitution further refines the approximation.

Equations (4.47) and (4.48) have the typical resonance structure with width γ_{nm} and frequency ω_{nm} of the resonance given by

$$\gamma_{nm} = \frac{4c^2\chi^0_{nm}}{g^2\omega_{nm}}\,T_{nn}\ , \qquad \omega_{nm} = c\sqrt{\frac{\nu_n^2}{b^2} + \frac{4\pi^2m^2}{g^2}}\ . \tag{4.49}$$

From this follows the estimate of the external Q-factor: $Q = 2\gamma_{nm}/\omega_{nm}$. The expression on the right-hand side of the first part of Eq. (4.49) is simply the ratio of the energy flow W_{nm} of the mode labeled n,m (which is given by the integral of the Poynting vector over the cross section of the pipe) to the energy W_{nl} stored in this mode:

$$\gamma_{nm} = -\frac{\dot{W}_{nm}}{W_{nm}}\ . \tag{4.50}$$

The loss factor κ^l_{nm} [cf. Eq. (2.10)] for a mode (n,m) can be found from Eq. (4.44) and Eqs. (4.47) and (4.48). For a mode $\chi_n = m\pi$, it is

$$\kappa^l_{nm} = \frac{16}{g}\,\frac{J_0^2(\nu a/b)}{\nu^2 J_1^2(\nu)}\,\sin^2\frac{\omega_{nm}g}{2c}\ , \tag{4.51}$$

and for a mode $\chi_n = (m+1/2)\pi$, it is

$$\kappa^l_{nm} = \frac{16}{g}\,\frac{J_0^2(\nu a/b)}{\nu^2 J_1^2(\nu)}\,\cos^2\frac{\omega_{nm}g}{2c}\ . \tag{4.52}$$

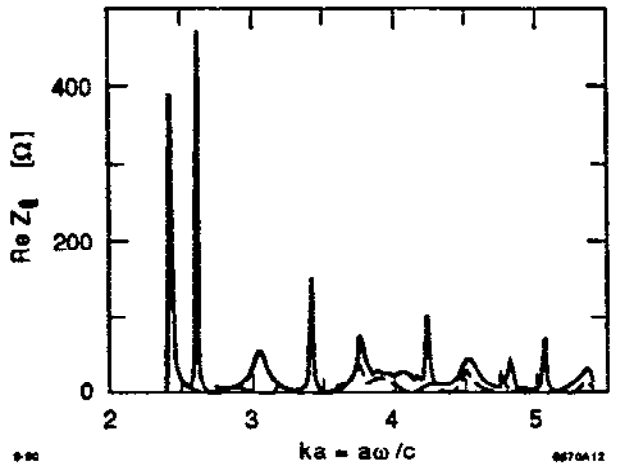

Figure 4.10. The real part of the impedance according to the perturbation model. A single mode nearest to ka is taken into account; $a/b = 0.318$, $g/2b = 0.600$ (the solid line). The dashed line gives the contribution of the nonresonant modes (see text).

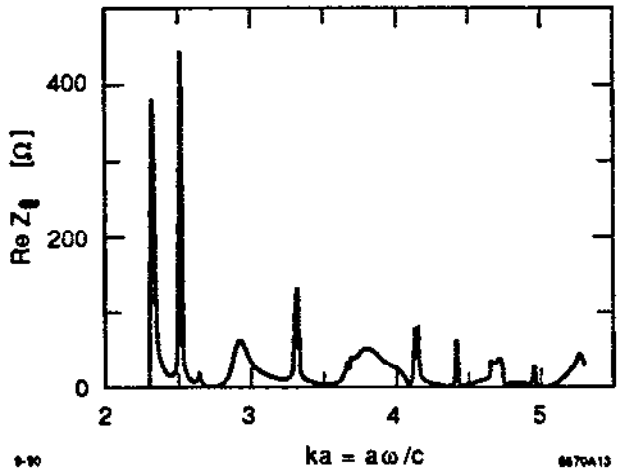

Figure 4.11
The real part of the impedance obtained by truncating the system of equations; $a/b = 0.318$, $g/2b = 0.600$.

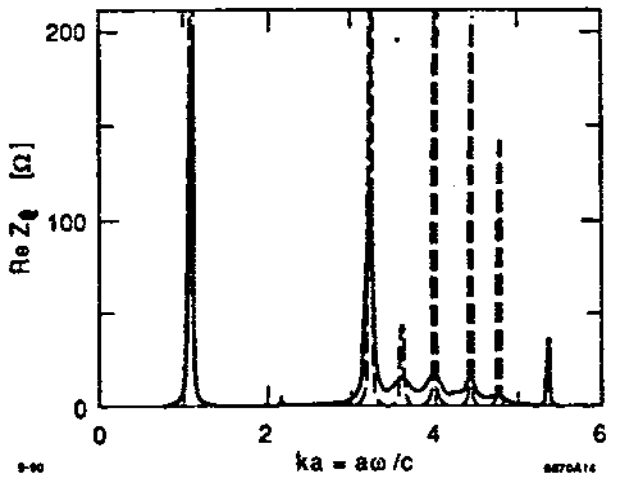

Figure 4.12
The broadening of the higher resonances due to radiation; solid line, loaded Q; dashed line, unloaded Q_0.

In calculating the longitudinal impedance, it is instructive to compare two approximate methods with each other and with purely numerical methods. The solid line in Fig. 4.10 [43] represents the real part of the longitudinal impedance Re $Z(ka)$ obtained from Eq. (4.44) by the following procedure. For a given frequency, we find the number n_0 of the nearest resonance that satisfies Eqs. (4.45) or (4.46). Then we calculate the impedance, retaining in Eq. (4.44) a single term with the number n_0 while the coefficients $d_n^{\pm}$ are defined by Eqs. (4.47) and (4.48). The dashed line gives the contribution of the nonresonant modes in some band $\pm\Delta n$ around the resonance. The parameters used are $a/b = 0.318$ and $g/2b = 0.600$. Figure 4.11 shows for comparison the real part of the impedance calculated by truncating the set Eqs. (4.39) and (4.40). In this example, the width of the band was $\Delta n = 10$ (in total, 20 equations were retained). The agreement between the results shown in Figs. 4.10 and 4.11 could be even better if, instead of one, the two nearest resonance modes were retained in Eqs. (4.39) and (4.40). The broadening of the resonance obtained by the perturbation method for the CEBAF cavity is illustrated in Fig. 4.12. The real part of the impedance

$$\text{Re } Z(\omega) = \sum_n \left[\frac{\kappa_n \gamma_n}{(\omega - k_n c)^2 + \gamma_n^2} + \frac{\kappa_n \gamma_n}{(\omega + k_n c)^2 + \gamma_n^2} \right] \qquad (4.53)$$

is shown here (solid line). The loss parameters κ_n and frequencies ω_n were calculated with the help of the program URMEL [121]. The widths γ_n (related to the external Q-factor) were calculated as defined in Eq. (4.49). The dashed line gives the impedance calculated with the widths caused by the finite conductivity of the walls (unloaded Q_0).

It is worth mentioning a calculation by Sands [100]—closely related to the subject of the present paper—which gives the low-frequency radiation from a small hole in a vacuum chamber. Sands' derivation is based on the perturbative analytical solution obtained by Bethe [9].

E. Trapped modes

Trapped modes are narrow resonances observed above the cutoff frequency both in experiments [28] and in numerical calculations [41]. Their field pattern corresponds to modes localized within a cavity with a relatively large Q-factor. A trapped mode of the pillbox cavity with side tubes can be seen in Fig. 4.11 as a small spike near $ka \approx 4.5$. Its amplitude is actually much higher than appears in Fig. 4.11 if plotted with higher resolution.

Calculations for different tube lengths using URMEL confirmed the existence of a trapped mode for a cavity with parameters $a/b = 0.318$, $g/2b = 0.600$. For the mode with frequency $f \approx 233.3$ MHz, which corresponds to $ka \approx 4.5$, the field outside the cavity goes rapidly to zero, thus conforming to the definition of trapped modes. The ratio R/Q for this mode is unusually small.

The origin of trapped modes is unclear. Several explanations have been suggested. One maintains that the sharp edges of the cavities can cause multiple reflection of a wave and, as a result, give a long decay time to the mode. This explanation seems unsatisfactory, because above the cutoff frequency the reflection rate is relatively small, even for the sharp edges. If the edges are rounded off,

the reflection rate goes rapidly to zero. The reflection rate becomes exponentially small when the function describing the edge boundary and its derivatives all are continuous.

Another hypothesis is that certain modes of a cavity produce waves in the tube that cancel each other. This assumption is probably also unsatisfactory if the modes are to be understood as those of a closed cavity unperturbed by the beam pipe openings [41].

A trapped mode may occur, however, if two degenerate modes of the closed cavity are mixed by the perturbation due to the pipe openings. One of the mixed modes may become a trapped mode.

This idea was studied on a mode corresponding to $ka = 4.5$. The mode was chosen because at the frequency $ka = 4.5$ there is only one wave that can propagate in the tube. This wave is generated mostly by the coupling of the two degenerate modes in the cavity. The degree of degeneracy of the modes can be varied by changing the parameters of the cavity. The analytical and numerical analysis supports the hypothesis of the connection between the mode degeneracy and the existence of the trapped modes. In particular, with the code URMEL it is shown that the mode remains trapped in a wide range of the cavity parameters, provided that the mode degeneracy is maintained.

F. The narrow-band impedance of bellows

Consider axially symmetric and longitudinally smooth periodic variations of a wall of a waveguide commonly known as *bellows*. Fig. 4.13 illustrates the geometry and the coordinate system. In this case application of the field-matching technique used in previous sections is very difficult. A more appropriate method for such cases will be described here. In general, all the Fourier harmonics of the polar angle θ, i.e. *modes* characterized by the number m, exist. However, our considerations will be restricted to an axial symmetric mode $m = 0$ and only the longitudinal impedance will be derived. The transverse impedance for the dipole mode $m = 1$ has been obtained [72].

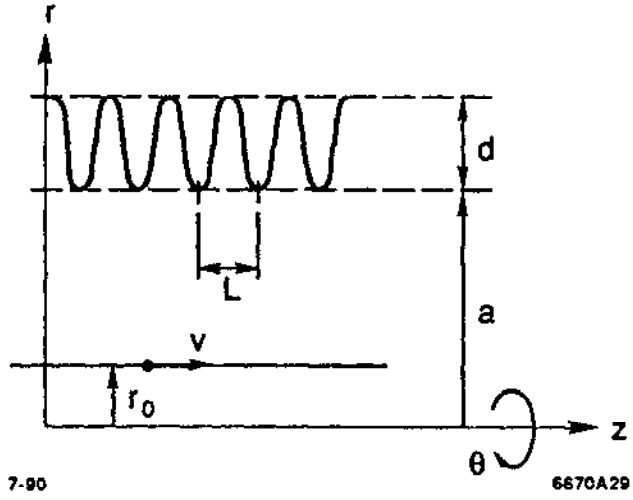

Figure 4.13
Geometry of bellows and the coordinate system.

Let us assume that the waveguide wall in the plane $\theta = constant$ is described by the function

$$r = r_b(z) , \tag{4.54}$$

which is periodic in z with period L. If the source particle moves along the axis of the waveguide, $r_0 = 0$, only the axial symmetric modes $m = 0$ are excited. The series that gives the general solution of the Maxwell equations suitable for this case is given by Krinsky and Gluckstern [75]. The expansions of the longitudinal and radial components of the electric field with unknown coefficients B_p in the limit $\gamma \to \infty$ are

$$E_{\omega z} = \frac{iq}{\pi ca} e^{ikz} \sum_{p=-\infty}^{\infty} B_p \, e^{2i\pi pz/L} \, \frac{I_0(\alpha_p r/a)}{I_0(\alpha_p)} , \tag{4.55}$$

$$E_{\omega r} = \frac{q}{\pi ca} e^{ikz} \left(\frac{a}{r} + \sum_{p=-\infty}^{\infty} B_p \, e^{2i\pi pz/L} \, (ka + 2\pi ap/L) \, \frac{I_1(\alpha_p r/a)}{\alpha_p I_0(\alpha_p)} \right), \tag{4.56}$$

where I_0 and I_1 are modified Bessel functions of the first kind of the zeroth and first order, respectively. The quantity α_p is defined by

$$\alpha_p^2 = \left(\frac{2\pi ap}{L} \right)^2 + 4\pi kap \, \frac{a}{L} . \tag{4.57}$$

The expansion coefficients B_p in this case are defined by the boundary condition [75]

$$E_{\omega z}(r_b, z) = -E_{\omega r}(r_b, z) dr_b/dz , \tag{4.58}$$

which leads to the following infinite set of linear algebraic equations:

$$\sum_{p=-\infty}^{\infty} M_{np} B_p = N_n , \qquad n = -\infty \ldots \infty , \tag{4.59}$$

where

$$M_{np} = \begin{cases} \left\langle \left[1 - \frac{i}{2} \, kr_b(z) \frac{dr_b}{dz} \right] \exp\left(-\frac{2i\pi nz}{L} \right) \right\rangle & p = 0 , \\ \left[\left(\frac{2\pi a}{L} \right)^2 pn + \left(\frac{2\pi a}{L} \right) ka(p+n) \right] \left\langle \frac{I_0(\alpha_p r_b(z)/a)}{\alpha_p^2 I_0(\alpha_p)} \exp\left[-\frac{2i\pi(n-p)z}{L} \right] \right\rangle & p \neq 0 , \end{cases} \tag{4.60}$$

and

$$N_n = \frac{2i\pi a}{L} \left\langle \frac{a}{r_b} \frac{dr_b(z)}{dz} \exp\left(-\frac{2i\pi nz}{L} \right) \right\rangle . \tag{4.61}$$

Here the brackets $\langle f \rangle$ are used to define the value of function $f(u)$ averaged over its period L. The longitudinal impedance per one period of bellows can be found by using Eq. (2.5):

$$Z_l(k) = -iZ_0 L B_0(k)/2\pi a . \tag{4.62}$$

The system of Eqs. (4.59) can be solved numerically. The computer code IMPASS (Impedances of Periodic Axially-Symmetric Smooth Structures [66]) enables one to calculate coefficients of the field expansions and to find both the longitudinal and the transverse impedances for $m = 0$ and $m = 1$ in the low-frequency region. The approach used here is not valid for the high-frequency region, where the impedance has a very complicated resonance structure.

Figure 4.14 [66] presents the coefficient B_0 found with the help of IMPASS as a function of the normalized frequency ka for three different values of bellows parameter $2\pi a/L$ and for the relative depth of the corrugations $d/2a = 0.09$. More results are given by Kheifets and Zotter [72].

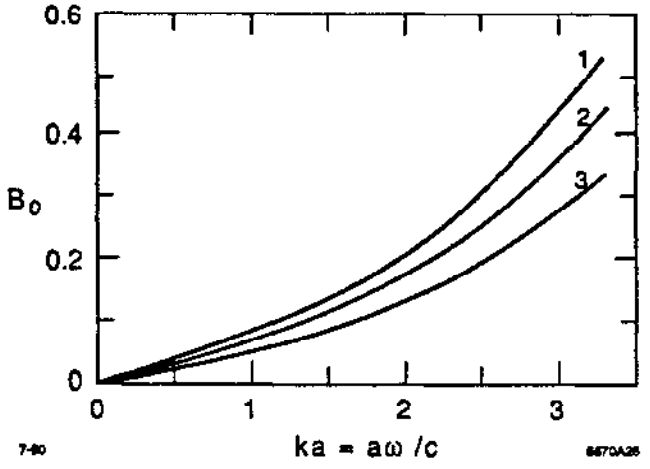

Figure 4.14 Coefficient B_0 which defines the longitudinal impedance of bellows, cf. Eq. (4.62), for bellows with the boundary defined by

$$r_b(z) = a(1 + \epsilon + \frac{4\epsilon}{\pi} \cos \frac{2\pi z}{L})$$

as a function of parameter ka for three values of the parameter $\eta = 2\pi a/L$: (1) η=31.42, (2) η=20.94, (3) η=12.57. The depth of corrugations is defined by $\epsilon \equiv d/2a$=0.09.

V. A DIFFRACTION MODEL FOR THE HIGH-FREQUENCY IMPEDANCE

Here we develop an approximate method that is suitable for studying the high-frequency behavior of the impedance. The integral equation that is equivalent to Maxwell's equations is solved by iteration using approximate boundary conditions [42,89]. This approach is very close to the diffraction models discussed by Bane and Sands [6,7] and by Palmer [90,92,93].

In Section V.A we define appropriate boundary conditions for the first iteration and study the implication of such a selection for a number of cases. In the next approximation the field on the boundary is assumed to be the field obtained

on the previous step. For some structures—such as an array of irises—for which the interference of waves diffracted on different irises is important, the correct answer may be easily found by such a method (Section V.D). For other structures—such as a taper—for which no solution is known, the method gives an estimate of the impedance (Section V.E).

A. A method of iteration

Consider an arbitrary metal structure with openings. Let its volume be bounded by the surface S. The total field inside the volume excited by a relativistic particle is the sum of its synchronous field and the radiated field $\mathbf{E}_\omega, \mathbf{H}_\omega$. The radiated field satisfies the homogeneous wave equation and its value inside the volume is defined by the fields on its inner surface [57]:

$$\mathbf{E}_\omega = \int dS' \, [ik(\mathbf{n}' \times \mathbf{H}'_\omega) \, G_k + (\mathbf{n}' \cdot \mathbf{E}'_\omega) \cdot \nabla' G_k + (\mathbf{n}' \times \mathbf{E}'_\omega) \times \nabla' G_k] \, , \quad (5.1)$$

$$\mathbf{H}_\omega = \int dS' \, [-ik(\mathbf{n}' \times \mathbf{E}'_\omega) \, G_k + (\mathbf{n}' \cdot \mathbf{H}'_\omega) \cdot \nabla' G_k + (\mathbf{n}' \times \mathbf{H}'_\omega) \times \nabla' G_k] \, , \quad (5.2)$$

where $\mathbf{n}'$ is the unit vector normal to the surface pointed inside the volume and

$$G_k(\mathbf{r}, \mathbf{r}') = \frac{e^{ikR}}{4\pi R} \, , \qquad R = |\mathbf{r} - \mathbf{r}'| = \sqrt{(z - z')^2 + r^2 + r'^{\,2} - 2rr' \, \cos\theta} \, , \quad (5.3)$$

is the Green's function of the wave equation. It satisfies the equation

$$(\nabla^2 + k^2) \, G_k = -\delta(\mathbf{r} - \mathbf{r}') \, .$$

In Eqs. (5.1) and (5.2) the derivatives in expression $\nabla' G_k$ are taken with respect to $\mathbf{r}'$.

For $k > 0$ the function can also be represented in the equivalent form

$$G_k(\mathbf{r}, \mathbf{r}') = \frac{i}{8\pi} \int_{-\infty}^{\infty} dp \;\; e^{ip(z - z')} \;\; \hat{G}_{kp}(r, r') \, , \quad (5.4)$$

where

$$\hat{G}_{kp}(r, r') \equiv \begin{cases} \sum_{m=0}^{\infty} \; A_m J_m(\Omega r) \; H_m^{(1)}(\Omega r') \; \cos m\theta & \text{for} \;\; r' > r \, , \\ \sum_{m=0}^{\infty} \; A_m J_m(\Omega r') \; H_m^{(1)}(\Omega r) \; \cos m\theta & \text{for} \;\; r' < r \, . \end{cases} \quad (5.5)$$

Here $A_m = 1$ for $m = 0$, $A_m = 2$ for all other m, and J_m and $H_m^{(1)}$ are the Bessel and the Hankel functions of order m, respectively. Function $\Omega(k, p)$ has a cut along the negative axis in the plane of its argument p. We define it as

$$\Omega = \sqrt{k^2 - p^2 + 2ik\varepsilon} \, , \qquad \varepsilon \to 0 \, .$$

Correspondingly, functions $H_m^{(1)}$ of the purely imaginary argument ix are defined as $H_m^{(1)}(ix) = 2(-i)^{m+1} K_m(x)/\pi$ [38]. For $k < 0$, G_k is defined by $G_k = G^*_{-k}$.

Consider now the azimuthally symmetric structure with a particle traveling along its z axis with the velocity of light. Let the metal wall of the pipe be described by $r = r_b(z)$. In this case it is sufficient to consider only the monopole modes $m = 0$. The method can also be extended to a general case $m \neq 0$.

The system of integral equations (5.1) and (5.2) can be solved approximately by the method of iteration. The field on the boundary chosen on the first iteration defines the field on all the successive steps. The choice of the field for the first iteration is crucial for the convergence of the solution.

To define the field on the surface of a pipe of arbitrary shape, let us first consider the situation in a straight pipe, $r_b = a = constant$. The EM field is the sum of the field of the particle in free space and the field of the image current in the wall (or the induced field). In the ultrarelativistic case, the electric field of a *particle* $\mathbf{E}_\omega^{(0)}$ has a large radial component (i.e. normal to the beam pipe wall) and a small longitudinal (tangential) component. The longitudinal component induces an image current in the wall. Since the image current has only a tangential component, it produces only a small tangential component of the *induced* field $\mathbf{E}_\omega^{(1)}$, which compensates for the tangential component of the particle field. The normal component of the induced electric field $E_{\omega n}^{(1)}$ and the tangential (azimuthal) component of the induced magnetic field $H_{\omega t}^{(1)}$ are zero on the pipe wall.

We now conjecture that in the high-frequency limit in the first approximation the boundary conditions for the *radiated* field in a pipe with a variable shape $r = r_b(z)$ are locally similar to those for a smooth pipe $a = constant$. The necessary condition for this assumption to be valid is that the length L of variation of the pipe shape, $dr_b/dz \approx a/L$, has to be large compared to the typical wavelength λ:

$$L \gg 1/k \, .$$

In other words, the assumption is that in the high-frequency limit in the first approximation the boundary condition for the normal component of the *radiated* electric field is zero on any conductive boundary, as it is for a smooth pipe, i.e.

$$E_{\omega n}^{(1)} = 0 \qquad \text{for } \; r = a(z-0) \, . \tag{5.6}$$

At the same time, the sum of the tangential component of the synchronous field of a particle $E_{t\omega}^{(0)}$ and the tangential component of the radiated field $E_{t\omega}^{(1)}$ on the metallic surface has to be zero:

$$E_{t\omega}^{(1)} = -E_{t\omega}^{(0)} \qquad \text{for } \; r = a(z-0) \, . \tag{5.7}$$

Hence, the components of the radiated field on the conductive boundaries are

$$E_{r\omega}^{(1)} = -E_{t\omega}^{(0)} \, \sin\alpha \, , \qquad E_{z\omega}^{(1)} = -E_{t\omega}^{(0)} \, \cos\alpha \, , \tag{5.8}$$

where

$$E_{t\omega}^{(0)} = E_{r\omega}^{(0)} \, \sin\alpha + E_{z\omega}^{(0)} \, \cos\alpha \, . \tag{5.9}$$

Here $E_{r\omega}^{(0)}$ is given in Eq. (2.27) and $E_{z\omega}^{(0)} \approx 0$. The angle $\alpha = \alpha(z)$ is defined by $\tan\alpha = dr_b(z)/dz$.

The magnetic field in the azimuthally symmetric case has only an azimuthal component $H_{\theta\omega}$. It can be shown [42] that from Eq. (5.6) follows

$$H^{(1)}_{\omega\theta} = 0 \qquad \text{for } r = a(z-0)\,. \tag{5.10}$$

The radiated field on the cross sections $z = 0$ and $z = g$ is the same as that in a straight pipe. This means that for the azimuthally symmetric mode $m = 0$, the radiated field is zero. Equations (5.8) and (5.10) specify the field on the boundary for the first iteration.

Equation (5.1) together with the radiation condition at infinity gives the component $E^{(1)}_z$ inside the pipe as the surface integral over the *metallic* walls of the pipe:

$$E^{(1)}_z = \int dS' \, \frac{\partial G_k}{\partial r'} \, E^{(0)}_t(r', z')\,. \tag{5.11}$$

For a smooth pipe $r_b(z) = a$, $dS = 2\pi a dz$, and $E^{(0)}_t$ is defined in Eq. (5.9). In this case Eq. (5.11) gives

$$E^{(1)}_z = \frac{2iq\tau^2}{\omega} \, I_0(\tau r) \, K_0(\tau a) \, e^{ikz}\,, \qquad \beta \approx 1\,, \tag{5.12}$$

which agrees with the exact solution for a straight pipe given by the first term in Eq. (4.5). Note that in this approximation $I_0(\tau a) \approx 1$.

Equation (5.1) may be used to find the radiated field in a cavity iteratively. The field in the cavity found in the first approximation defines the radiated field on the boundaries, including beam pipe openings. It may be taken as the value of the field on the boundary for the next iteration. The series obtained in this way are analogous to the Born's series of scattering theory. The expansion parameter of the series is the ratio of the amplitude of the tangential component of the radiated field $E^{(1)}_t$ to the amplitude of the tangential component of the particle field in Eq. (2.27). Note that the first approximation allows one to estimate this parameter and find the amplitude of the diffracted waves in the side pipes.

This method is next used to evaluate the impedance of a pillbox cavity with side pipes.

B. A diffraction model for a cavity

Consider a pillbox cavity of length g, and radius b, with side pipes of radius a. The surface integral Eq. (5.1) for this geometry is the sum of two integrals. The first integral, and the main contribution to the sum, is over the sides of the cavity at $z = 0$ and $z = g$ for $a < r < b$. This is given by Eq. (5.11) with $E^{(0)}_t$ defined in Eq. (2.27). The second integral is over the cylindrical wall $r = b$for $0 < z < g$, which gives a negligibly small contribution of order $(1/\gamma)^2$. Similar considerations are used by Gluckstern and Neri [34-36] to obtain the narrow-band longitudinal impedance above the cutoff frequency of the beam pipe.

For the region $0 < r < a$,

$$E_{\omega z}^{(1)}(r,z) = \frac{iq}{2c} \int_{-\infty}^{\infty} dp \;\; e^{ipz} \left[1 - e^{i(k-p)g}\right] \;\; J_0(\Omega r) \left[H_0^{(1)}(\Omega b) - H_0^{(1)}(\Omega a)\right] . \quad (5.13)$$

This expression gives the first approximation for the diffracted field inside the cavity. Hence, to find the impedance as defined in Eq. (2.5), we have to choose the path of integration along the beam pipe wall $r = a$ in accordance with the discussion in Section III.B [120]. Since on the pipe wall outside the cavity $E_{\omega z}(a,z) = 0$, the range of integration in Eq. (2.5) is $0 < z < g$. For $k > 0$, we therefore have

$$Z_l(k) = \frac{Z_0}{2\pi} \int_{-\infty}^{\infty} \frac{dp}{k-p} \;\; J_0(\Omega a) \left[H_0^{(1)}(\Omega a) - H_0^{(1)}(\Omega b)\right] \sin^2 \frac{g}{2} (k-p) . \quad (5.14)$$

An estimate of the integral in Eq. (5.14) is obtained by Heifets [46]. For the region of parameters where $g \ll ka^2$ (a cavity regime), it reproduces the Lawson-Dôme formula [24,80]:

$$Z_{\mathrm{cav}}(k) = (1+i) \frac{Z_0}{2\pi a} \sqrt{\frac{g}{k\pi}} . \quad (5.15)$$

For the region of parameters where $ka^2 \ll g \ll kb^2$, there is a transition regime

$$Z_{\mathrm{trans}}(k) = \frac{Z_0}{2\pi} \;\; \ln \frac{g}{ka^2} , \quad (5.16)$$

and for the region of parameters where $g \gg kb^2$, one obtains the impedance of a step found by Balakin and Novokhatski [1] and independently by Kheifets [63], cf. Eq. (6.79):

$$Z_S(k) = \frac{Z_0}{\pi} \;\; \ln \frac{b}{a} . \quad (5.17)$$

The difference between the impedances of a cavity, Eq. (5.15), and a step, Eq. (5.17), corresponds to different diffraction regimes. For $g \ll ka^2$ the transverse dimension of the area illuminated by the diffracted wave increases with z as $r \sim \sqrt{2z/k}$, which characterizes Fresnel diffraction. For larger g for which $r \sim z/ka$, Fraunhofer diffraction occurs.

The real part Re $Z_l(k)$ of Eq. (5.14) is produced by the values p in the range $-k < p < k$:

$$\mathrm{Re}\; Z_l(k) = \frac{Z_0}{2\pi} \int_{-k}^{k} \frac{dq}{k-p} \; J_0(\Omega a) \left[J_0(\Omega a) - J_0(\Omega b)\right] \; \sin^2 \; \frac{g}{2} (k-p) . \quad (5.18)$$

The results of the numerical integration of Eq. (5.18) are shown in Fig. 5.1 [42], together with the estimate, Eqs. (5.15) and (5.17). According to these calcu-

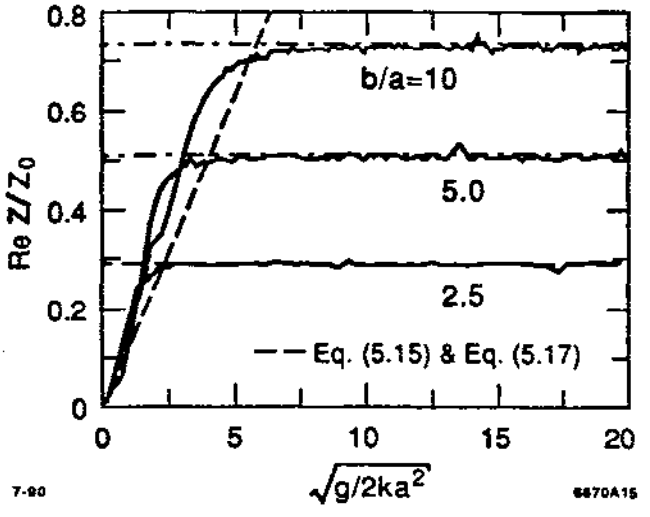

Figure 5.1
The transition from a cavity regime to a step regime.

lations, the transition from the cavity to the step regime occurs for values of the cavity parameters such that

$$\eta = \frac{g}{k(b-a)^2} \approx 1 \ . \tag{5.19}$$

Let us now evaluate the radial component of the radiated field $E_r^{(1)}$. It can be derived from Eq. (5.1), where the surface integral has to be taken over the surfaces $z = 0$ and $z = g$, for $a < r < b$. In the high-frequency region $ka \gg 1$, neglecting terms of order of $1/ka$, we obtain

$$E_{\omega r}^{(1)}(r,z) \ = \ \frac{q}{2\pi c} \sum_{n=1}^{2} (z - z_n) \ \exp[ikz_n]$$

$$\times \int_0^{2\pi} d\theta \left[\frac{\exp[ikR_n(a)]}{(a - r\cos\theta)\ R_n(a)} - \frac{\exp[ikR_n(b)]}{(b - r\cos\theta)\ R_n(b)} \right] , \tag{5.20}$$

where $R_n^2(x) = r^2 + x^2 - 2rx\cos\theta + (z - z_n)^2$, $n = 1, 2$, and the summation is performed over two waves radiated from the surfaces $z_1 = 0$ and $z_2 = g$. It is easy to see that the wave radiated from the surface $z = 0$ does not contribute to $E_r^{(1)}$ at $z = 0$. Only the wave scattered from the other surface changes the field in the next approximation. This is similar to the situation in scattering theory. The phase of this wave is proportional to the wave vector k and is large for $kg \gg 1$, giving, on average, a small correction. $E_{\omega r}^{(1)}(r,z)$ has a singularity $(r-a)^{-1/2}$ at $r = a$ as is well known [108]. Note that, at least in this approximation, similar singularity appears also at $r = b$. These singularities leave the field energy finite. They are not essential in evaluating the integral in Eq. (5.1).

C. Loss factors in the diffraction model

The total impedance of the accelerator vacuum chamber is usually approximated by the sum of the impedances of its elements. This is equivalent to calculating the impedance of a given element while neglecting the diffracted EM field arising from all the other elements. In general this is incorrect. The interference of the EM field generated on different elements can be important. This will be illustrated below for an array of cavities. But, even neglecting the interference, the estimate of the impedance of a given element is not a simple task, especially for the high-frequency impedance.

Fortunately, in most cases an element can be represented either as a pillbox cavity with the beam pipes or as an abrupt change of the beam pipe radius. The second structure (a step) can be considered as a very long cavity. The estimates of the impedances for these two types of structures [12] according to the diffraction model discussed above give the correct dependence on all the physical parameters. This was verified by numerical calculations using the code TBCI over a wide range of parameters. The results are also valid for a very short bunch where direct numerical calculations require too much computing time and computer memory.

The high-frequency longitudinal impedance of a pillbox cavity with gap g, radius b, and side pipes of radii a, which is valid for $ka \gg 1$, is given by Eq. (5.15). The impedance falls off as $k^{-1/2}$ in agreement with the results of Lawson [80, 81] and Dôme [24]. For a short Gaussian bunch, for which $\sigma \ll a$, this high-frequency tail of the impedance gives the main contribution to the energy loss for a cavity:

$$\kappa^{l}_{\mathrm{cav}}(\sigma) = \frac{\Gamma(1/4)}{\pi a}\sqrt{\frac{g}{\pi\sigma}}\,, \qquad \frac{\Gamma(1/4)}{\pi} = 1.154\,. \tag{5.21}$$

Equation (5.21) has been checked by TBCI calculations for three different sets of parameters of CEBAF rf structures: (a) the fundamental power coupler, $a = 3.5$ cm, $g = 2.5$ cm, $b = 5.5$ cm; (b) the higher-order mode coupler, $a = 3.75$ cm, $g = 3.75$ cm, $b = 5.5$ cm; and (c) the gate valve $a = 1.75$ cm, $g = 2$ cm, $b = 3.5$ cm. The rms length of the bunch σ was varied over the range 0.75 to 1.5 mm. The observed agreement is within 10%; see Fig. 5.2 [12].

The transverse impedance can be estimated from the longitudinal impedance of the dipole mode by using the Panofsky-Wenzel theorem (see Section III.A). The estimate for the transverse loss factor is

$$\kappa^{\perp}_{\mathrm{cav}}(\sigma) = \frac{\sqrt{\pi g\sigma}}{a^3}\,. \tag{5.22}$$

This formula also agrees well with the results obtained by the code TBCI; see Fig. 5.3 [12]. For a very long cavity (a step), Eq. (5.21) is not applicable. The longitudinal impedance of a step is given by Eq. (5.17). Note that the frequency-

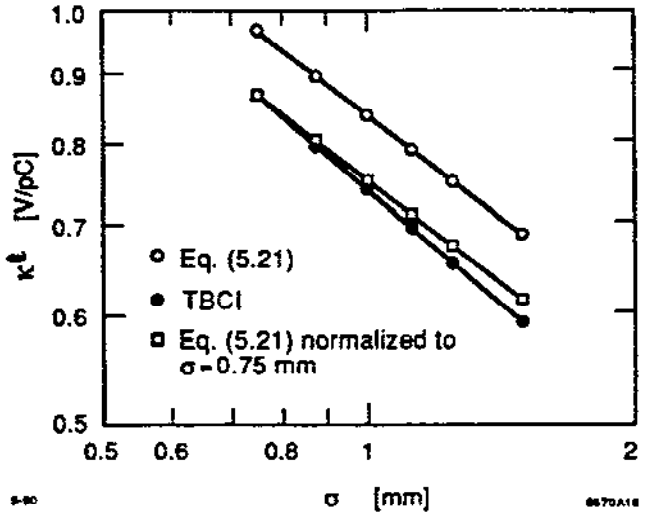

Figure 5.2 The longitudinal loss factor as a function of the rms bunch length; $a = 3.5$ cm, $b = 5.5$ cm, $g = 2.5$ cm.

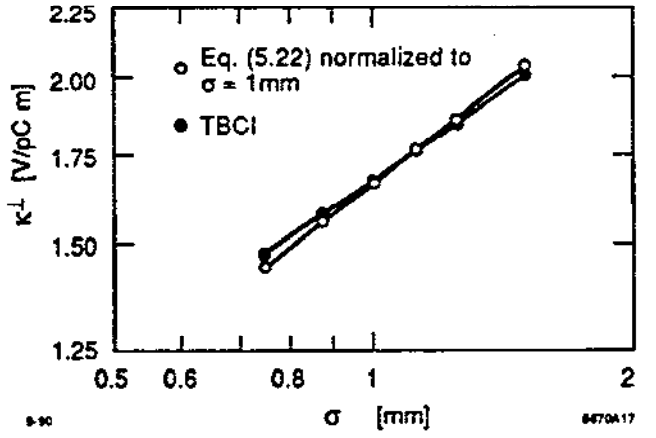

Figure 5.3 The transverse loss factor (kick) as a function of the rms bunch length; $a = 3.5$ cm, $b = 5.5$ cm, $g = 2.5$ cm.

independent impedance corresponds to a point wake function which is proportional to a δ function. The longitudinal loss factor for a step is

$$\kappa_S^l(\sigma) = \frac{2}{\sqrt{\pi}\sigma} \ln\frac{b}{a} . \tag{5.23}$$

The exact expression for the transverse loss factor of a step is unknown. Bisognano *et al.* [12] obtained the following estimate:

$$\kappa_S^\perp(\sigma) = \frac{2}{\sqrt{\pi a^2}} \ln\frac{b}{a} \ln\frac{b}{\sigma} . \tag{5.24}$$

These formulae contain both radii a and b, in contrast to Eqs. (5.15) and (5.21) for a short cavity. The regime of the cavity differs from the regime of the step in that in the second case the signal from the outer wall of the cavity has enough time to reach a bunch traveling inside it, thus probing the outer radius of the cavity. If the parameter η [cf. Eq. (5.19)] for $k \sim 1/\sigma$

$$\eta \equiv \frac{2g\sigma}{(b-a)^2} \tag{5.25}$$

is small, $\eta \ll 1$, the formulae for a cavity are valid. In the opposite case, when $\eta \gg 1$, the regime of a step is fulfilled. This is illustrated in Fig. 5.4 [12], which shows the dependence of the longitudinal loss factor κ_l on the radius b of the cavity. The longitudinal and transverse loss factors, as functions of the rms bunch length σ, are plotted in Figs. 5.5 and 5.6. In all cases the agreement of the estimates with numerical calculations is quite good. Eqs. (5.21) to (5.25) are convenient for a fast and reasonably accurate estimate of the impedance budget of an accelerator. However, Eq. (5.24) should be considered as an empirical estimate.

D. A periodic array

The EM waves generated in one element of an accelerator propagate into the elements downstream of the system. There the waves interfere with the locally radiated field. Even if the impedance of each element assumed to be mutually independent is known, finding the impedance for the whole system is, in general, nontrivial.

In the high-frequency region, the previously described method of iteration is applicable. As an example of its application, we consider here a periodic structure. For an array of cavities with a large number of cavities, the interference can drastically change the impedance. Another example where the interference is important (two adjacent cavities) is considered by Heifets [42].

Let us consider an rf structure of a linear accelerator. It can be approximated by a periodic array of cavities built of irises in a waveguide. The irises, having equal round beam holes of radius a, are separated by a distance L. In the high energy accelerator the signal reflected from the outer cavity wall does not reach the bunch moving with the velocity of light along the accelerator axis. For simplicity we therefore assume the outer radius to be infinitely large.

The radial component of the radiated field at location z of the accelerator, to good approximation, is the sum of the field Eq. (2.27) and a field of unknown amplitude $f(k,r)$ diffracted on the upstream irises:

$$E_{\omega r}^{(0)}(z,r) = -\frac{2q}{cr}\ e^{ikz/\beta}\ \vartheta(r-a) + \frac{2q}{c}\ f(k,r)\ \ e^{ikz}\ \vartheta(a-r)\ . \tag{5.26}$$

Here $\vartheta(x)$ is a step function. We use this expression as the zeroth approximation for E_t in Eq. (5.1). For the longitudinal field between the irises, $0 < z < L$, Eq. (5.1) yields

$$E_{\omega z}^{(1)}(z,r) \ = \ \frac{iq}{2c}\int\limits_{-\infty}^{\infty} dp\ e^{ipz}\left[1-e^{i(k-p)L}\right]\int\limits_{0}^{\infty} dr'\left[\vartheta(r'-a) - r' f(k,r')\ \vartheta(a-r')\right]$$

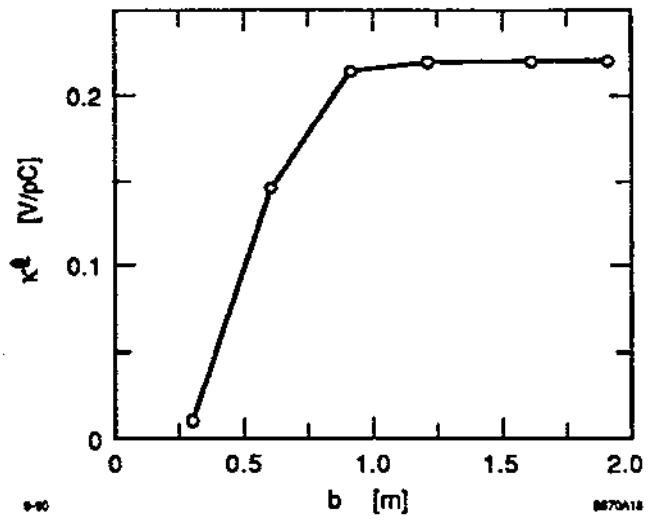

Figure 5.4
The longitudinal loss factor as a function of b; $a = 0.25$ m, $g = 6.0$ m, $\sigma = 0.06$ m.

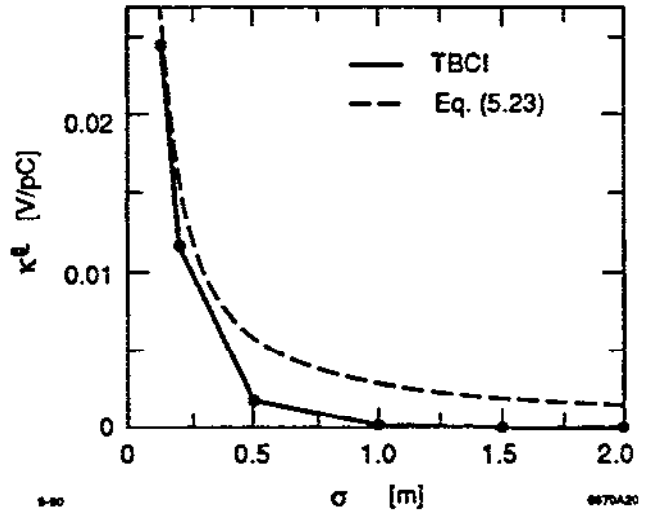

Figure 5.5
The longitudinal loss factor as a function of σ; $a = 1.5$ m, $b = 2.0$ m, $g = 20.0$ m.

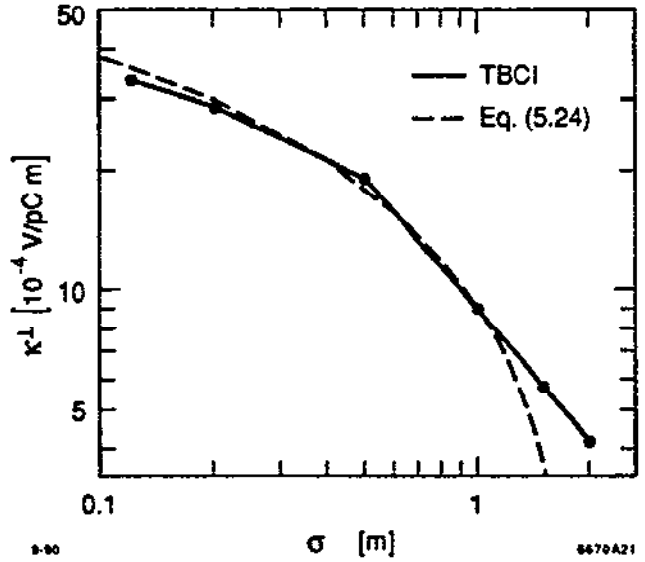

Figure 5.6
The transverse loss factor as a function of σ; $a = 1.5$ m, $b = 2.0$ m, $g = 20.0$ m.

$$\times \frac{\partial}{\partial r'} \left[J_0(\Omega r)\, H_0^{(1)}(\Omega r')\, \vartheta(r'-r) + J_0(\Omega r')\, H_0^{(1)}(\Omega r)\, \vartheta(r-r') \right] , \qquad (5.27)$$

where $\Omega = \sqrt{k^2 - p^2}$. The impedance per cell is

$$Z_l(k) = \frac{Z_0}{2\pi} \int\limits_{-\infty}^{\infty} \frac{dp}{k-p} \sin^2 \frac{L}{2} (k-p)\, J_0(\Omega a)\, H_0^{(1)}(\Omega a)\, [1 + a f(k,a)]$$

$$- \frac{2}{c} \int\limits_{-\infty}^{\infty} \frac{dp}{k-p} \sin^2 \frac{L}{2} (k-p)\, H_0^{(1)}(\Omega a) \int\limits_0^a dr' J_0(\Omega r') \frac{\partial}{\partial r'} r' f(k,r') \, . \qquad (5.28)$$

The first term here is the same as that for a single cavity, as given by Eq. (5.14), except for the additional factor $[1 + af(k,a)]$. We will see that this factor is of order $1/k$. The second term in Eq. (5.28) is small. Hence, the high-frequency impedance of a periodic array becomes $Z_l(k) \propto k^{-3/2}$.

The equation defining function $f(k,r)$ can be obtained from the condition of periodicity for the radial component of the field $E_{\omega r}(z,r)$. The expression for $E_{\omega r}^{(1)}(z,r)$ can be found from the equation $\nabla \cdot \mathbf{E} = 0$ and Eq. (5.27). At $z = L$ this yields

$$E_{\omega r}^{(1)}(L,r) = -\frac{q}{2c} \int\limits_{-\infty}^{\infty} p\, dp\; e^{ipL} \int\limits_0^{\infty} dr' \left[\vartheta(r'-a) - r' f(r')\, \vartheta(a-r') \right]$$

$$\times \left[J_1(\Omega r)\, H_1^{(1)}(\Omega r')\, \vartheta(r'-r) + J_1(\Omega r')\, H_1^{(1)}(\Omega r)\, \vartheta(r-r') \right] . \qquad (5.29)$$

For $f(k,r)$ we thus obtain the following integral equation:

$$f(k,r) = \Phi(r) + \int\limits_0^r r' dr'\; \Psi(r',r)\, f(k,r') + \int\limits_r^a r' dr'\; \Psi(r,r')\, f(k,r') \, , \qquad (5.30)$$

where

$$\Psi(r,r') = \frac{1}{4} \int\limits_{-\infty}^{\infty} p\, dp\; e^{-i(k-p)L}\; J_1(\Omega r)\, H_1^{(1)}(\Omega r') \, , \qquad (5.31)$$

and

$$\Phi(r) = -\int\limits_a^b dr'\; \Psi(r,r') \, . \qquad (5.32)$$

Note that $f(k,0) = 0$.

Function $\Psi(r,r')$ describes the Fresnel diffraction on a circular hole. An estimate of the integral in Eq. (5.31) in the diffraction zone $r \simeq a$, $r'-r \gg \sqrt{2L/k}$ gives

$$\Psi(r,r') \simeq \Psi_0(r,r') \equiv \sqrt{\frac{k}{2\pi L r r'}} \exp\left\{ i\frac{k}{2L}(r-r')^2 - i\frac{\pi}{4} \right\} . \quad (5.33)$$

Equation (5.30) in this approximation simplifies to

$$f(k,r) = \Phi_0(r) + \int_0^a r'dr' \, \Psi_0(r,r') \, f(k,r') , \quad (5.34)$$

where

$$\Phi_0(r) \simeq \frac{-iL}{k} \frac{1}{a-r} \Psi_0(r,a) \quad \text{for } a-r \gg \sqrt{2L/k} . \quad (5.35)$$

Function $\Phi_0(r)$, describing the diffraction on a single iris, rapidly oscillates for $(a-r) > \sqrt{2L/k}$, and in this region is negligibly small. A solution of Eq. (5.34) can be found by an iterative procedure in which the solution f_n on the nth step is found by substituting f_{n-1} for $f(k,r)$ (with $f_1 = \Phi_0$) in the integrand of Eq. (5.34). Subsequent iterations take into account the diffraction from the consecutive irises of the array. The iterative solution on the nth step is

$$f_n(k,r) \propto \exp\left\{ \frac{ik}{2L(n+1)}(r-a)^2 \right\} . \quad (5.36)$$

This function has a width that increases with n as $(a-r) \simeq \sqrt{(2L/k)(n+1)}$. Its amplitude decreases rapidly when the width becomes of the order of a, i.e. for $n > M \simeq ka^2/L$. Palmer [91] noted that M defines the minimal number of cavities sufficient for the impedance of a *finite* array to be approximated by the impedance of an *infinite* periodic structure. We discuss this in more detail in Section VI.

Function $\Psi_0(r,r')$ has a sharp peak as a function of $r-r'$. In the limit as $k \to \infty$ it can be approximated by the δ function:

$$\lim_{k\to\infty} \Psi_0(r,r') = \frac{1}{r} \delta(r-r') . \quad (5.37)$$

The solution of Eq. (5.34) in this limit is $f(\infty,a) = -1/a$. For finite but large $k \gg L/a^2$, we have $1 + af(k,a) \sim (1/k)$, see Eq. (5.41) below. The amplitude of the radiated field $f(k,r)$ at the iris increases from $f=0$ at $r=0$ to $f \approx -1/a$ at $r=a$, and then decreases as $-1/r$ for $r > a$. Recall that for a single cavity $E^{(1)}_{\omega r}$ has a discontinuity at $r=a$, changing from zero to $-1/a$. The continuity of the function $f(k,r)$ and, correspondingly, of the radiated field $E^{(1)}_{\omega r}$ at the point $r=a$ arises from the interference of the diffracted waves in the periodic structure. This is the reason that the asymptotic frequency dependence of the impedance for a single cavity differs from that of a periodic array of cavities.

To solve Eq. (5.34) numerically, it is convenient to introduce a new function, $F(a-r)$, defined by

$$\frac{\partial}{\partial r}\, r\, f(k,r) = -\Lambda\, F(a-r)\ , \tag{5.38}$$

where

$$\Lambda = 1 + a f(k,a)\ . \tag{5.39}$$

The function $F(a-r)$ satisfies the integral equation

$$F(a-r) = \sqrt{ra}\ \Psi_0(a,r) + \int_0^a dr'\ F(a-r')\ \sqrt{rr'}\ \Psi_0(r,r')\ , \tag{5.40}$$

with $\Psi_0(r,r')$ defined in Eq. (5.33). Equation (5.40) was solved numerically for different wave numbers k. The typical behavior of function $r\, f(k,r)$ is shown in Fig. 5.7 [42]. The parameter $\Lambda(k)$ has been found from these calculations; its dependence on $ka^2/2L$ is shown in Fig. 5.8. It wobbles around [42]

$$\Lambda \approx \frac{4\pi L}{ka^2}\ . \tag{5.41}$$

Function $F(a-r)$ oscillates rapidly (see Fig. 5.9); therefore, the last term in Eq. (5.30) is small. The remaining term has the same structure as that for a single cavity, but has an additional factor $\Lambda \propto 1/k$. Hence, the impedance of the periodic array decreases with the wave number as $k^{-3/2}$. For the real part of the impedance we obtain

$$\mathrm{Re}\ Z(k) = Z_0\ \frac{2}{\sqrt{\pi}}\ \left(\frac{L}{ka^2}\right)^{3/2}\ , \tag{5.42}$$

while the same quantity decreases as $k^{-1/2}$ for a single cavity. The same dependence on k, i.e. Re $Z(k) \propto k^{-3/2}$, was obtained in the optical resonator model [13, 58, 101, 106]. A more rigorous analytical derivation of these results is given in Section VI.D.

E. A taper

Consider a gradual transition—a *taper*—between two cross sections of the beam pipe from a smaller radius a to a larger radius b. In such a case the energy loss of a bunch is expected to be smaller than it would be while passing through a step. Until recently, no analytic methods for evaluating the effects of a taper were available. Here we use the method of iteration to estimate the effect of a linear taper, i.e. a taper in which the slope of the wall is constant. For short bunches, $\sigma \ll a < b$, the energy loss is dominated by the high-frequency modes $kb > ka \gg 1$. This allows one to estimate the loss and the impedance using Eq. (5.11).

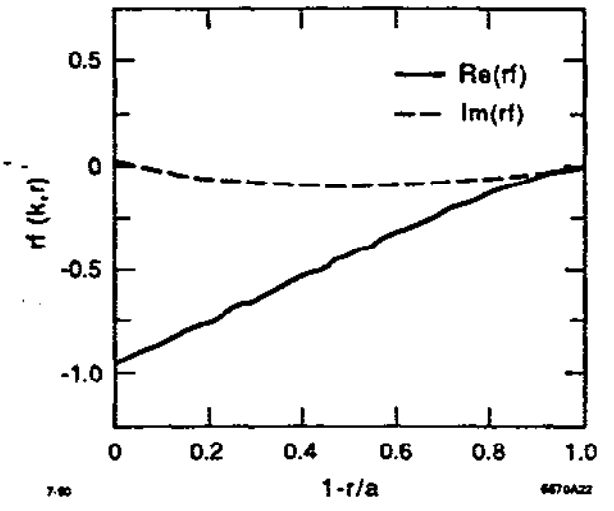

Figure 5.7
Function $r\,f(k,r)$ (see text).

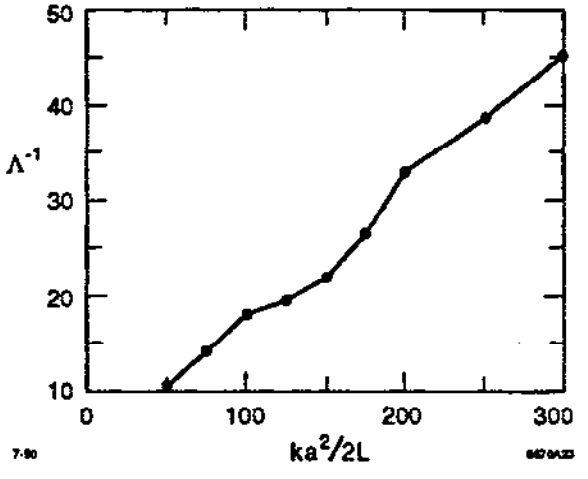

Figure 5.8
Parameter Λ^{-1} as a function of $ka^2/2L$ (see text).

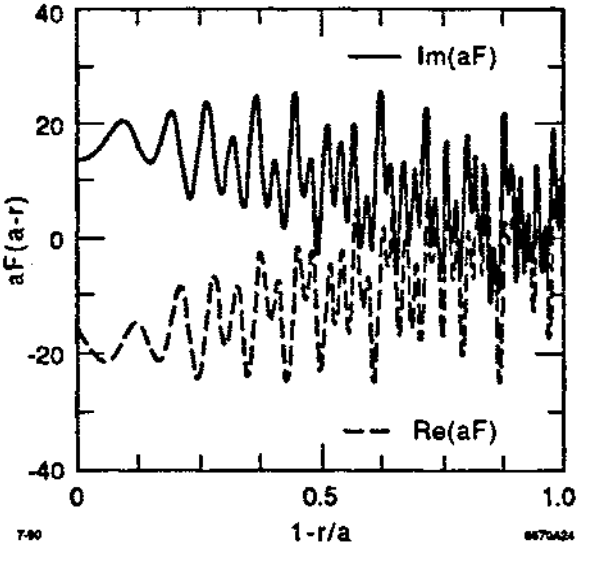

Figure 5.9
Function $aF(a-r)$ (see text).

Let us characterize the taper by an angle α at which the taper wall is inclined to the axis z: $\cot\alpha = g_1/(b-a)$, where g_1 is the length of the taper. For a step we have $g_1 = 0$ and $\alpha = \pi/2$. On the basis of the previous discussion, we expect the main contribution to the impedance to come from the waves with large k diffracted at small angles. The taper may be expected to reduce the impedance or the loss factor of the transition effectively, if its angle is comparable to or smaller than the Fresnel diffraction angle.

As shown below, for a bunch of rms length σ, the loss factor decreases with increasing taper length g_1 until it reaches a minimal value at $g_1 \simeq (b-a)^2/\sigma$, and it remains constant with further increases of g_1. A short taper, for which $g_1\sigma/2(b-a)^2 \ll 1$, is not effective in reducing the energy loss.

Consider a cylindrical cavity of total length g with slanted side walls comprising two symmetrical tapers of length g_1 on both sides. The symmetry of the cavity significantly simplifies calculations. We follow here the considerations given by Heifets [42]. Equation (5.11) for such a cavity gives:

$$E_{\omega z}^{(1)}(r,z) = \frac{iq}{2c}\int_a^b dr' \int_{-\infty}^{\infty} dp\ e^{ipz}\left[\exp\{i(k-p)(r'-a)\cot\alpha\}\right.$$

$$\left. - \exp\{i(k-p)[g-(r'-a)\cot\alpha]\}\right]\ J_0(\Omega r)\ \frac{\partial H_0^{(1)}(\Omega r')}{\partial r'}\ . \qquad (5.43)$$

Here $\Omega = \sqrt{k^2-p^2}$ and $\cot\alpha = g_1/(b-a)$. The two terms in Eq. (5.43) describe the waves generated at the two tapers: the taper-out at $z=0$ and the taper-in at $z=g$. For $g_1 = 0$ Eq. (5.43) becomes Eq. (5.13). The longitudinal impedance of a taper-out can be obtained by integrating the first term over z in the interval $0 < z < L$ and considering the limit $L \to \infty$. A taper-in is considered in a similar way. This gives

$$Z_l(\omega) = \lim_{L\to\infty}\left(-\frac{1}{c}\right)\int_{-\infty}^{\infty}\frac{dp}{k-p}\ J_0(\Omega a)\ [1-\exp\{\mp i(k-p)L\}]$$

$$\times \int_a^b dr'\ \exp\{\pm i(k-p)(r'-a)\cot\alpha\}\ \frac{\partial H_0^{(1)}(\Omega r')}{\partial r'}\ , \qquad (5.44)$$

where the signs $\pm$ correspond to a taper-out and a taper-in. In the limit $L \to \infty$,

$$\lim_{L\to\infty}\frac{1}{k-p}\left[1-e^{\mp i(k-p)L}\right] = \frac{1}{k-p} \pm i\pi\delta(k-p)\ . \qquad (5.45)$$

Hence, the impedance is

$$Z_l(\omega) = \pm\frac{1}{c}\ \ln\frac{b}{a} - \frac{1}{2c}\int_{-\infty}^{\infty}\frac{dp}{k-p}\ J_0(\Omega a)$$

$$\times\int_a^b dr'\ \exp\{\pm i(k-p)(r'-a)\cot\alpha\}\ \frac{\partial H_0^{(1)}(\Omega r')}{\partial r'}\ . \qquad (5.46)$$

The first term corresponds to the difference in the field energies of a particle in beam pipes of different radii. It is independent of the angle α. The real part of the second term describes the loss to the radiation, which is the same for a taper-out and a taper-in. The sum of the impedances of two tapers gives the impedance of the long tapered cavity; for $\alpha = 0$, it gives Eq. (5.14). The difference between the losses for two tapers with the same angle α is independent of α:

$$\kappa^l_{out} - \kappa^l_{in} = \frac{2}{\sigma\sqrt{\pi}}\ \ln\frac{b}{a}\ . \qquad (5.47)$$

This was noted in numerical simulations [14]. As shown by Heifets [41], a substantial contribution for a step is given by the region of variable p, for which $1/b \ll \Omega \ll 1/a$. Hence, if

$$\tan\alpha > \frac{b-a}{2ka^2}\ , \qquad (5.48)$$

the exponent in Eq. (5.46) may be replaced by unity and the impedance of a taper is the same as the impedance of a step. In the opposite case of small α, the exponent oscillates rapidly unless

$$(k-p)(r'-a)\ \cot\alpha \ll 1\ . \qquad (5.49)$$

Restricting the area of integration by this condition, we obtain for the real part of the impedance

$$\mathrm{Re}\ Z(\omega) = \mathrm{Re}\ Z_S(\omega) - \Delta Z_l(\omega)\ , \qquad (5.50)$$

where Z_S is the impedance of a step, Eq. (5.17), and the correction term is

$$\Delta\ Z_l = \frac{1}{2c}\int_{-1}^{x_0}\frac{dx}{1-x}\ J_0(ka\sqrt{1-x^2})\left[J_0(kr_m\sqrt{1-x^2}) - J_0(kb\sqrt{1-x^2})\right]\ . \qquad (5.51)$$

Here,

$$r_m = a + x_0\ , \qquad x_0 = \frac{\tan\alpha}{k(b-a)}\ . \qquad (5.52)$$

To estimate the integral, we note that ΔZ_l may be large only if the argument of the Bessel function in the integrand $\psi = kr_m\sqrt{1-x^2}$ is small within the range

of integration. This is possible only if $ka \tan\alpha \ll 1$. If this condition is fulfilled, the correction term is

$$\Delta Z_l = \frac{1}{c} \ln\frac{1}{\zeta}, \tag{5.53}$$

where

$$\zeta = \begin{cases} a/b & \text{if } kb \tan\alpha < 1 , \\ 2ka \tan\alpha & \text{if } 2kb \tan\alpha > 1 . \end{cases} \tag{5.54}$$

The loss factor for a taper may be obtained by the convolution of Eq. (5.50) with the bunch distribution of rms length σ. In the case $b \gg a$, the correction term to the loss factor is

$$\Delta\kappa_l = \begin{cases} -\frac{1}{2\pi a} \cot\alpha , & \text{if } \tan\alpha \gg \sigma/a , \\ -\frac{1}{2\sigma\sqrt{\pi}} \ln\frac{b}{a} & \text{if } \tan\alpha \ll \sigma/b . \end{cases} \tag{5.55}$$

Thus, the energy loss for a taper-out may be smaller than that for a step-out ($\alpha = \pi/2$) maximum by a factor of two, even if the angle α is very small [42, 126]. For a long cavity tapered symmetrically from both ends, the correction Eq. (5.55) doubles, which, for a sufficiently small angle, $\tan\alpha \ll \sigma/b$, reduces the loss for a cavity to zero.

The dependence of the longitudinal loss factor of a one-sided taper on its angle can be approximated by

$$\kappa_T^l = \frac{2}{\sigma\sqrt{\pi}} \left(1 - \frac{\tilde{\eta}_1}{2}\right) \ln\frac{b}{a}, \tag{5.56}$$

where $\tilde{\eta}_1 = \min(1.0, \eta_1)$, and

$$\eta_1 = \frac{g_1\sigma}{(b-a)^2} . \tag{5.57}$$

For $\eta_1 > 1$, the loss factor of a taper reaches half the value of the loss factor for a step, and it remains constant with further increase of η_1.

The results of Eq. (5.56) are compared with calculations by code TBCI in Fig. 5.10 [44] for a cavity tapered from one side, of length $g/a = 115$, where $a = 1$ cm. The bunch length is assumed to be $\sigma/a = 0.3$. Curves are plotted for the ratios $b/a = 4.0$ and $b/a = 2.0$. The two sets of results are in reasonably good agreement.

For a symmetric taper, $\tilde{\eta}_1/2$ should be replaced by $\tilde{\eta}_1$:

$$\kappa_T^l = \frac{2}{\sigma\sqrt{\pi}} (1 - \tilde{\eta}_1) \ln\frac{b}{a}. \tag{5.58}$$

A long symmetric taper reduces losses to zero.

The lack of dependence of the losses on the direction of beam propagation is also confirmed in these calculations.

A quite different approach to the problem of a taper was recently developed by Yokoya [125].

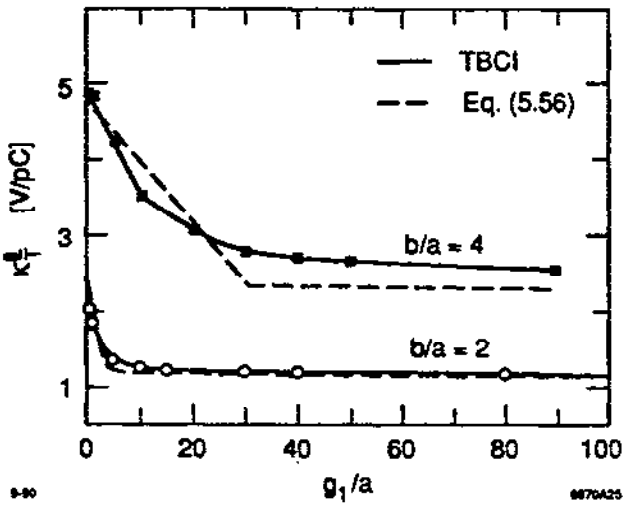

Figure 5.10 The longitudinal loss factor of a taper as a function of taper length g_1/a; $a = 1$ cm, $\sigma/a = 0.3$.

VI. ANALYTICAL RESULTS FOR THE HIGH-FREQUENCY IMPEDANCE

When the structure under consideration can be separated into simple parts for which the solutions of the Maxwell equations are known or can be found, a natural method for obtaining the solution for the whole structure is the field-matching technique. The application of this method for calculating the narrow-band impedance is discussed in Section IV.A.

Here we use this method to derive an exact system of equations suitable for the high-frequency region. An approximate solution of the system is obtained for several simple cylindrically symmetric structures. The high-frequency impedance is found for a step, for a cavity, and for a periodic array of a finite number of cavities. It is shown that the observed transition from one regime (characteristic of a single cavity) to another regime (appropriate for an infinite periodic structure) can be explained by the interference of the EM waves diffracted from different cavities. The criterion governing such a transition is given. The results agree with the results obtained above with another approximation: the diffraction model. This supports the reliability of the approximations, and allows us to use them in more complicated cases where analytical methods do not exist. For example, Gluckstern and Neri [37] used a similar approach to obtain the longitudinal impedance of a small obstacle.

The situation for a semi-infinite circular waveguide is unique . In this case, an exact solution of the Maxwell equations can be found in a closed form. The Wiener-Hopf technique used for that purpose, and the derivation of the longitudinal impedance for that structure, are described in Section VI.F.

A. The basic system of algebraic equations

The starting point for calculating the high-frequency longitudinal impedance is a system of linear algebraic equations for unknown coefficients of the field expansion. We will derive the system of equations for the general case of a periodic array of M equal cylindrical cavities of radius b placed on an infinitely long beam pipe of constant radius a [48, 49]. A particle with charge q and velocity $v \sim c$ (i.e. $\beta \sim 1$) is assumed to move along the axis of the system $r_0 = 0$. We choose the plane $z = 0$ to coincide with the beginning of the first cavity. Figure 6.1 gives the layout of the geometry considered and the coordinate system used.

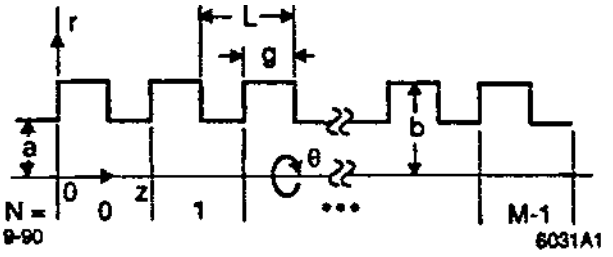

Figure 6.1
A periodic array of cavities. The layout of geometry and the coordinate system.

A particular case of a single cavity can be obtained by assuming $M = 1$. Likewise, a particular case of a periodic array of cavities can be obtained in the limit as $M \to \infty$.

For the cylindrically symmetric (monopole) modes, the Fourier harmonics of the electric field generated by a particle can be written as a sum of the *field of a particle* in a pipe and the *radiation field* due to the presence of the cavities. The radiation field satisfies the homogeneous wave equation and must be finite at $r = 0$. It can be represented as a superposition of cylindrical eigenfunctions with unknown coefficients $A(p)$. For the region inside the pipe, $r \le a$, the radial and longitudinal Fourier components of the electric field are, respectively,

$$E_{r\omega} = Q\gamma \;\; e^{ikz}\; G_1(r,a) - i\,\frac{qa}{\pi c}\int\limits_{-\infty}^{\infty} dp\; A(p)\;\frac{p}{\Omega}\; J_1(\chi_p r/a)\;\; e^{ipz}, \qquad (6.1)$$

and

$$E_{z\omega} = -iQ \;\; e^{ikz}\; G_0(r,a) + \frac{q}{\pi c}\int\limits_{-\infty}^{\infty} dp\; A(p)\; J_0(\chi_p r/a)\;\; e^{ipz}\;, \qquad (6.2)$$

where $k = \omega/c$, $Q = qk/\pi c\gamma^2$, $G_{0,1}(r,a)$ are defined in Eqs. (4.3) and (4.2), and

$$\chi_p = a\Omega\;, \qquad \Omega = \sqrt{k^2 - p^2 + 2ik\varepsilon}\;, \qquad \varepsilon \to 0\;. \qquad (6.3)$$

An infinitely small imaginary part ε is added to the wave number k to comply with the radiation condition.

The radiation field components inside the Nth cavity, $a < r < b$, $NL \leq z < NL + g$, are

$$E_r^N = \sum_{n=0}^{\infty} \lambda_n \, D_n^N \, g_n^{(1)}(r) \, \sin(\lambda_n \zeta_N) \, , \tag{6.4}$$

and

$$E_z^N = \sum_{n=0}^{\infty} (\mu_n / b) \, D_n^N \, g_n^{(0)}(r) \, \cos(\lambda_n \zeta_N) \, , \tag{6.5}$$

where

$$g_n^{(0,1)}(r) = J_{0,1}(\mu_n r/b) \, Y_0(\mu_n) - Y_{0,1}(\mu_n r/b) \, J_0(\mu_n) \, , \tag{6.6}$$

$$\mu_n = b\sqrt{k^2 - \lambda_n^2} \, , \qquad \lambda_n = n\pi/g \, , \qquad \zeta_N = z - NL \, , \tag{6.7}$$

and D_n^N are unknown coefficients for the Nth cavity, $N = 0, 1, \ldots, M-1$. Here $Y_{0,1}$ are Bessel functions of the second kind, of the zeroth and first order. The field components in Eqs. (6.1), (6.2), (6.4), and (6.5) are constructed in such a way that their tangential projections are equal to zero on all the metallic surfaces: at $r = a$ in the pipe and $r = b$ in the cavities for appropriate values of z, and at $z = NL$ and $z = NL + g$ for arbitrary values of r in the interval $b > r > a$.

To find the unknown expansion coefficients D_n^N, one can use the field-matching method described in Section IV.A. Matching the radial components of the field from Eqs. (6.1) and (6.4) in the Nth cavity on the surface $r = a$, $0 \leq \zeta_N < g$, defines the coefficients D_n^N in terms of the radial component of the radiation field. After that, matching the z-components of the field, Eqs. (6.2) and (6.5), at $r = a$ produces the following integral equation for the function $A(p)$:

$$A(p) = \sum_{N=0}^{M-1} \sum_{n=0}^{\infty} \frac{C_n(k)}{\pi g} \frac{V_n(p)}{J_0(\Omega)} \exp\{i(k-p)NL\}$$

$$\times \left[\frac{i}{ka} \, V_n^*(k) + a \int_{-\infty}^{\infty} dp' \, V_n^*(p') \, \frac{J_1(\chi_{p'})}{\chi_{p'}} \exp\{i(p'-k)NL\} \, A(p') \right] \, , \tag{6.8}$$

where the following notations are introduced:

$$C_n(k) = \frac{\mu_n}{b} \frac{g_n^{(0)}(a)}{g_n^{(1)}(a)} \approx \sqrt{k^2 - \lambda_n^2} \, \tan\left[(b-a) \sqrt{k^2 - \lambda_n^2} \right] \, , \tag{6.9}$$

$$V_n(p) = \int_0^g dz \; e^{-ipz} \, \cos(\lambda_n z) \, . \tag{6.10}$$

Note that

$$|V_n(p)|^2 = \frac{4p^2 \sin^2 \frac{g}{2}(p-\lambda_n)}{(p^2-\lambda_n^2)^2} \tag{6.11}$$

and that the functions $V_n(p)\ \exp\{-ipNL\}$ are orthogonal:

$$\int_{-\infty}^{\infty} dp\ V_n^*(p)\ V_m(p)\ \exp\{-ipL(N-N')\} = \pi g\, \delta_{n,m}\, \delta_{N,N'}\ . \tag{6.12}$$

The longitudinal impedance is given by the coefficient $A(k)$:

$$Z(k) = -Z_0\ A(k)\ , \qquad Z_0 = 377\ \Omega\ . \tag{6.13}$$

In what follows we assume that $b > a$, since when $b = a$ all $C_n(k) = 0$ identically. Consequently, all $A(p) = 0$, which means that no radiation occurs in a smooth pipe.

We seek a solution of Eq. (6.8) in the form

$$A(p) = \sum_{N=0}^{M-1} \sum_{n=0}^{\infty} B_n^N\ \frac{V_n(p)}{J_0(\chi_p)}\ \exp\{i(k-p)\ NL\}\ , \tag{6.14}$$

which gives the following system of linear algebraic equations for B_n^N:

$$B_n^N = \frac{a}{\pi g}\ C_n(k) \left\{ \frac{i}{ka^2}\ V_n^*(k) + \sum_{N'=0}^{M-1} \sum_m\ \Gamma_{nm}^{N-N'}\ B_m^{N'} \right\}\ . \tag{6.15}$$

Here $N = 0,\ 1,\ \ldots,\ M-1$, and the following notation for matrix elements $\Gamma_{nm}^{N-N'}$ is introduced:

$$\Gamma_{nm}^{N-N'} = \int_{-\infty}^{\infty} \frac{dp}{\chi_p}\ \frac{J_1(\chi_p)}{J_0(\chi_p)}\ V_n^*(p)\ V_m(p)\ \exp\{i(p-k)\ L(N-N')\}\ . \tag{6.16}$$

To evaluate this integral, we use analytical continuation of functions in its integrand into the complex plane of the variable p. According to the radiation condition, cf. Eq. (6.3), the path of integration in Eq. (6.16) must be shifted above the negative real axis and below the positive of that plane. With the path closed by a circle of large radius in either the upper or the lower half-plane, it is easy to show that the integral is equal to the sum of residues in the zeros of the Bessel function $J_0(\nu_l) = 0$:

$$\Gamma_{nm}^{N-N'} = \sum_l \frac{2\pi i}{u_l a^2} \begin{cases} V_n^*(u_l) V_m(u_l)\ \exp\{iL(u_l-k)(N-N')\} & \text{for } N > N' \\ V_m^*(u_l) V_n(u_l)\ \exp\{-iL(u_l+k)(N-N')\} & \text{for } N < N' \end{cases} \tag{6.17}$$

where

$$u_l = \begin{cases} \sqrt{k^2 - (\nu_l/a)^2} & \text{for } \nu_l < ka \\ i\sqrt{(\nu_l/a)^2 - k^2} & \text{for } \nu_l > ka \end{cases} . \tag{6.18}$$

All terms with $\nu_l > ka$ in the sum of Eq. (6.17) are exponentially small. Hence, the summation over l may be truncated at $\nu_l = ka$. The imaginary part of the diagonal term is

$$\text{Im } \Gamma^0_{nn} = \sum_{l=0}^{l_{\max}} \frac{2\pi}{u_l a^2} \; |V_n(u_l)|^2 \; , \tag{6.19}$$

where the integer $l_{\max}$ on the upper limit of the summation is defined by the inequality $\nu_{l_{\max}} \leq ka$.

The longitudinal impedance in terms of the coefficients B^N_n is

$$Z(k) = -Z_0 \sum_{N=0}^{M-1} \sum_{n=0}^{\infty} V_n(k) \; B^N_n(k) \; . \tag{6.20}$$

So far, the system Eq. (6.15) constitutes the exact set of equations defining the radiation of an ultrarelativistic particle.

B. The impedance of a cavity in the zeroth-order approximation

In the high-frequency limit, we expect that the system Eq. (6.15) can be solved by the method of iteration. In the zeroth-order approximation, we neglect the second term in brackets in Eq. (6.15):

$$B^N_n = \frac{iC_n(k)}{\pi g k a} \; V^*_n(k) \; . \tag{6.21}$$

Then the impedance per cell is

$$\frac{Z}{M} = -i \, \frac{Z_0}{\pi g k a} \sum_{n=0}^{\infty} |V_n(k)|^2 \; C_n(k) \; . \tag{6.22}$$

Note that in the zeroth-order approximation the impedance per cell given by this formula does not depend on the number of cells in the array and, as seen shortly, is the impedance of a single cavity.

For large wave numbers k the impedance, Eq. (6.22), is a fast changing function of k and goes to infinity at the resonance values

$$k_{nl} = \sqrt{\left(\frac{\pi n}{g}\right)^2 + \left(\frac{\pi(l+1/2)}{b-a}\right)^2} \tag{6.23}$$

defined by the equation $C_n^{-1}(k_{nl}) = 0$. The impedance can be presented as a sum of the resonances with infinitely small width. With $C_n^{-1}(k)$ in the vicinity of a resonance represented as

$$C_n^{-1}(k) = R_{nl}^{-1}(k - k_{nl} + i\varepsilon) \; , \tag{6.24}$$

where

$$R_{nl} = -\frac{[\pi(l+1/2)]^2}{k_{nl}(b-a)^3} , \tag{6.25}$$

the real part of the impedance is given by the sum of δ-functional terms

$$\mathrm{Re}\,\frac{Z}{M} = \frac{Z_0\pi^2}{gka(b-a)^3} \sum_{n,l} |V_n(k)|^2 \, \frac{(l+1/2)^2}{k_{nl}} \, \delta(k-k_{nl}) . \tag{6.26}$$

Practically, we are interested in Re Z averaged over some interval of wave numbers Δk, which should be large compared with the difference between neighboring resonance frequencies δk, given by

$$\delta k = k_{n(l+1)} - k_{nl} \approx \frac{\pi l}{k(b-a)^2} . \tag{6.27}$$

We can chose an appropriate Δk in the following way. The factor $|V_n(k)|^2$ given by Eq. (6.11) has a maximum value of order $(g/2)^2$ for $n = n_0$, where

$$n_0 = \left[\frac{kg}{\pi}\right] , \tag{6.28}$$

and decreases as $(n-n_0)^{-2}$ for $n \neq n_0$. The brackets denote the integer part of an argument. The main contribution to the impedance is therefore given by mode n_0 which, of course, is different for different k. Hence, it is convenient to choose the interval of averaging as

$$\Delta k \approx \pi/2g , \tag{6.29}$$

which is large compared to δk, if k is large.

To estimate the real part of the impedance in Eq. (6.26), it suffices to consider only the term $n = n_0$. The average impedance is then

$$\left\langle \mathrm{Re}\,\frac{Z}{M} \right\rangle = \frac{\pi^2 g}{4ka(b-a)^3} \, \frac{Z_0}{\Delta k} \sum_{l=0}^{l_{\max}} \frac{(l+1/2)^2}{k_{n_0 l}} , \tag{6.30}$$

where

$$l_{\max} = (b-a) \sqrt{\frac{k}{\pi g}} . \tag{6.31}$$

This estimate of the real part of the impedance, with Δk defined by Eq. (6.29), differs from the real part of Lawson's estimate [80]

$$\frac{Z}{M} = (1+i) \, \frac{Z_0}{2\pi} \sqrt{\frac{g}{\pi a}} \, \frac{1}{\sqrt{ka}} \tag{6.32}$$

only by a factor $\pi/3$. Numerical calculations confirm that this result is independent of the size chosen for the interval Δk.

We conclude that the main contribution to the impedance comes, with good accuracy, from eigenmodes with eigennumbers

$$n = n_0 \quad \text{and} \quad 0 \le l \le l_{\max} . \tag{6.33}$$

This result has a simple physical meaning. The eigenmode with the eigennumbers $(n, l) \gg 1$ is characterized by the wave vector $\mathbf{k}$ with components $k_\perp = \pi l/(b-a)$ and $k_\parallel = n\pi/g$, corresponding to the wave number k_{nl} in Eq. (6.23) and the frequency $\omega/c \approx k_{nl}$. The interaction of a particle with a mode contributes substantially to the impedance if, in the time of flight through the cavity g/v, the phase slippage is small:

$$(\omega - k_\parallel v)\ \frac{g}{v} < \frac{\pi}{2} . \tag{6.34}$$

Substituting $v \approx c$ and $n = n_0$ from Eq. (6.28), we obtain the condition Eq. (6.33) with $l_{\max}$ from Eq. (6.31).

The zeroth-order approximation does not take into account either the interference of the radiation from different cavities or the energy escape into the cavity openings. We next derive a method that allows us to take into account both these effects.

C. The high-frequency impedance of a cavity in the diagonal approximation

We start with the somewhat simpler case of a single cavity, $M = 1$. In this case, the interference of the radiation from different cavities plays no role, but the energy flow into the side pipes must be taken into account. For $M = 1$, Eq. (6.15) takes the form

$$B_n = \frac{a}{\pi g}\, C_n(k) \left\{ \frac{iV_n^*(k)}{ka^2} + \sum_m \Gamma^0_{nm} B_m \right\} . \tag{6.35}$$

In the zeroth-order approximation, the sum on the right-hand side of this equation is neglected altogether. In the next approximation, we include the main diagonal term $m = n$ contributing to the sum. All the other terms give only small corrections and can be taken into account by the method of iteration. In this *diagonal approximation* [48, 49], we obtain the following expression for the impedance:

$$Z(k) = -i\, \frac{Z_0}{ka^2} \sum_n \frac{|V_n(k)|^2}{y(k)} , \tag{6.36}$$

where we define

$$y(k) \equiv \frac{\pi g}{a}\, C_n^{-1} - \Gamma^0_{nn} \approx \frac{\pi g}{a}\, \frac{\cot\left[(b-a)\sqrt{k^2 - \lambda_n^2}\right]}{\sqrt{k^2 - \lambda_n^2}} - \Gamma^0_{nn} . \tag{6.37}$$

The sum in Eq. (6.36) is again determined mainly by terms $n \approx n_0$.

By treatment similar to that of Eq. (6.22), the impedance given by Eq. (6.36) can be represented as a sum over the resonance terms with finite widths. The resonance frequencies are now given by the condition Re $y(k) = 0$, while the resonance widths are defined by Im Γ^0_{nn}. Evaluation of Γ^0_{nn} has been done [49]; for large $k \approx n\pi/g$, a good estimate is

$$\Gamma^0_{nn} = (i-1)\,\frac{g}{a}\,\sqrt{\frac{\pi g}{2k}}\,. \tag{6.38}$$

The resonance frequency shift given by Re Γ^0_{nn} is small, and the expansion around a resonance frequency k_{nl} takes the form

$$y(k) = R_{nl}^{-1}(k - k_{nl} + i\gamma_{nl})\,, \tag{6.39}$$

where

$$R_{nl} = -\frac{al^2}{g^2(b-a)l^2_{\max}}\,, \tag{6.40}$$

and

$$\gamma_{nl} = \frac{1}{g\sqrt{2}}\left(\frac{l^2}{l^3_{\max}}\right)\,. \tag{6.41}$$

Hence, in the diagonal approximation, Re Z is not singular as it was in the zeroth approximation Eq. (6.26), although it may have rather sharp peaks if γ_{nl} is small. This is the main qualitative feature of the diagonal approximation for a single cavity.

The ratio of the resonance width γ_{nl} to the distance δk between adjacent resonances is small for resonances with $l < l_{\max}$:

$$\frac{\gamma_{nl}}{\delta k} \approx \frac{l}{l_{\max}} < 1\,. \tag{6.42}$$

Therefore, averaging over Δk for resonances with different l may be performed independently. Since the integral over a resonance curve does not depend on its width, the real part of the impedance is the same as that given by Eq. (6.32). The diagonal approximation allows one to estimate correction, given by the next iteration, and to prove that such corrections are small in the high-frequency limit [49]. Recently, Gluckstern [30] showed that Eq. (6.32) holds for a cylindrically symmetric cavity of general shape.

D. The high-frequency impedance of an array of cavities

Consider now an array consisting of M identical cells. In this case the interference of waves generated in different cells must be taken into account. We describe the interaction of a particle with each cell in a manner similar to the previous treatment of a single cavity. Therefore, we consider Eq. (6.15) in the

diagonal approximation for the lower indices, retaining only the terms $m = n = n_0$, but keeping the summation over the upper indices N'. This gives [48, 49]

$$B_n^N y(k) = \frac{iV_n^*}{ka^2} + \sum_{N'=0, N' \neq N}^{M-1} \Gamma_{nn}^{N-N'} B_n^{N'} , \qquad (6.43)$$

where $N = 0, 1, \ldots, M-1$; $\Gamma_{nn}^{N-N'}$ is defined in Eq. (6.17); and $y(k)$ is defined by Eq. (6.37).

The system Eq. (6.43) is difficult to solve numerically for an interesting case, namely $M \sim ka \gg 1$. Indeed, the rank of the corresponding matrix is M. In addition, the coefficients in Eq. (6.43) oscillate rapidly with a typical period of $1/M$. Therefore, the computational time for the calculation of the averaged impedance increases with M as M^3.

To simplify Eq. (6.43), consider the behavior of its matrix elements given in Eq. (6.17). All the elements with $N < N'$ contain factors that oscillate with large sum frequencies $u_l + k \sim 2k$. After averaging over a frequency interval, their contribution is negligibly small. On the other hand, all the matrix elements with $N > N'$ contain factors that oscillate with small difference frequencies $u_l - k$. These terms describe the interaction of a particle with the waves traveling in the same direction. Therefore, we may assume that

$$\Gamma_{nn}^{N-N'} = 0 \quad \text{for} \quad N < N' \qquad (6.44)$$

and rewrite Eq. (6.43) in the form

$$B_n^N y(k) = \frac{iV_n^*}{ka^2} + \sum_{N'=0}^{N-1} \Gamma_{nn}^{N-N'} B_n^{N'} . \qquad (6.45)$$

By omitting the terms with $N' > N$ we neglect the interaction of a particle with the waves traveling in the opposite direction. In particular, we neglect the decay of the modes inside cavities into these waves. Since we do this in the nondiagonal terms, for consistency, we should do the same in the diagonal terms as well. In other words, Im Γ_{nn}^0 in the definition of $y(k)$, Eq. (6.37), should be divided by 2.

Equations (6.45) are the recurrence relations between coefficients B_n^N. Thus the coefficients can be found sequentially starting with the zeroth one :

$$B_n^0 = \frac{iV_n^*}{ka^2 y(k)} . \qquad (6.46)$$

Note that this expression gives the impedance of a single cavity.

It is also possible to solve the system of Eqs. (6.45) explicitly. To do this we note that the Nth coefficient is expressed through coefficients with indices $N' < N$. Although we are interested in only the first M coefficients, the procedure can be formally extended to any N. Since the matrix $\Gamma_{nn}^{N-N'}$ depends only on the differences $N - N'$, Eq. (6.45) can be solved by applying the discrete Laplace

transformation. The Laplace transforms of B_n^N and Γ_{nn}^N are defined for a complex argument s as follows:

$$B_n(s,k) \;=\; \sum_{N=0}^{\infty} \; e^{-Ns}\, B_n^N \;, \tag{6.47}$$

$$\Gamma_n(s,k) \;=\; \sum_{N=1}^{\infty} \; e^{-Ns}\, \Gamma_{nn}^N \;, \tag{6.48}$$

with $\sigma \equiv \mathrm{Re}\; s > 0$.

Then the Laplace transform of a solution of Eq. (6.45) is

$$B_n(s,k) \;=\; \frac{iV_n^*}{ka^2}\, \frac{1}{[y(k) - \Gamma_n(s,k)]\,(1 - e^{-s})} \;. \tag{6.49}$$

The inverse transformation now gives the solution of Eq. (6.45):

$$B_n^N \;=\; \int_{-i\pi+\sigma}^{i\pi+\sigma} \frac{ds}{2\pi i}\; e^{Ns}\, B_n(s,k) \;, \qquad \sigma > 0 \;. \tag{6.50}$$

Hence, the impedance of an array with an arbitrary number of cells M is given by the following expression [cf. Eq. (6.20)]:

$$Z(k) \;=\; -\frac{Z_0}{4\pi k a^2} \sum_{n=0}^{\infty} |V_n(k)|^2 \int_{-i\pi+\sigma}^{i\pi+\sigma} ds\; \frac{e^{Ms} - 1}{[y(k) - \Gamma_n(s,k)]\,(\cosh s - 1)} \;. \tag{6.51}$$

Here

$$\Gamma_n(s,k) \;=\; \sum_{l=0}^{\infty} \frac{2\pi i |V_n(u_l)|^2}{a^2 u_l \left(e^{iL(k-u_l)+s} - 1\right)} \tag{6.52}$$

and

$$u_l \;=\; \sqrt{k^2 - (\nu_l/a)^2 + 2ki\epsilon} \;, \qquad \nu_l \approx \pi l \;. \tag{6.53}$$

The integrand in Eq. (6.51) has the same value on two parallel lines, $s = -i\pi + \sigma$ and $s = +i\pi + \sigma, -\infty < \sigma < 0$. Therefore, we can add and subtract integrals over these two lines, thereby extending the contour of integration in the complex plane s from $-\infty - i\pi$, then from $-i\pi + \sigma$ to $i\pi + \sigma$, and back to $-\infty + i\pi$.

The integral is then equal to the sum of the residues at the roots of the respective equations $\cosh s = 1$ and

$$y(s) = \Gamma_n(s,k) \; . \tag{6.54}$$

It is easy to see that all the roots of Eq. (6.54) are purely imaginary. Using that fact, we average the impedance over the interval $\Delta k = \pi/2g$, cf. Eq. (6.29), as in Section VI.C for a single cavity [47]. The result is

$$\left\langle \mathrm{Re}\left(\frac{Z}{M}\right)\right\rangle \;=\; \frac{2Z_0}{(ka)^{3/2}}\left(\frac{2L}{\pi a}\right)^2\sqrt{\frac{\pi a}{g}}\;\Phi(k,M)\;, \tag{6.55}$$

where

$$\Phi(k,M) \;=\; k\pi g\left(\frac{a}{4L}\right)^2\int\limits_{-\pi}^{\pi} dt\;\frac{F(t,M)}{2\pi}\;\Xi(\xi)\;, \tag{6.56}$$

$$F(t,M) \;=\; \frac{\sin^2\left(Mt/2\right)}{M\sin^2\left(t/2\right)}\;, \tag{6.57}$$

$$\Xi(\xi) \;=\; \frac{1}{\xi^2}\left(1-\frac{\arctan\xi}{\xi}\right)\;, \tag{6.58}$$

$$\xi \;=\; \frac{a}{2L}\;\sqrt{k\pi g}\;\frac{J_1(p)}{pJ_0(p)}\;, \tag{6.59}$$

and

$$p \;=\; \sqrt{-\frac{2ka^2}{L}\,t}\;. \tag{6.60}$$

For an array with only a few cavities ($M \approx 1$) the expansion of the expression Eq. (6.51) was obtained by Heifets and Kheifets [49]. Apart from small corrections, the impedance per cavity is the same as that for a single cavity, cf. Eq. (6.32).

To evaluate the average impedance for $M \gg 1$ we note that, for large M, function $F(t,M)$ has a sharp peak at $t \sim 0$. Hence, a good approximation for it is

$$F(t,M) \approx \begin{cases} M & \text{if } |t| < \pi/M\;, \\ 0 & \text{if } |t| > \pi/M\;. \end{cases} \tag{6.61}$$

Then Eq. (6.56) can be simplified to

$$\Phi(k,M) \;=\; \frac{M}{8}\;\frac{g}{a}\;\left(\frac{a}{4L}\right)\;[R_1(P)+R_2(P)]\;, \tag{6.62}$$

where

$$R_1(P) \;=\; \int\limits_0^P pdp\;\;\Xi(\xi_1)\;, \tag{6.63}$$

$$R_2(P) = \int_0^P p dp \; \Xi(\xi_2) \,, \tag{6.64}$$

$$\xi_1 = \frac{a}{2L} \sqrt{k\pi g} \; \frac{J_1(p)}{pJ_0(p)} \,, \tag{6.65}$$

$$\xi_2 = \frac{a}{2L} \sqrt{k\pi g} \; \frac{I_1(p)}{pI_0(p)} \,, \tag{6.66}$$

and

$$P = \sqrt{\frac{2\pi k a^2}{LM}} \,. \tag{6.67}$$

We will evaluate integrals R_1 and R_2 in two regions of the parameter P.

(a) Suppose first that $P \ll 1$ or

$$M \gg \frac{ka^2}{L} \,. \tag{6.68}$$

Since $P \ll 1$, we can expand functions ξ_1 and ξ_2 in the vicinity of $p = 0$: $\xi_1 = \xi_2 = (a/4L)\sqrt{\pi k g}$. Both values are large for large k everywhere inside the interval of the integration in Eqs. (6.63) and (6.64). Hence, function $\Xi \approx \xi^{-2} \approx (4L/a)^2(1/\pi k g)$. For the integrals R_1 and R_2 we get $R_1 = R_2 \approx 16L/gM$ and $\Phi(k, M) \approx 1$. Thus we obtain

$$\left\langle \mathrm{Re} \left(\frac{Z}{M} \right) \right\rangle = \frac{2Z_0}{(ka)^{3/2}} \left(\frac{2L}{\pi a} \right)^2 \sqrt{\frac{\pi a}{g}} \quad \text{for } M \gg \frac{ka^2}{L} \,. \tag{6.69}$$

In other words, the real part of the average impedance per cell decreases with frequency as $\omega^{-3/2}$.

(b) Suppose now that $P \gg 1$ or

$$1 \ll M \ll \frac{ka^2}{L} \,. \tag{6.70}$$

In this case, the main contribution to the integral R_1 comes from the vicinities of the roots of $J_1(p)$: $p_m = \nu_{1m}$, where $\xi_1 \approx 0$. Near the root p_m, the function Ξ can be approximated by

$$\Xi \approx \frac{1}{3 + [\xi'(p - \nu_{1m})]^2} \,. \tag{6.71}$$

This expression has the correct behavior in the vicinity of the roots $p = \nu_{1m}$, and decreases as ξ^2 far from them. The estimate of the integral R_1 is then

$$R_1 \approx \frac{\pi k a^2}{M\sqrt{gML}} \,, \tag{6.72}$$

where we used the formula [38]

$$\sum_{m=1}^{P/\pi} \nu_{m1}^2 \approx \frac{P^3}{3\pi}, \qquad P \gg 1 .$$

Unlike the situation with R_1, the integrand of R_2 does not oscillate, and the relative contribution of R_2 to Eq. (6.62) is small [it is of order of $(gM/L)^{-1/2} \ll 1$ with respect to R_1]. The physical reason for such a difference is that the interaction of a particle with the diffracted waves is substantial only when both travel in the same direction. Therefore, in this case

$$\left\langle \mathrm{Re}\left(\frac{Z}{M}\right)\right\rangle = \frac{Z_0}{2\pi}\sqrt{\frac{g}{\pi k a^2}}\sqrt{\frac{2L}{gM}}, \qquad 1 \ll M \ll \frac{ka^2}{L}, \tag{6.73}$$

In other words, the real part of the average impedance per cell decreases as $(kaM)^{-1/2}$. This result was first qualitatively obtained by Palmer [91]. A result similar to Eq. (6.73) was later obtained by Gluckstern [31, 32], albeit with a different coefficient.

An intermediate parameter region $M \sim ka^2/L$ is the transition area. The transition from one regime to another is illustrated in Fig. 6.2 [49]. The curves represent function Φ versus ka^2/ML for different values M, and were obtained by numerical integration of Eq. (6.56).

Let us summarize the results [49]. The real part of the impedance per cell for a small number of cavities decreases with frequency as $k^{-1/2}$. For a large number of cavities the asymptotic frequency region is divided into two parts. For an extremely high frequency, the real part of the impedance depends on frequency in a way similar to that for a single cavity, i.e. as $k^{-1/2}$, but falls off as $M^{-1/2}$ with the number of cells M because of the interference of the radiated waves emitted from different cavities. The interference also takes place for moderate (but still large) frequencies satisfying the criterion Eq. (6.70), resulting in a much faster decrease of the impedance, $\sim k^{-3/2}$. There is a continuous transition from the regime where the parameter M satisfies Eq. (6.70) to another where M satisfies Eq. (6.68). This result agrees both with numerical calculations for a small number of cavities [7] and with the optical resonator model [13, 58, 101, 106].

The fast decrease of the real part of the impedance as $k^{-3/2}$ has a direct implication for the design of a short bunch accelerator. Indeed, if the asymptotic decrease of the longitudinal impedance followed the law $k^{-1/2}$, the main contribution to the total energy loss would be given by the high-frequency tail of the impedance, and the total energy loss would depend on the longitudinal rms size of the bunch σ as $\sigma^{-1/2}$. The situation is quite different when the impedance falls off as $k^{-3/2}$. In this case the total energy loss is defined by the low-frequency range of the impedance and is generally smaller.

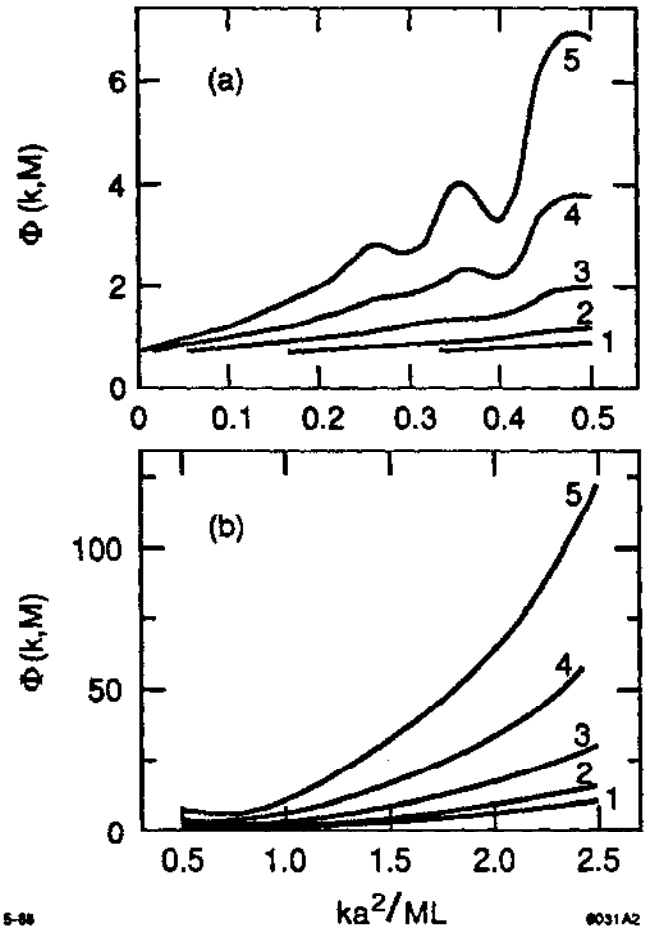

Figure 6.2 The transition from a cavity regime to a periodic array regime. The function Φ is plotted versus the parameter ka^2/ML for different values of the number M of cavities. (a) Blowup of the region of small values ka^2/ML of (b). Curves are labeled as follows: (1) $M = 500$, (2) $M = 1000$, (3) $M = 3000$, (4) $M = 10,000$, (5) $M = 30,000$.

E. The high-frequency impedance of a collimator

The longitudinal impedance of a collimator in the high-frequency region (and in the relativistic case $\gamma >> 1$) can be found analytically by using formula (4.28). Since asymptotically $\widetilde{\lambda}_b \approx \widetilde{k}$, only the diffracted field, i.e. the field depending on coefficients z_n, contributes to the impedance. Physically this arises because only the diffracted field radiated forward can reach a relativistic particle. Hence,

$$Z_{col}(k) \;=\; -2(Z_0/\pi)\,\widetilde{k}\,\Sigma_n\, z_n\; J_0\,(\nu_n/p)\;, \qquad \cdot\cdot (6.74)$$

where $p = b/a$, a is the pipe radius, and b is the collimator radius.

Coefficients z_n can be found from the matrix Eq. (4.23), with the matrix elements and the right-hand side of it taken from Table II:

$$z_l \tilde{k} J_1^2(\nu_l) = -\frac{J_0\,(\nu_l/p)}{\nu_l^2} + 2p^{-2}\,\tilde{k}\,\Sigma_m(t_m - y_m E_-)\,\phi_{lm}\,(p^{-1})\,, \qquad (6.75)$$

where quantities $\phi_{lm}(p^{-1})$ are defined in Eq. (4.24), and E_- in Table II.

Dividing Eq. (6.75) by $J_1^2(\nu_l)$, multiplying by $J_0(\nu_l/p)$, and summing over l, we obtain

$$\tilde{k}\,\Sigma_l z_l\,J_0\,\frac{\nu_l}{p} \;=\; -\frac{\Sigma_l\,J_0^2\,(\nu_l/p)}{\nu_l^2\,J_1^2(\nu_l)} + \;2\tilde{k}\,\Sigma_l\,J_0^2\,(\nu_l/p)$$

$$\times\,J_1^{-2}(\nu_l)\,\Sigma_m(t_m - y_m E_-)\,\nu_m\,J_1(\nu_m)\,(\nu_m^2\,p^2 - \nu_l^2)^{-1}\,. \qquad (6.76)$$

Summation here can be performed explicitly by using the following particular form of the Kneser-Sommerfeld formula [27, 116]:

$$\Sigma_l\,J_0^2\,(\nu_l/p)\,(\nu_l^2 - x^2)^{-1}\,J_1^{-2}\,(\nu_l)$$

$$= \frac{\pi\,J_0(x/p)\,[J_0(x/p)\,Y_0(x) - \;J_0(x)\,Y_0(x/p)]}{4J_0(x)}\,, \qquad (6.77)$$

where Y_0 is a Bessel function of the second kind. From here it follows that the second term on the right-hand side of Eq. (6.76) containing coefficients t_m and y_m vanishes, since the sum over l is zero. The first sum in Eq. (6.76) according to the same formula is

$$\frac{\Sigma_l\,J_0^2\,(\nu_l/p)}{\nu_l^2 J_1^2(\nu_l)} \;=\; \frac{\pi}{4}\;\lim\,[Y_0(x) - Y_0(x/p)]_{x\to 0} \;=\; \frac{\ln p}{2}\,. \qquad (6.78)$$

Hence, in the high-frequency region, the impedance of a collimator does not depend on frequency and is the following constant:

$$Z(\tilde{k}) = \frac{Z_0}{\pi}\;\ln\frac{a}{b} \quad \text{for}\;\; \gamma > \tilde{k} >> 1\,. \qquad (6.79)$$

The same expression holds for the high-frequency impedance of a pipe cross-section step for the case of a bunch exiting the narrow pipe. In the opposite case, the impedance is zero, cf. Section IV.C.

Formula (6.79) is not valid for $\tilde{k} > \gamma$. In this range of frequencies the impedance decreases at least as k^{-2}.

It is interesting to estimate the total energy loss $\Delta\mathcal{E}$ of a charge passing through a collimator, cf. Eqs. (2.1) and (2.15). For a Gaussian bunch of rms length σ, the total energy loss is

$$\Delta\mathcal{E} \;=\; \frac{2q^2}{\sigma\,\sqrt{\pi}}\;\ln\,\frac{a}{b}\,. \qquad (6.80)$$

This expression is valid for $\sigma > 1/\gamma$, and agrees with the formula for the total energy loss of a charge passing through a sudden change in a pipe cross section [1, 63].

If Re Z is assumed to be constant for $\widetilde{k} < \gamma$ and zero for $\widetilde{k} > \gamma$, as previously discussed, then the total energy loss of a *point* charge, $\sigma = 0$, is proportional to γ. For a charge passing through a hole in a screen, this conclusion is in agreement with the estimate obtained by Lawson [80] and with numerical calculations [25, 26].

F. The impedance of a semi-infinite circular waveguide

Here we describe the application of the Wiener-Hopf factorization method [107, 122] for calculating the impedance of a semi-infinite waveguide with a circular cross section of radius a [69, 70]. A similar structure—a semi-infinite circular pipe inside an infinite circular pipe of larger radius—is considered by Palumbo [94]. These structures have a unique feature: the Maxwell equations in these cases can be solved exactly. Levine and Schwinger [83] used the same method to obtain an explicit solution to the problem of the radiation of sound from the end of an open pipe.

As discussed in Section III.D, the impedance in this case depends on the direction of the charge motion. Consider for example, a charge entering a waveguide whose open end is placed at $z = 0$. Because of the axial symmetry of the problem, the current density has only the z component and can be expressed as the sum of the current densities of the source charge and the induced charge.

The starting point of the method is a set of integral equations for the longitudinal current density distribution induced in the wall of the pipe. The system can be obtained from Eq. (6.2). In the ultrarelativistic limit $\gamma \to \infty$, Eq. (6.2) can be rewritten as

$$E_{z\omega}(r,z) = -iQ\ e^{ikz} K_0(\tau r) - \frac{q}{2cka} \int_{-\infty}^{\infty} dp\, F(p)\, \chi_p^2\, J_0\left(\chi_p \frac{r}{a}\right)\, H_0^{(1)}(\chi_p)\ e^{ipz}\,, \qquad (6.81)$$

where $k = \omega/c$, $\tau = k/\gamma$, $Q = qk/\pi c\gamma^2$, and $\chi_p = a\sqrt{k^2 - p^2 + 2ki\varepsilon}$. In Eq. (6.81) the unknown function $A(p)$ was replaced by another function $F(p)$ according to the formula

$$A(p) = -\frac{\pi}{2ka}\, \chi_p^2\, H_0^{(1)}(\chi_p)\, F(p)\,. \qquad (6.82)$$

As shown by Kheifets *et al.* [70], function $F(p)$ defined in this way can be interpreted as the Fourier component of the induced current density. In Eq. (6.81) we have also replaced $G_0(r,a)$ by $K_0(\tau r)$ to take into account that the second term in Eq. (4.4) also comes from the induced current (cf., Section V.B), and thus is already included in the second term of Eq. (6.81).

Function $F(p)$ is defined by the boundary condition which here can be written as

$$E_{z\omega}(a,z) \;=\; 0\,, \qquad \text{for } \; z>0\,. \tag{6.83}$$

We define

$$L(p) \;=\; \pi\chi_p^2\, J_0(\chi_p)\, H_0^{(1)}(\chi_p)\,; \tag{6.84}$$

then Eq. (6.83) gives

$$\int_{-\infty}^{\infty} dp\, F(p)\, L(p)\, \exp(ipz) \;=\; \hat{Q}\, \exp(ikz) \qquad \text{for } \; z>0\,, \tag{6.85}$$

where $\hat{Q} = -2ik^2 a K_0(\tau a)/\gamma^2$. Since there is no metallic surface for $z<0$, the induced current density for negative z is zero

$$\int_{-\infty}^{\infty} dp\, F(p)\, \exp(ipz) \;=\; 0\,, \qquad \text{for } \; z<0\,. \tag{6.86}$$

Equations (6.85) and (6.86) constitute a system of linear integral equations for function $F(p)$. Provided the function $F(p)$ is found, the longitudinal impedance can be found by integrating Eq. (6.81) according to formula (2.5).

The solution of the system (6.85) and (6.86) can be obtained by factoring the kernel $L(p)$ in such a way as to satisfy the following requirements [107]:

(1) In the upper half-plane of the complex variable p, the product $F(p)L(p)$ has one pole at $p_0 = k$. The value of the residue of this pole is $\hat{Q}/2i\pi$. In all other points of the upper half-plane this product is an analytic function. As $|p| \to \infty$ in the upper half-plane, $F(p)L(p) \to 0$.

(2) In the lower half-plane, $F(p)$ is an analytic function and tends to zero as $|p| \to \infty$.

The analytic behavior of $F(p)$ and $F(p)L(p)$ described above causes $F(p)$ to be the solution of the system defined by Eqs. (6.85) and (6.86). The function $F(p)$ satisfying both the above requirements is [107]

$$F(p) = \frac{i\hat{Q}}{2\pi\Gamma_+(ka)\sqrt{ka}}\, \frac{\Gamma_-(pa)}{(ka-pa)^{3/2}}\,, \tag{6.87}$$

where functions $\Gamma_\pm$ are

$$\Gamma_\pm(u) = [2\rho\, I_0(\rho)\, K_0(\rho)]^{\pm 1/2} \exp\left\{ -\frac{u}{i\pi} \int_0^{ka} dt\, \frac{\ln[\pi\sigma_1\, J_0(\sigma_1)\, H_0(\sigma_1)]}{u^2 - t^2} \right.$$

$$\left. + \frac{u}{i\pi}\, PV \int_{ka}^{\infty} dt\, \frac{\ln[2\sigma_2\, I_0(\sigma_2)\, K_0(\sigma_2)]}{t^2 - u^2} \right\}, \qquad (6.88)$$

where $\rho = \sqrt{u^2 - (ka)^2}$, $\sigma_1 = \sqrt{(ka)^2 - t^2}$, and $\sigma_2 = \sqrt{t^2 - (ka)^2}$. Note that at $u = ka$ there is no singularity.

In terms of these functions, the impedance produced by the radiation on the open end of the waveguide [70] for $\beta \approx 1$ is

$$Z(k) = \frac{Z_0\, ka\, K_0(\tau a)}{2\pi\, \gamma^2\, I_0(\tau a)} \left[\frac{\gamma I_1(\tau a)}{I_0(\tau a)} - \frac{\Gamma_+'(ka)}{\Gamma_+(ka)} - \frac{1}{4ka} \right]. \qquad (6.89)$$

Figure 6.3 presents the real part of the longitudinal impedance Re $Z(k)$, Eq. (6.89), for several values of the Lorentz factor γ.

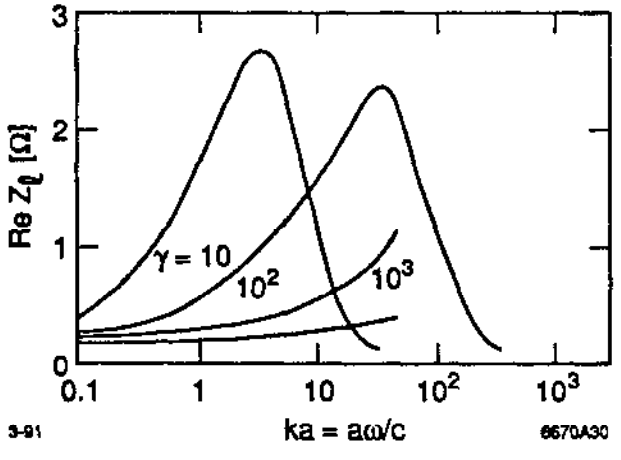

Figure 6.3 The real part of the longitudinal impedance of a semi-infinite circular waveguide as a function of parameter $ka = a\omega/c$ for three different values of the Lorentz factor γ.

In the asymptotic region $ka \gg 1$, the contribution of the discontinuity to the longitudinal impedance is

$$Z(k) = \frac{Z_0}{2\pi} \ln\frac{2\gamma}{ka}. \qquad (6.90)$$

This result is similar to that for a step with infinitely large outer radius.

VII. CONCLUSIONS

Substantial progress has recently been achieved in understanding the physics of the bunch-environment interaction in modern accelerators and in the development of analytical and numerical methods of estimating the coupling impedances and the loss factors. We have tried to describe the present level of understanding and the main theoretical results in the field. Clearly, the methods presented are limited to rather simple cylindrically symmetric geometries. Nevertheless, it is difficult to overestimate the importance of the comprehension and insight which they help to develop. Certainly much more work is needed for other geometries such as tapers, bellows, etc. This is especially true for cylindrically nonsymmetric structures.

ACKNOWLEDGMENTS

We are grateful to B. Zotter, R. Gluckstern, P. Wilson, M. Sands, and K. Bane for their valuable comments.

This work was supported by the U. S. Department of Energy under contract DE–AC03–76SF00515.

REFERENCES

1. Balakin, V.E., and A.V. Novokhatski, 1983, "VLEPP: Longitudinal Beam Dynamics," in *Proc. 12th Int. Conf. on High Energy Accelerators* (Fermilab), pp. 117-118.
2. Bane, K., 1980, "Constructing the Wake Potentials from the Empty Cavity Solutions of Maxwell's Equations," CERN/ISR-TH/80-47.
3. Bane, K.F.L., 1986, "Wakefield Effects in Linear Colliders," SLAC-PUB-4169.
4. Bane, K.F.L., and P.B. Wilson, 1980, "Longitudinal and Transverse Wake Potentials in SLAC," in *Proc. 11th Int. Conf. on High-Energy Accelerators* (Birkhauser, Geneva), p. 592.
5. Bane, K.F.L., P.B. Wilson, and T. Weiland, 1984, "Wakefields and Wakefield Acceleration," SLAC-PUB-3528.
6. Bane, K.L., and M. Sands, 1987, "Wakefields of Very Short Bunches in an Accelerating Cavity," SLAC-PUB-4441.
7. Bane, K.L., and M. Sands, 1990, "Wakefields of Very Short Bunches in an Accelerating Cavity," Part. Accel. **25**, 2-4, 73-96.
8. Bassetti, M., and D. Brandt, 1986, "Transverse Electro-Magnetic Force in Circular Trajectory," CERN/LEP-TH/86-04.
9. Bethe, H.A., 1944, "Theory of Diffraction by Small Holes," Phys. Rev. **66**, 7-8, 163-182.
10. Bisognano, J.J., 1990, "Comments on the High-Frequency Behavior of the Coupling of an Accelerator Beam to Its Environment," Part. Accel. **25**, 2-4, 253-262.
11. Bisognano, J.J., 1990, "On the Independence of the Longitudinal Wakefield on Direction of Transit through a Cavity," CEBAF-TN-0109.
12. Bisognano, J.J., S.A. Heifets, and B.C. Yunn, 1988, "The Loss Parameters for Very Short Bunches," CEBAF-PR-88-005.
13. Brandt, D., and B. Zotter, 1982, "Calculation of the Wakefield with the Optical Resonator Model," CERN-ISR/TH/82-13.
14. Chan, K.C.D., and R. Schweinfurth, 1987, "Beam Energy Spread Induced by Beampipe Steps," LANL-AT-6:ATN-87-24.
15. Channell, P.J., 1986, "Energy Independent Radial Space Charge Forces in Circular Machines," LANL-AT-6: ATN-86-15.
16. Chao, A., 1982, "Coherent Instabilities of a Relativistic Bunched Beam," SLAC-PUB-2946.
17. Chao, A., 1983, "Coherent Instabilities of a Relativistic Bunched Beam," in *Physics of High Energy Particle Accelerators,* M. Month, ed., AIP Conf. Proc. **105**, 353-523.
18. Chatard-Moulin, M., and A. Papiernik, 1979, "Energy Losses of an Electron Bunch Moving along the Axis of a Circular Waveguide with Periodically Perturbed Wall," IEEE Trans. Nucl. Sci. **NS26**, 3, 3523-3525.
19. Chin, Y.H., 1988, "ABCI (Azimuthal Beam Cavity Interaction) User's Guide," CERN/LEP-TH/88-3.
20. Collin, R.E., 1966, *Foundations for Microwave Engineering* (McGraw Hill, New York), p. 56.